Diss. ETH No. 15162 Zürich, 2003

Mathias Zwahlen

Orientation in Ultrathin Self-Assembled Organic Films for Functional Coatings: A NEXAFS study

A dissertation submitted to the Swiss Federal Institute of Technology Zürich for the degree of:
Doctor of Natural Sciences

Accepted on the recommondation of
Prof. Dr. N. D. Spencer, examiner
Prof. Dr. S. Virtanen, co-examiner
Prof. Dr. W. Steurer chair

Mathias Zwahlen
Dipl. Physics, University of Zürich, Switzerland
Born on the 1st of November, 1975
Citizen of Wahlern (BE), Switzerland

Mathias Zwahlen, 2003

Diss. ETH No. 15162 Zürich, 2003

Mathias Zwahlen

Orientation in Ultrathin Self-Assembled Organic Films for Functional Coatings: A NEXAFS study

A dissertation submitted to the Swiss Federal Institute of Technology Zürich for the degree of:
Doctor of Natural Sciences

Accepted on the recommondation of
Prof. Dr. N. D. Spencer, examiner
Prof. Dr. S. Virtanen, co-examiner
Prof. Dr. W. Steurer chair

Mathias Zwahlen
Dipl. Physics, University of Zürich, Switzerland
Born on the 1st of November, 1975
Citizen of Wahlern (BE), Switzerland

Zusammenfassung

Der Begriff “SAM” (Self-Assembled Monolayer) bezeichnet komplexe und hochgeordnete Strukturen, zu welchen sich Moleküle spontan bei der Adsorption auf ein Substrat organisieren können. Dank dieser internen Ordnung und des modularen Aufbaus ist es möglich, mit solchen Filmen, gezielt und flexibel, funktionelle chemische Gruppen auf der Oberfläche eines Substrats anzubringen und damit die Oberflächenchemie relativ unabhängig von derjenigen des Volumens zu beeinflussen. Die Flexibilität und der erzielte Effekt von SAMs, sowie die Einfachheit und Robustheit der Technik, lassen SAMs auch für zahlreiche technische Anwendungen reizvoll erscheinen.

Messungen zu der internen Struktur und Ordnung von monomolekularen Filmen nehmen eine zentrale Rolle für deren Erfolg ein. Prinzipbedingt kann sich das volle Potential einer SAM-Beschichtung nur dann entfalten, wenn tatsächlich eine hochgeordnete Struktur entsteht. Es ist ausserdem besonders bemerkenswert, dass SAMs eine beträchtliche Wirkung auf makroskopisch beobachtbare Eigenschaften (z. Bsp. Benetzbarkeit) haben und dass man die Mechanismen, durch welche diese entsteht auf molekularer Ebene verstehen kann. Aus all diesen Gründen, ist eine genaue Kenntnis über das physikalisch chemische Verhalten im Allgemeinen und die interne Struktur und Ordnung im Besonderen, unabdingbar für eine Entwicklung solcher Filme.

Strukturaufklärungen an selbstorganisierten Filmen ziehen als roter Faden durch diese Arbeit. Dazu habe ich vornehmlich NEXAFS (Near Edge X-Ray Absorption Fine Structure spectroscopy) verwendet, und wo nötig mit anderen oberflächenanalytischen Methoden ergänzt. Diese synchrotron-basierte Photoelektronenspektroskopie ist sensitiv auf interne Ordnung in SAMs und kann damit insbesondere die letzte Phase der Filmbildung, welche für die Definiertheit der Schicht entscheidend ist aber den meisten experimentellen Tech-

niken verschlossen bleibt, quantitativ verfolgen. In dieser Arbeit werden Ergebnisse von SAMs auf Muskovit-Glimmer, Metall- sowie Metalloxidoberflächen präsentiert.

Eine Modifikation der Oberflächenchemie von Muskovit-Glimmer mittels SAMs wird als wertvolles Hilfsmittel für die Herstellung massgeschneiderter Glimmer-Partikelverbundwerkstoffen erachtet. Unsere Studien konnten dabei Präparationsbedingungen und Moleküle identifizieren, mit denen sich hochgeordnete SAMs erzielen lassen.

Die Experimente zu SAMs auf Titanoxid dienen dazu, etablierte Filme genauer zu verstehen. NEXAFS konnte erfolreich dazu verwendet werden, kleine Unterschiede in der Ordnung von Phosphat-basierenden Filmen zu detektieren, wie sie beispielsweise aus dem Wechsel der Kopf- oder Endgruppe oder des Lösungsmittels erfolgen. Hier erweist sich die bereits angetönte Sensitivität auf den Grad der Ordnung als äusserst wichtig und bringt zum Beispiel die bessere Eignung der Phosphonat- gegenüber der Phosphatgruppe zu Tage.

Schliesslich tragen NEXAFS Experimente auf Oligo(ethylene glycol) terminierten SAMs auf Gold dazu bei, die “makroskopische” Fähigkeit dieser Filme, der nicht-spezifischen Proteinadsorption zu widerstehen, zu enträtseln. Wie in jedem SAM, sind auch hier detaillierte Kenntnisse der Filme nötig um deren “makroskopisch” beobachtbaren Eigenschaften zu erklären. Quantitative NEXAFS-Analysen gepaart mit Simulationen an vorgeschlagenen Modellstrukturen, geben Aufschluss über die Konformation der Moleküle, welcher im heute gängigen Modell grosse Bedeutung zugemessen wird obwohl die Kenntnis darüber immer noch Lücken aufweist.

Summary

The term “SAM” (Self-Assembled Monolayer) describes a class of complex and highly ordered structures, to which molecules can agglomerate upon adsorption onto a substrate. Owing to the internal order, and the modularity of the molecular building blocks provides a possibility to deposit specifically targeted chemical groups at the surface of a substrate and thus changing the surface chemistry (relatively) independent of that in the bulk. The flexibility of this method and well as the effects that can be achieved with SAMs in combination with the simple preparative procedure with which such films can be established, also make them a technique worth transporting to high-technology.

The only way in which the full potential of such films can benefit the researcher, is if they indeed adopt an “ideal” structure. Only then is the position of the functional endgroups guaranteed, can maximal effect be achieved an possibly most notably, can the properties of the modified surfaces be understood on a molecular level. All these reasons imply, that the use of monomolecular films will only bring their desired advances if a lot of effort is undergone in order to investigate their physical chemistry and internal structure respectively order. This explains why the development of SAMs has gone hand in hand with that of experimental techniques with which molecular structures can be proven.

Structural studies on self-assembled films are the common denominator of all the chapters in this thesis. The majority of the work was made possible by the synchrotron-based NEXAFS (Near Edge X-Ray Absorption Fine Structure) spectroscopy, which was in some cases complemented by other experimental techniques. NEXAFS is a photo-electron spectroscopy which is highly sensitive to the internal order of organic films and can most notably investigate the final stage of SAM formation, which is crucial for the resulting structure in a quantitative way, thus excelling over most other surface analytical methods.

In this thesis, I will present studies of conformational order and film structure in SAMs on Muscovite mica, metal- and metal-oxide substrates.

The modification of the surface chemistry of muscovite with SAMs is deemed beneficial for the production of tailored (mica) particle-composites. Our experiments focussed on alkylammonium ions and have clarified preparative procedures as well as concrete surfactants, with which highly order SAMs suitable for the intended modification can be established.

Alkanephosphates have been known to form well-ordered SAMs on titanium-oxide surfaces for some time. The NEXAFS results for these films have successfully revealed minor differences in the order of such films such as arise from a change in head- or endgroup or upon changing the solvent. Only with the already mentioned quantitative sensitivity to the internal order of the NEXAFS technique was it possible to detect these differences, which may prove to be crucial for future applications. At this point, the most prominent consequence of the experiments was proving the superiority of the phosphonate- over the phosphate-group as binding headgroup for the resulting order in the films.

Finally, we performed NEXAFS experiments on Oligo(ethylene glycol) terminated SAMs on gold. These films posses the unique (and bio-chemically valuable) ability to resist the non-specific adsorption of proteins. In accordance with the significance of this property, a lot of effort has gone into the investigation of the molecular mechanisms, which underly protein resistance of SAMs. Quantitative NEXAFS analysis combined with simulations of proposed model conformations have led to new insights concerning the internal structures of such films, which are believed to play a decisive role for protein resistance.

Table of Contents

Zusammenfassung **5**

Summary **7**

I Experimental **12**

1 Theory and instrumentation of NEXAFS spectroscopy **13**

1.1 Introduction 13

1.2 Structure of this chapter 14

1.3 NEXAFS physics -X-ray photon absorption. 14

1.4 Angular dependence of a NEXAFS signal 17

1.5 The synchrotron — a continuous source of linearly polarised X-rays 19

1.6 Instrumentation 23

1.7 Data analysis 27

2 Supplementary experimental techniques **31**

2.1 Contact-angle measurement 31

2.2 X-ray photoelectron spectroscopy (XPS) 35

II Self-Assembled Monolayers on metal (oxide) surfaces **39**

3 Dodecylphosphate- and -phosphonate-based molecules on Titanium oxide surfaces **40**

3.1 Motivation/ Introduction 40

3.2 Experimental . . . 43
3.3 Results . . . 46
3.4 Discussion . . . 60
3.5 Conclusions and outlook . . . 65

4 Oligo(Ethylene glycol) functionalised Alkanethiols on Gold 67
4.1 Motivation/ Introduction . . . 67
4.2 Experimental . . . 70
4.3 Results . . . 73
4.4 Discussion . . . 78
4.5 Conclusions and outlook . . . 81

III Self-assembly in ion-exchanged films on muscovite mica 83

5 General 84
5.1 Introduction . . . 84
5.2 The structure of muscovite mica. . . . 89
5.3 Quaternary ammonium salts. . . . 91
5.4 Experimental . . . 94
5.4.1 Materials . . . 94
5.4.2 Methods . . . 96

6 Solvent dependence of conformational order and film formation. 104
6.1 Introduction . . . 104
6.2 Experimental . . . 107
6.3 Results . . . 109
6.4 Discussion . . . 116
6.5 Conclusions . . . 123

7 Chain length dependence of order in dialkylammonium SAMs. 126
7.1 Introduction . . . 126
7.2 Experimental . . . 129

7.3 Results . . . 130
7.4 Discussion . . . 134
7.5 Conclusions . . . 140

8 Change of binding head-group — Pyridinium ions 142
8.1 Introduction/ Motivation . . . 142
8.2 Experimental . . . 143
8.3 Results . . . 144
8.4 Discussion . . . 150
8.5 Conclusions and Outlook . . . 152

Acknowledgements 154

Curriculum Vitae 156

Bibliography 159

Part I

Experimental

Chapter 1

Theory and instrumentation of NEXAFS spectroscopy

1.1 Introduction

Near-**E**dge **X**-Ray **A**bsorption **F**ine **S**tructure (**NEXAFS**) spectroscopy is an X-ray absorption technique which deals with the absorption cross section near the (1s) ionisation step. Omitting a background from electrons bound to different orbitals, two fundamental types of transitions can occur near the 1s edge. The final states can either be discrete molecular orbitals or may alternatively be free vacuum states if the exciting energy is sufficient to excite the electron above the Fermi level.

Although one generally refers to the photon absorption process as an electronic transition, the rest of the molecule is also affected by such an excitation. The hole in the inner shell of the molecule leaves this in an excited state which subsequently decays. Energy which is set free during this relaxation can either be discharged via the emission of a secondary photon (fluorescence) or can be transferred to another electron in a higher shell, enabling it to escape the molecule (Auger process). The latter is the predominant relaxation channel for atoms with low atomic numbers ($z \leq 15$) [1] and the number of Auger electrons is proportional to the number of primary excitations. For a constant flux of incoming photons the number of Auger electrons emerging from the sample hence quantifies the absorption cross-section in a non-normalised fashion.

The energy of NEXAFS resonances yields information on the chemical state of atoms within the probed depth (compare XPS-section 2.2). Additionally, the absorption cross-section into a molecular final state depends on the relative orientation of the electric field vector of the photon with respect to the direction of the transition dipole moment, which is in turn related to the charge distribution in a molecular orbital. If the photons are linearly polarised, then ordered structures, such as self-assembled monolayers of organic molecules, produce spectra that inherently depend on the angle of photon incidence.

1.2 Structure of this chapter

This chapter aims to explain enough of the fundamentals of NEXAFS spectroscopy for the reader to be able to understand the experiments in this thesis. The technique is described in much more details in a specialised book [2] and in a number of books which are devoted to synchrotron radiation [3,4] or photo-electron spectroscopy [5]. The first section serves as a discussion of the photon-absorption cross-section. It will clarify why regularly aligned bonds give rise to distinctively angle-dependent resonances in NEXAFS spectra. I will additionally introduce all the mathematical formalisms used in this thesis. In the next section a description of synchrotron radiation aims to explain the light source which enables NEXAFS experiments to be carried out. It focuses on the origin and properties of synchrotron radiation and follows a more detailed theoretical treatise by Feynman [6]. After the explanation of all the fundamental concepts I will then present the experimental setup of our experiments, covering the beamline and the equipment in the end-chamber. Finally, a discussion of the data-analysis procedures completes the chapter.

1.3 NEXAFS physics -X-ray photon absorption.

For the NEXAFS technique, the differential cross-section of photon absorption by an electron is particularly interesting, since it is the basis of how to detect order in a mono-molecular film. Fermi derived an expression for the electronic transition probability (P_{fi}) of a transition from an initial ($|i>$) to a final state($|f>$) per unit time under the influence of a time-dependent perturbation (V(t)), which is known as "Fermi's golden rule"and

is shown in equation 1.1. $\rho_f(E)$ denotes the density of states in the region of the final state.

$$P_{fi} = \frac{1}{h}| < f|\overline{V}|i > |^2 \rho_f(E) \tag{1.1}$$

Although it was derived with the formalism of perturbation theory, this expression is believed to be universally valid and has indeed proven to be a reliable workhorse. Of course, the absorption of an X-ray photon may not strictly comply with the exact concept of a mathematical perturbation. Within the frame of non-relativistic quantum mechanics, the absorption of the photon cannot be explained but its effect on an electron can nevertheless be calculated by inserting its electromagnetic potential into "Fermi's golden rule" (eq. 1.1) as the perturbing potential. Equation 1.2 shows the vector potential for a linearly polarised photon ($\vec{e}$ stands for the unit vector in direction of its electric field) which propagates in the direction of the wave vector $\vec{k}$ and oscillates with the frequency $\omega/2\pi$:

$$\vec{A} = A_0 \vec{e} \cos(\vec{k} \cdot \vec{x} - \omega t) \tag{1.2}$$

After several omitted mathematical transformations (see [2]) this explicit form of photon potential (eq. 1.2) turns equation 1.1 into:

$$P_{fi} = \frac{\pi e^2}{2\hbar m^2 c^2} A_0^2 | < f|e^{i\mathbf{k}\cdot\mathbf{x}} \vec{e} \cdot \vec{p}|i > |^2 \tag{1.3}$$

Until now the calculation was exact apart from a possible misuse of perturbation theory. In a next step equation 1.3 will now be simplified by a linear approximation of the exponential function. This cut-off is well justified due to the very low values of $\mid \vec{k} \cdot \vec{x} \mid$(k$\leq$ 1nm^{-1}, $|r| \approx$ 1Å [2]) and we end up with the "dipole" approximation of the X-ray absorption cross-section:

$$P_{fi} \propto | < f|\vec{e} \cdot \vec{p}|i > |^2 \rho_f(E) \tag{1.4}$$

The final step is to express the momentum operator in its more intuitive spatial representation [2]:

$$\vec{p} = \frac{\mathrm{i}m(E_f - E_i)}{\hbar} \vec{r} \tag{1.5}$$

And hence:

$$\begin{aligned} \sigma_x \propto P_{fi} &\propto \rho_f(E)| < f|\vec{e}\cdot\vec{r}|i > |^2 \\ &= \rho_f(E)|\vec{e}\cdot\underbrace{< f|\vec{r}|i >}_{TDM}|^2 \end{aligned} \tag{1.6}$$

The incident photon can therefore excite an electronic transition $|i > \rightarrow |f >$ if three conditions are all fulfilled. First of all, the density of states (ρ_f) in the energy region into which the photon could excite the electron has to be non-zero. Secondly, the vector of the transition dipole moment (TDM) must not be vanishing. This is a vectorial quantity which is determined by the two states involved and reflects the symmetry of the system. Group theory states [7, 8] that the direct product of the irreducible representations of the initial and final states contains the irreducible representations of the x, y and z-coordinates. This requirement can be verified by a comparison with (readily available for standard molecular orbitals) character tables so that it is not necessary to analytically calculate the TDM in order to test whether a transition is symmetry allowed. For molecular states where the final orbital corresponds to a bond, the TDM normally points in a distinctive direction with respect to the involved atoms. (e.g. in the common transition 1s $\rightarrow \sigma$ it points along the interatomic axis). Due to this relation, the orientation of a TDM is directly related to that of its associated bond. The final requisite is that the vector of the TDM must have a component which is parallel to the electric field vector of the (linearly polarised) photon in order for the scalar product to differ from zero.

Transitions into molecular orbitals. According to quantum mechanics, the energy spectrum of a molecule contains discrete levels. On the photon energy scale the individual transitions can hence be observed as a series of peaks. As mentioned above, the transition dipole moment varies from zero if and only if the comination of initial and final moment varies exhibits the correct behaviour under symmetry transformations. Of all systems in this thesis, this restriction only plays a role for the pyridinium ions on mica (See section 8.3). For TDMs which are fixed in space, the transition probability depends on the relative angle between the incident photon and the TDM. By measuring this angle dependence (i.e. with a series of spectra at different angles of incidence), we can hence conclude the absolute direction into which the TDM of an oriented molecular orbital is pointing.

Transitions into vacuum states — ionisation. The energy spectrum of free particles is continuous and lacks any directional preferences due to the isotropy of space, so that the three requirements of equation 1.6 are always met if the energy of the incoming photon is high enough to lift an electron above the Fermi level. Transitions into vacuum states show a relatively weak dependence (exponential decrease) on the energy of the photon (decay width>20eV) [2] and are not influenced by the direction from which the photon hits the atom. They manifest themselves as a step-like angular-independent feature in the spectra.

1.4 Angular dependence of a NEXAFS signal

The following section is devoted to the way in which a NEXAFS signal can be analysed to deliver the mean tilt angle of molecular orbitals. I will calculate the angle dependence of the NEXAFS signal of such a resonance for a concrete choice of coordinate system and partially linearly polarised light (see section 1.5). The intensity of the experimental signal (I) is proportional (see also section) to the transition probability (P_{if}) of the electronic transition. Assuming that the other conditions are met ($\rho_f(E) > 0$, TDM$\neq \vec{0}$), the focus is turned towards the angle-dependent term in equation 1.6:

$$I \propto |\vec{e} < f|\vec{r}|i > |^2 \equiv |\vec{e} \cdot \vec{o}|^2 \tag{1.7}$$

As previously, $\vec{e}$ denotes a unit vector in the direction of the electric field vector and $|i>$ and $|f>$ are the initial and final states of the transition respectively. As a direct result of Maxwell's equations the electric field vector of a photon is always perpendicular to its propagation direction. It is decomposed into a component in the plane of the electron ring($E^{\parallel}$) and one perpendicular($E^{\perp}$), the sense of which will become clear from the electromagnetic field of a bending magnet (See section 1.5). For light that is partially linearly polarised in the plane of the electron ring, then the two components are connected via the degree of polarisation [9]:

$$P \equiv \frac{|E^{\parallel}|^2}{|E^{\parallel}|^2 + |E^{\perp}|^2} \tag{1.8}$$

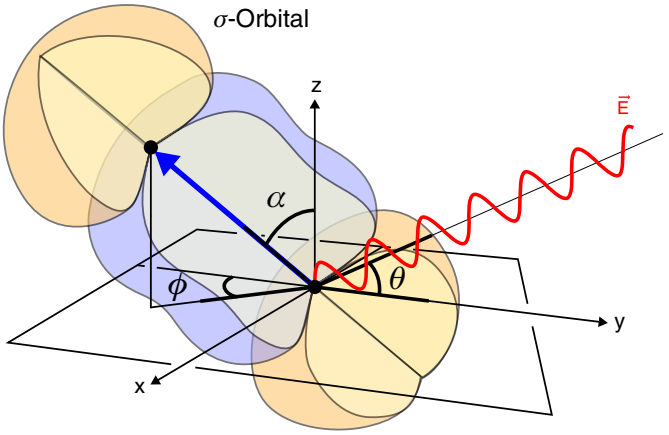

Figure 1.1: A linearly polarised photon with a wave vector and electric field vector in the yz-plane that hits the sample and the TDM-vector for the transition it excites. The attention is drawn to the reference axis from where the different angles are measured.

We now obtain a form for equation 1.7 which explicitly uses these notations:

$$I \propto P|<f|\vec{e}^{\parallel}\cdot\vec{r}|i>|^2+(1-P)|<f|\vec{e}^{\perp}\cdot\vec{r}|i>|^2 \tag{1.9}$$

$$\equiv P\cdot I^{\parallel}+(1-P)\cdot I^{\perp} \tag{1.10}$$

where $\vec{e}^{\parallel}$ and $\vec{e}^{\perp}$ are unit vectors of the in-plane and perpendicular electric field components. In the next step, equation 1.9 is evaluated for an explicit choice of direction for the incoming photon and of the TDM. This situation as well as the coordinates with which we will subsequently describe this situation are shown in figure 1.1.
For this coordinate system the intensities can be rewritten for the in-plane and perpendicular components:

$$\begin{aligned} I^{\parallel} &\propto P(\cos^2\theta\cos^2\alpha+\sin^2\theta\sin^2\alpha+2\sin\alpha\cos\alpha\sin\theta\cos\theta\cos\phi) \\ I^{\perp} &\propto (1-P)(\sin^2\alpha\sin^2\phi) \end{aligned} \tag{1.11}$$

These expressions are the general forms of the two intensities. For transitions on substrates with three- or higherfold rotational symmetry, the azimuthal (ϕ) dependence is, however, averaged out — thus simplifying the equation. All the substrates in this thesis either

intrinsically feature this characteristic or lack any azimuthal anisotropy due to the size of the macroscopic beam spot (Area approx. 1mm^2) which covers a large number of differently oriented domains. After this simplification, the final, most simple form of equation 1.11 for the intensity emerges:

$$I = A(P(\cos^2\theta\cos^2\alpha + \frac{1}{2}\sin^2\theta\sin^2\alpha) + (1-P)(\frac{1}{2}\sin^2\alpha)) \tag{1.12}$$

The newly introduced scaling factor A contains all the physical and experimental constants (e.g. overlap integral, detector efficiency etc.) Molecular orbitals are sometimes divided into two categories called "vector"- and "plane"-type orbitals for practical reasons [2]. As is intuitively graspable the two are characterised by a vector parallel or orthogonal to the orbitals respectively.

The calculations in this section were all performed for vector orbitals. Because the plane type is calculated analogously and its derivation has been published elsewhere I refer to the original reference [2].

For the sake of completeness I will at this point mention a special form of equation 1.12. It describes the difference between intensities at two different angles of photon incidence and will open a route for substantially simplifying the data analysis in some cases [10] (see section 1.7):

$$I(\theta_1) - I(\theta_2) = C(1 - \frac{3}{2}\sin^2\alpha)(\cos^2\theta_1 - \cos^2\theta_2) \tag{1.13}$$

Equation 1.13 factorises into three distinct expressions. The first one (C), contains all the physical and machine constants, the second is only a function of the angle by which the transition dipole moment is tilted and finally the last factor is solely determined by the two angles of incidence.

1.5 The synchrotron — a continuous source of linearly polarised X-rays

Synchrotron radiation is named after its place of discovery: circular electron accelerators which are called "synchrotrons" because the guiding magnetic field in them rises synchronously with the energy of the particles in order to maintain a constant radius of orbit. In high energy physics it is perceived as a nuisance because it presents a substantial source

of power loss. Today, synchrotron light is appreciated as an invaluable tool for condensed-matter research so that a number of accelerators have been built and optimised specifically for the production of synchrotron radiation.

Light emission from a moving charge is directly connected to Maxwell's unification of electricity and light. Within this framework, light is simply one manifestation of the electromagnetic field that is generated by a (moving) charge. Additionally synchrotron radiation obtains special properties because the electrons are highly relativistic i.e. signal speeds are comparable to the electron velocity. Equation 1.14 describes the full electric and magnetic fields generated by a charge [6, 9] and serves as a starting point for this short description of synchrotron radiation:

$$\begin{aligned} \vec{E} &= -\frac{q}{4\pi\epsilon_0}\left(\frac{\vec{e}_{r'}}{r'^2} + \frac{r'}{c}\frac{d}{dt}\left(\frac{\vec{e}_{r'}}{r'^2}\right) + \frac{1}{c}\frac{d^2}{dt^2}\vec{e}_{r'}\right) \\ \vec{B} &= -\vec{e}_{r'} \times \frac{\vec{E}}{c} \end{aligned} \tag{1.14}$$

Apart from the conventional terms (q, ϵ_0), $\vec{r}$, ($|\vec{r}| \equiv r$) is the apparent position of the charge in a given coordinate system and $\vec{e}_{r'}$ is a unit vector pointing from the origin towards the charge. This equation contains additional terms to the conventional "Coulomb's law" (only the first term). Indeed, this obsolete description breaks down when velocities approach the speed of light. The electric field of a charge has a component which is proportional to its acceleration — more precisely the acceleration perpendicular to the line of sight (towards the charge) because the crucial factor is the change in the unit vector towards the charge [6]. Exactly this acceleration-dependent term explains the light, which an accelerated charge emits as it has the slowest decrease with the distance (light will obviously be seen far away!) of the three. For our purposes it is hence sufficient to consider a simplified version of equation 1.14 in which the other two terms have fallen off:

$$\vec{E} = -\frac{q}{4\pi c\epsilon_0}\frac{d^2\vec{e}_{r'}}{dt^2} \tag{1.15}$$

The expression for the magnetic field stays the same as in equation 1.14. In analogy to electron storage rings, I will now concentrate myself on the electric field evoked by an electron on a circular orbit and describe how an observer in the plane of the circle would perceive it. The observer is considered to be far away from the circle itself so that equation 1.15 is valid. For a non-relativistic electron, the observer sees a harmonically oscillating

field with maxima whenever the electron is flying directly towards or away from him. It corresponds to monochromatic electromagnetic radiation with the frequency of the particle on its orbit (oscillating dipole).

However, when the particle approaches the speed of light, the observer's perception of the electron path is significantly distorted because the signal speed is comparable to the speed of the particles and both time and space have to be Lorentz-transformed [3]. At such high velocities the acceleration appears greatly increased (i.e. proportional to γ^4 with $\gamma = sqrt1 - v^2/c^{2^{-1}}$) in the short time interval in which the particle flies towards him and is commensurately reduced when it moves away from him [3]. Now the observer experiences a cycloidal, periodical electric field with sharp and high peaks every time the particle flies directly towards him, compared to which the field at every other point of the electron orbit is low. The Fourier spectrum of this electric field possesses a substantial amplitude at diverse frequencies, notably also at such that are much higher than the oscillating frequency [3] (or equivalently higher photon energies). In reality, the spectrum is continuous since synchrotrons transport bunches of electrons with a distribution of velocities and internal movements within the bunch [5]. It is due to this altered perception of the circular movement, that the observer detects X-ray instead of IR photons [6].

A similar transformation also occurs to the solid angle into which the radiation is emitted. At more and more relativistic speeds this gets increasingly squeezed together and finally looks like a "sweeping flashlight" (entrance cone $\propto \frac{1}{\gamma}$) [3].

Finally, synchrotron light also distinguishes itself through another interesting property which can be understood through a study of equation 1.15. For our well known observer, the electric field vector direction will always point into nearly the same direction, perpendicular to the line of sight and in the plane of the electron ring i.e. the radiation is completely linearly polarised. Above and below this plane, the radiation is elliptically polarised [3]. In practise, a finite solid angle of emission is accepted by the experimental apparatus, so that a bending magnet produces a beam which is 80-90% linearly polarised [9]. Other insertion devices such as Wigglers and Undulators may produce different polarisation patterns (e.g. circularly polarised light) [3].

We performed all the NEXAFS experiments for this thesis at beamline U1A of the National Synchrotron Light Source at Brookhaven National Laboratory (Upton, NY, USA).

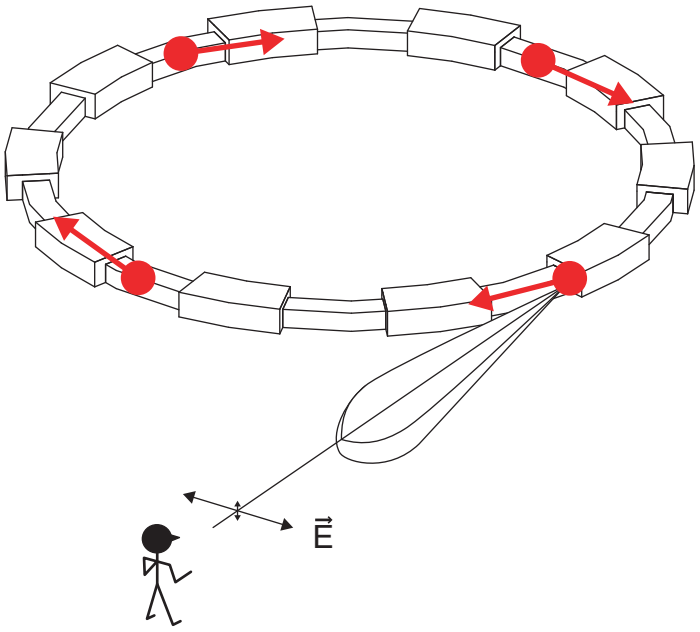

Figure 1.2: This image depicts the different unique properties of synchrotron light and shows the position of the observer that was always referred to in this section.

This research center harbours two electron rings called "VUV" and "X-Ray" ring according to their emission regimes which have the following machine parameters [11]: Electrons are preaccelerated before their insertion into the storage rings where they reach their nominal energies and are then stored for a certain amount of time (Typically 4-6 hours in the case of the VUV ring after which losses due to collisions with residual gas molecules necessitate a refill). Five VUV beamlines, of which we always used U1A, are equipped for NEXAFS studies. This beamline belongs to EXXON corporation and uses the radiation from a bending magnet.

[1] depending on the operational field

	VUV	X-Ray
Electron energy	0.808GeV	2.8GeV
Electron current	Max. 1A	280mA
Circumference	51m	170.1m
Critical energy [3]	622eV	7.1keV
		26.1keV[1]
Number of beam ports	18	28
Number of beam lines	22	53

Table 1.1: Experimental parameters for the two electron storage rings at NSLS in Brookhaven.

1.6 Instrumentation

For the most part, NEXAFS experiments have to be performed under UHV conditions because of the mean free path-length of X-ray photons (hence the name "**V**acuum **U**ltra **V**iolet") and electrons in gases. As a nice side-effect of this environment, unwanted contamination is substantially reduced so that the integrity of the samples is retained for a significant time (e.g. measuring time per sample approx. 1h).

Beam optics. After their production, the X-rays have to be guided to the sample. All the optical components for X-rays are operated in reflection, because it is not possible to manufacture lenses for X-rays (insignificant contrast in refractive index) [5]. Fairly stringent criteria apply to the materials that are used for the optical components. They have to be UHV-compatible, free from absorption features in their operational energy range and resistant to the intense X-ray irradiation. For an optimal throughput of the photons and in order to prevent an excessive heating of the optical components by refracted light, all instruments are operated close to or below the critical angle for total reflection, which is very grazing due to the high frequency of the photons [12]. From this optical arrangement, "precise workability" accrues as an additional requirement for the materials. The general scheme of their production is hence by a polishing and subsequent coating process.

On its way to the sample, the first optical device that the light encounters is a mirror which focuses it onto the entrance slit of the monochromator. Due to minor changes in

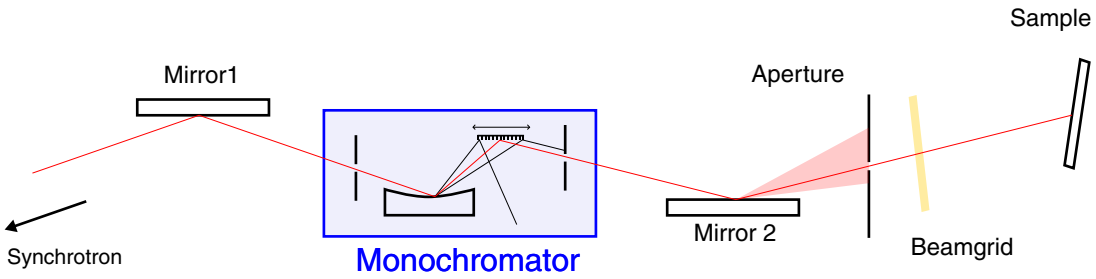

Figure 1.3: Side view of the beam guiding system. The angles and deflections of the light have been overproportionally scaled for illustration purposes.

the position of the electron beam, this mirror has to be adjusted after every injection to maximise the intensity of light that enters the monochromator.

In a next stage a **monochromator** selectively allows photons of only a single energy to pass through to the samples while all others are deflected. For this purpose, the incident beam is widened to a focussed image in which the different wavelengths are spatially separated. This is achieved by a diffraction at a curved grating in the geometry of a Rowland circle [13]. After this splitting-up, the photons pass through a series of gratings. Because of their initial spatial separation and the alignment of the gratings only photons within a narrow energy band reach the exit-slit of the monochromator. In our case a special design called "extended range grasshopper"-monochromator was used in which the energy of the passing photons is seamlessly tuned via a linear movement of the internal gratings.

Inevitably, photons with a multiple of the fundamental energy also pass the optical arrangement because they possess higher-order diffraction maxima at the same angle as the primary photons. This undesirable effect can be reduced by operating the monochromator at incidence angles which are above the angle for total internal reflection of the second harmonics while being below that of the primary energy. Higher order photons are then partially refracted into the optical devices. Nevertheless a fraction of higher (especially second) order photons still passes the monochromator and can excite transitions in other atoms than the designated one (see chapter 3 for an example).

The construction of the monochromator and most notably the width of its exit slit es-

sentially determine the energy resolution of a NEXAFS experiment. Under the conditions in our experiments it was 0.5eV at the C1s edge, 0.8eV for the N1s edge and 1.1eV at the O1s edge (Determination via absorption spectra of reference gases upon installation of the monochromator). Three in situ interchangeable gratings enable the monochromator to operate between 25eV and 1000eV [14].

Light emerging from the monochromator then hits a mirror which directs it onto the sample. Before hitting the sample the beam is collimated by a series of apertures and passes a nearly completely transparent gold grid. The radiation-induced electron signal on this grid is measured during each experiment and can be used as an in situ monitor of the spectral transmission if the grid itself is free from (mainly hydrocarbon) contamination and its associated absorption features in the experimental energy region. We always used the signal on this grid for the compensation of minor fluctuations of the photon flux.

Endstation: Two interconnected vacuum chambers, an experimental chamber in which the experiments are performed, on top of a chamber designated for sample preparation, form the end-station. The vacuum chamber is equipped with a turbomolecular pump (and a roughing pump) with which it is evacuated down to its working pressure of less than $2 \cdot 10^{-7}$mBar.

Up to two samples are simultaneously inserted into the chambers by flooding the experimental chamber to atmospheric pressure with nitrogen. A linear manipulator serves for the positioning of the samples in the two vacuum chambers. By rotating this around its longitudinal axis, the polar angle, at which the photons hit the sample, can be adjusted. The system lacks an in situ control of the azimuthal angle of incidence so that this can only be changed by extracting and reaffixing the sample to the manipulator in a different orientation.

Preparation chamber. The lower chamber serves for sample treatment under vacuum conditions. An (Argon) gas inlet and a sputter-gun allow a (destructive) sputter-cleaning. Gold-coated samples which served as a reference of the spectral transmission function (see section 1.7) needed to be free of absorption features in their designated energy ranges. We hence used this piece of equipment to remove (predominantly hydrocarbon) contaminants from them. (Typical operating parameters $5 \cdot 10^{-5}$mBar Argon, 20–25mA current in the sputtergun, 2kV acceleration voltage, ca 30–60 minutes, no current detectable on the sam-

ple)

Experimental Chamber. The detection system is a charge detector called **"channeltron"**. It is a tube in the shape of a twisted cone made out of lead silicate glass, a material which is insulating yet has a high yield of secondary electrons [15]. An electron that enters the channeltron and hits its walls, triggers off an avalanche of secondary electrons. These are accelerated by a high voltage (approx. 2kV) as they are drawn towards the exit of the channeltron which further increases the number of secondary electrons. In total, an entering charge is amplified by a factor of about 10^7–10^8 by the time it reaches a collector plate at the end of the channeltron. The effluent current is converted into a voltage by a current-to-voltage amplifier (KEITHLY 427, Keithley Instruments, USA) with a gain of approximately $10^7 V/A$.

In addition to standard channeltrons, a grid was fitted directly in front of the entrance to the tube in our setup. By setting this to a retarding voltage (typically: -150V) all electrons below a certain kinetic energy can be excluded from the detector. This modification is known under the name "partial yield detection" [2]. The reduction of the total electron signal is more than compensated by a significant rise in the signal-to-noise ratio [2]. It is also only with this blocking grid that a low energy electron floodgun can be operated in the proximity of the channeltron without over-saturating the detector.

Floodgun. The charging of insulating samples upon removal of electrons provokes a sharp decrease in electron yield and hence necessitates the use of a low energy floodgun. We typically operated a filament at 1.2A heating current and 20-30V driving voltage. Two dangers are associated with the use of an electron gun. Thin organic films can be damaged by electron irradiation [16]. Such damage is often accompanied by appearance of additional peaks in the spectrum, the absence of which indicated to us that the films were not changed by the electron current. In order to allay fears of damage over a long period of time (e.g. over the course of a measurement) two spectra can be taken under the same conditions but after different exposure times and then compared with each other. It is however not readily possible to detect very rapid changes in films. The second risk is a saturation in the electron detector due to this additional electron source which emits a much higher electron current than the sample itself. Under improper circumstances this could render the detection of the photoelectrons impossible. A detector that allows the exclusion of all

electrons below a certain kinetic energy (see the description of the detector 1.6) however elegantly avoids this problem. The electron floodgun was always operated below the energy threshold of the detector and we assured ourselves that the electron source was not interfering with the signal on the detector prior to every experiment.

Computer Control All the NEXAFS measurements were computer controlled by a VAX/VMS ([17]) system which allows the control over the monochromator and an automated readout of the signals on the channeltron and the grids in the beam axis.

1.7 Data analysis

A NEXAFS signal is the sum of a (constant) background, discrete transitions and an ionisation step. In principle it is possible to deconvolute the individual components by fitting a number of spectral features to the data as is routinely done to XPS (see section 2.2) data [18]. This is, however, comparatively more complicated because the library of reference values (i.e. energies, widths and forms) for the various features is not as extensive and the spectral resolution is often insufficient to resolve the individual features. At first, the experimental data have to be precisely energy calibrated. The raw data are saved as a function of the monochromator setting. Although the position of its moveable inner mirror (see 1.6) is approximately calibrated to the photon energy, this is not sufficiently precise. The energy calibration is performed by shifting a prominent feature in one of the spectra to a reference (often known from literature) energy by hand. Once this energy reference has been set up, all other spectra can automatically be calibrated by bringing the (constant) signals on the grid in the beam axis (see section 1.3) into an optimal overlap (maximisation of the mutual correlation).

In a next step, the spectral transmission of the beam optics has to be taken into account. Several methods for this are known [2] of which we always used the division of the raw spectra by the spectrum of a reference sample with no absorption features in its operational energy regions. Such a spectrum is considered to be a direct measurement of the number of photons hitting the sample. In practise, a sputter-cleaned, gold-coated silicon wafer served as this spectral reference. The signal-to-noise ratio of the spectra can be increased by including the signal on the beam grid (see section 1.6) into the

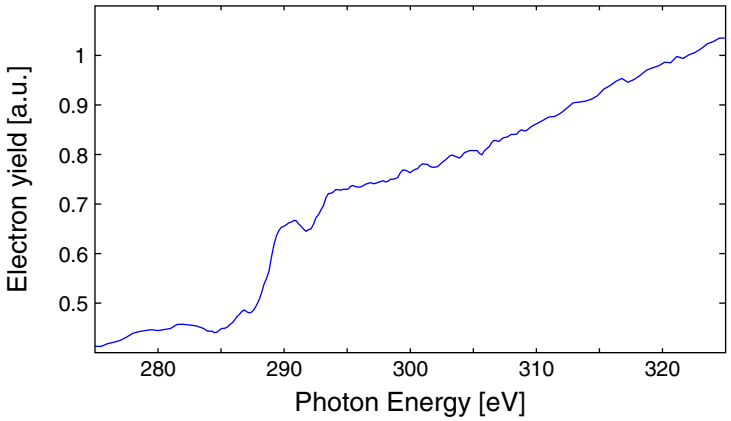

Figure 1.4: Typical Carbon 1s spectrum of a sputter-cleaned gold substrate which we used as a monitor of the transmission reference

division. These additional factors (see equation 1.16) reduce the contribution from minor temporary fluctuations in the transmission function. Equation 1.16 shows the complete algorithm with which we took the transmission function into account:

$$I_{\text{calibrated}} \equiv \frac{channeltron_{\text{sample}}}{channeltron_{\text{transmission}}} \frac{beamgrid_{\text{transmission}}}{beamgrid_{\text{sample}}} \tag{1.16}$$

A quantitative comparison between different spectra is only possible if the intensities are normalised to a common scale. We always used the absorption step between the lower and the upper energy boundary of the regions as a unit of electron yield. The assumption behind our method of including the transmission function is that the number of electrons from the reference sample is directly proportional to the number of incoming photons [2] i.e. that the photo-electron cross-section remains constant. For gold, this is not strictly the case so that a quasi-linear background has to be subtracted.

We are now in the possession of calibrated spectra, which can be analysed and mutually compared. At first, the various spectral features are identified. Their energy positions are sensitive to the chemical environments of the atoms, so that they can help to determine or confirm the surface chemistry (compare XPS-section 2.2).

Apart from chemical information, angle dependent resonances give information on the structure and order in ordered monomolecular layers (see section 1.4). For this part of the

analysis we now seek to calculate the average tilt angles of the different transition dipole moments. The exhaustive way to achieve this is by identifying and fitting all the components and then quantifying their angle-dependence. As mentioned before, this is tedious and often not viable because of the insufficient signal-to-noise ratio and the comparatively low numbers of reference spectra.

Alternatively, the method of "difference spectra" [10] presents a way to eradicate angle-independent features such as a background from the absorption step. As suggested by its name, this method looks at the difference in intensities between two different angles of photon incidence which only contains contributions from angle-dependent features. The equation (eq. 1.13) for this analysis was derived in section 1.4 and decomposes into three distinctively different factors. In order to determine the tilt angle of a transition dipole moment, the so-called "machine factor" (C, see section 1.4), which contains physical constants and experimental parameters has to be determined. Once this is known for a certain transition, the tilt angle of a TDM can then be obtained from a linear fit of the differences between the intensities versus the differences of the $\cos^2$ of the corresponding angles of incidence using:

$$\sin^2\alpha = \frac{2}{3}\left(1 - \frac{1}{M}\frac{I_{\theta_1} - I_{\theta_2}}{\cos^2\theta_1 - \cos^2\theta_2}\right) \tag{1.17}$$

It can be determined by measuring an ordered monolayer with the same molecular building block, for which the tilt angle is already known from other experiments. We routinely used a hexadecanethiol SAM on gold as a reference for alkane-based systems (tilt angle of 33° from the surface normal (see [19] and numerous complimentary references therein). After this calibration, the tilt angle of the actual system of interest only requires a linear fit of the differences in intensities versus the differences in the square of the cosines (see figure 1.5 for an example of such a $\cos^2$–fit). At this point, the strength of this method becomes apparent, since the difference between intensities at different angles of photon incidence can be quantified by a simple numerical integration in the difference spectra. The exact degree of linear polarisation and the concrete form of the investigated features do not need to be known. Unfortunately this simplified method of data analysis can only be applied if a reference sample for the appropriate transition is available to fix the machine factor. Whenever this is not the case, e.g. if novel chemical units are investigated, tilt angles have

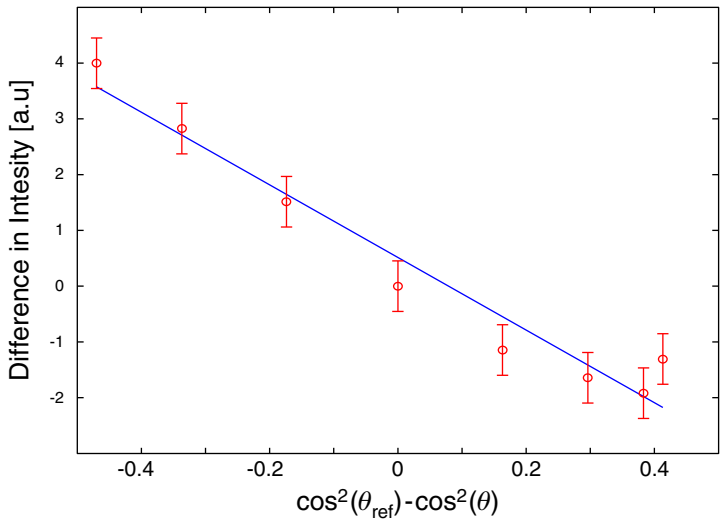

Figure 1.5: Typical linear fit of intensity differences spectra versus $\cos^2$ differences as used to determine the tilt angle of a TDM according to the method of "difference spectra"

to be calculated by quantifying the intensities of the individual resonances in the original spectra.

Error calculation. Data analysis differentiates between two estimations for the error of a quantity calculated from experimental data [20] . The "internal error" arises from the intrinsic limitations of the measuring system (mainly: uncertainty in the angle of incidence and in the intensity). This uncertainty in all measured values then propagates if arithmetic operations are carried out with the experimental data. The "external error" stems from the fact, that one only measures a finite number of samples and that the experimental histogram hence only approximately reproduces the ideal distribution. In practise, we always estimated the confidence interval according to the internal and the external error and published the higher of the two values.

Chapter 2

Supplementary experimental techniques

2.1 Contact-angle measurement

In the proximity of the boundary between two phases, the chemical environment differs from those in the undisturbed continuum phases [21]. This inhomogeneous region is called the "interfacial" or "surface layer" and normally extends into the continua by about 1–10nm depending on the types of phases [21]. If the two phases in contact are immiscible, then the energy of molecules in the interfacial region is higher than in the bulks because the attractive forces on them are on average reduced compared to the force on those that are completely embedded in the bulks. As a direct consequence of this energy increase, a system of two immiscible phases strives to minimise the contact area. Any increase of the mutual contact area accordingly requires work to be put into the system. The energy per unit area, which is associated with this work, is called "surface tension" and is a property for a concrete combination of the two continuua (1,2) in contact.

$$dW = \underbrace{\gamma_{12}}_{\text{surface tension}} \quad dA \tag{2.1}$$

Instead of the view as energy per area, surface tension can also be interpreted as a force per unit length, which acts tangentially to the surface [22]. This interpretation fits the older yet intuitive model of two phases being separated by a membrane under tension —

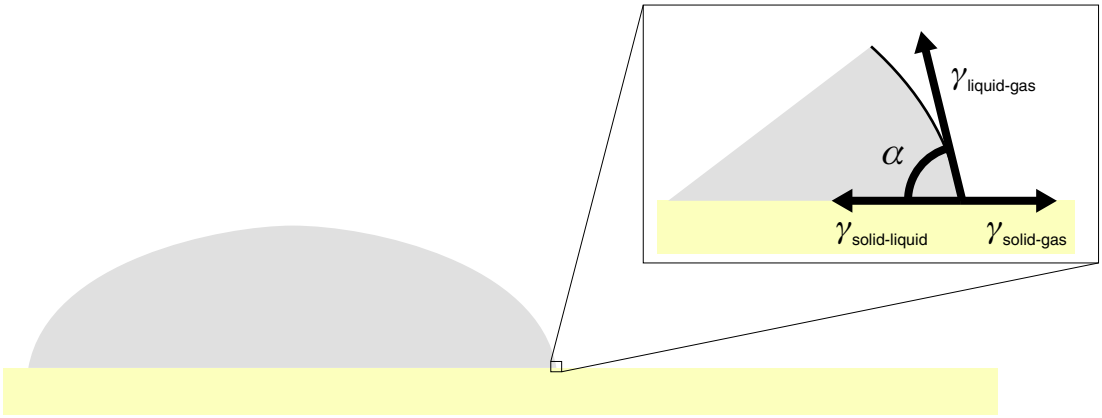

Figure 2.1: A sessile drop of liquid on a solid surface. The arrows indicate the different acting surface tensions at the points, where all three phases meet. In the equilibrium situation these have to cancel out.

from which the name is derived. In this model, an increase in the mutual contact area is equivalent to a stretching of the membrane. For a drop of liquid on a solid surface, this model proves helpful to obtain the relationship between the different acting surface tensions. In static equilibrium, the net force at any point on the borderline, where the three phases (see figure 2.1) meet, must vanish [23]:

$$\gamma_{lg} \cos \alpha + \gamma_{sl} = \gamma_{sg} \tag{2.2}$$

From the contact angle of a liquid drop on a solid surface we can hence deduce the surface tension between the liquid and the solid (γ_{sl}) if the other two involved surface tensions (solid-gas γ_{sg}, liquid-gas γ_{lg}) are known. Under constant experimental conditions (same liquid and atmosphere) this property (γ_{sl}) depends on the chemical composition of the surface region — notably also of the topmost layer of chemical groups. It can significantly vary between different substrates as suggested by expressions like “non-wetting” or “completely wetting” surfaces.

In addition, because the surface tension between substrate and the atmosphere (γ_{sg}) is usually low compared to that between the substrate and the liquid (γ_{sl}), contact angles of the same liquid on different substrates can be compared with each other to primarily learn about the interaction between the substrate and the liquid. Reference values are available

(see [24] for examples) for numerous types of well-defined substrates (e.g. bare substrates or methyl-, methylene- respectively hydroxyl-functionalised films). With their help an uncomplicated method of chemically characterising relatively well-defined samples such as thin organic films is available. In most such cases, the above-mentioned reference values can be used to predict the (water) contact angle for a concrete surface composition, which can then be compared to the experimental values. In the example of organic molecules which adsorb onto a surface and form a densely packed and ordered monomolecular film, the adsorption kinetics can be followed by the contact angle (transition from the contact angle of the bare substrate to the standard value for the complete film) or the existence of order (with very specific chemical groups at the topmost layer) can be proven. Another example, where the contact angle for ultra-thin films can be helpful, is the coadsorption of two chemical species, where the experimental contact angle is determined by the relative fractions of the two species [25]. The contact angle technique is a macroscopic measuring method which averages over the contact area of the drop ($\approx$0.1mm^2). This means that "perturbed regions" (e.g. domain boundaries) are not directly detectable and gives rise to effects from the surface topography (e.g. Lotus-effect [26], shark-skin [27] or SAMs on rough surfaces [25]). Because of this texture dependence, the experimental procedure of measuring the contact angle influences its outcome. One commonly differs between an "advancing" and "receding" contact angle. The first is measured immediately as a drop of liquid is deposited on a surface while the latter is determined during the removal of the drop from the surface. For rough substrates the two method significantly vary, while for stable, highly ordered monomolecular films on an ideally smooth substrate no hysteresis is expected [23].

The surface sensitivity of the contact angle technique strongly depends on the system under examination and is normally higher if there is a strong contrast between the interactions of the chemical groups in different depth zones. (E.g. hydrophobic functionalisation of a hydrophilic substrate or hydroxyl-functionalised alkane chains)

Even alongside other quantitatively superior or more flexible techniques like XPS or NEXAFS, the contact-angle technique assures a valuable position. This is without doubt because of the very easy and fast experimental procedure which does not require any calibration or vacuum apparatus, as well as the simple data-analysis. Especially in the initial

stage of a research project or for a quick quality control within a batch of samples before starting more elaborate experiments one hence often performs a contact angle measurement.

All data shown in this thesis are advancing contact angles. Where not stated differently, they were acquired on a NRL C.A Goniometer (Ramé-Hart inc., Mountain lakes, NJ, USA). A sessile drop of a given volume ($\approx 3\mu$l) is deposited on a sample with a syringe and the contact angle is measured by adjusting a cross-hair to the shape of the drop in a magnifying glass (Accuracy $\approx .3^\circ$).

2.2 X-ray photoelectron spectroscopy (XPS)

X-ray photoelectron spectroscopy makes use of the photo-electric effect to quantitatively measure the chemical composition at the surface of a sample. A heated filament emits an electron current which is directed and accelerated (E_{kin} approx. 15keV) towards an anode where it evokes both a continuous X-ray spectrum (Bremsstrahlung, see section 1.5) as well as discrete Roentgen lines due to radiative relaxation processes (Al K_α 1486.6eV or Mg K_α 1253.6eV). Anode materials are chosen in such a manner that they have one dominating X-ray line with an energy that is sufficient to knock electrons out of the inner shells of numerous elements.

On their way to the electron detector, the liberated electrons pass a system of electron lenses and an energy analyser. The purpose of the lenses is to flexibly alter the kinetic energy of electrons by imposing an electric field. Its form can be adjusted to affect electrons from different spatial regions of emission differently. In the (hemispherical) analyser the electrons are then deflected by two electrodes. The geometry and construction is such that only electrons entering the analyser in a given direction and with a given energy, reach a fixed electron detector. This working principle allows the separation of electrons according to their kinetic energy as well as their point emission (imaging XPS, see [18]). An XPS-measurement hence yields the number of electrons as a function of their kinetic energy which can be directly transformed into a spectrum as a function of the original binding energy:

$$E_{Binding} = h\nu - E_{kin} - \Phi \tag{2.3}$$

Where $h\nu$ is the energy of the incoming photon, E_{kin} stands for the kinetic energy of the electron and Φ denotes the work function of the apparatus. In figure 2.2 the survey spectrum of a dodecyl-phosphate ($DDPO_4$) monolayer on titanium oxide is exemplarily shown (Please refer to chapter 3 for more details). In an XPS spectrum, peaks appear at all those binding energies at which electrons are bound in the sample. The peak positions are characteristic for the atomic species which are present in the sample so that the individual peaks can be attributed to a specific element by comparison with extensive reference libraries. The energy resolution of the analyser is also sufficient to discriminate between

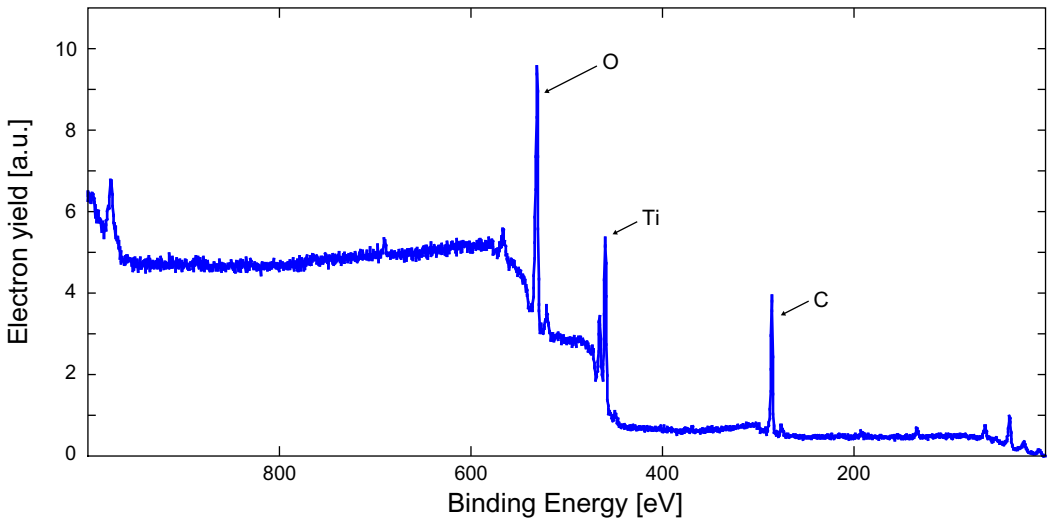

Figure 2.2: Survey Spectrum of a dodecyl-phosphate monolayer on titanium oxide. The electron yield is plotted as a function of the binding energy. Each atomic species leads to characteristic peaks which act as a chemical fingerprint.

different chemical states of an atomic species (such as Ti-**O**, P=**O** or P-**O**-C in the case of $DDPO_4$ on titanium oxide (see chapter 3)) After this "initial stage" of the analysis, one hence knows the qualitative chemical composition of the sample. By inclusion of the elemental photon absorption cross-sections (also known from reference measurements and called "sensitivity factors" in this specific context) and a consideration of the experimental transmission function, the significance of an XPS-spectrum strongly rises. Apart from identifying the different chemical species, an XPS-measurement on such a calibrated system now also quantifies their proportions (accuracy approx $\pm 10\%$).

The XPS method owes its surface sensitivity to the short mean-free path of electrons in a solid (See [28, 29] for summaries of mean free paths in various solids). Typical electron escape depths range from approximately 0.5–1.5nm in the energy region of 10–1000eV for normal substrates.

XPS is an invaluable surface-analytical technique because of its capability to quantitatively analyse the surface chemistry and its ability to discriminate between different oxidation states and is hence available in most surface science laboratories. For a skilled scientist who performs his experiments on a modern (commercial) XPS-apparatus, the acquisition of an

XPS-spectrum is a routine measurement. Often these machines are regularly calibrated so that the effort to obtain a spectrum is comparatively low. Much more diligence is however required during the subsequent analysis of a spectrum as the designated information is often obscured by a range of effects. I will briefly describe the ones relevant for the spectra in this thesis.

Charging. Insulating samples (e.g. Mica) charge up positively when (photo-)electrons are removed from them. This adds an additional electrostatic energy barrier which subsequent electrons have to overcome, causing them to appear at higher binding energies. In the case of non-monochromatised X-rays the charging process is self-limited by the (low energy) stray electrons (i.e. from the anode) in the experimental chamber. Before the actual analysis, the spectra have to be shifted by this constant energy offset (of the order of 5eV under normal operating parameters). Such a calibration is usually performed by using a well known absorption line as energy reference (e.g. $C1s_{aliphatic} \equiv 285.0eV$). Alternatively a low energy floodgun may be used to neutralise the sample. This is necessary for measurements with an X-ray monochromator [18] but its high number of electrons can damage thin organic films [16] so that its use is avoided whenever possible in an examination of such systems.

Secondary emission lines. Although the commonly used anodes (Al, Mg) are dominated by one X-ray fluorescence line, they also to a lesser extent radiate at other discrete energies (example $K_{\alpha 3}$ 1496.4eV with a relative intensity of approx. 6.4% for Al). These secondary emission lines duplicate the primary spectrum at a constant energy offset and do not normally disturb an analysis as they are significantly less pronounced than the primary ones and well separated from them. It is however mandatory to identify the associated features and not to mistake them for additional species. Using a monochromatised X-ray source eradicates such features from a spectrum but one wherever possible refrains from this measure, since it reduces the photon flux drastically, bringing with it a significantly poorer signal-to-noise ratio or commensurately longer acquisition times.

Subtraction of a background. The signal at a given electron energy does not solely stem from electrons with one unique binding energy but also contains electrons with a lower binding energy which were inelastically scattered on their way to the analyser [18]. This background appears in spectra as a multi-step structure which lies underneath the

photoelectric peaks and has to be subtracted in order to isolate the peaks. A number of models for the background have been presented, ranging from purely empirical ones to models which take the underlying physical processes into account. For the quantification of all the spectra in this thesis, a model proposed by Shirley [30] was used.

Instrumentation. All the XPS-spectra in this thesis were acquired on an ESCA 5400 instrument (Physical Electronics, Eden Prairie, MN, USA) equipped with a twin (Al/ Mg) anode. During the operation the working pressure in the experimental chamber was lower than $< 4 \cdot 10^{-9}$mBar, the standard anode was Aluminium at 300W electron emission power. The aperture of the apparatus which determines the included area of a measurement and the electron flux, was set to 3, corresponding to a sampled area of $\sim$3mm^2. The pass energy denotes the accepted energy of the energy analyser and determines the energy resolution of the XPS machine. All the detail spectra were measured at a value of 35.75eV which is the "optimal" compromise between energy resolution and signal-to-noise ratio, while survey spectra were acquired at a higher pass energy of 71.55eV to lower the acquisition time. In all cases the electrons emerged from the sample towards the analyser at a take-off angle of 45° . The experimental settings of an XPS machine and their immediate effect on the spectrum are explained in detail in reference [18] to which I refer for more information. In addition to detailed scans in the designated energy regions, I always confirmed the chemical integrity with a survey scan before the experiment.

Part II

Self-Assembled Monolayers on metal (oxide) surfaces

Chapter 3

Dodecylphosphate- and -phosphonate-based molecules on Titanium oxide surfaces

3.1 Motivation/ Introduction

Historically the science of SAMs was developed for two systems, namely that of alkanethiols on gold and organosilanes on silicon oxide [19]. Numerous researchers established a base of knowledge of these films which covered the influence of chain length [31], packing density [32,33] and thermal stability [34], but the main impact of these initial studies was, however, restricted to fundamental science. From this original field the focus of research has recently moved into different directions, one of which are substrates with a higher practical relevance such as the oxide surfaces of technically relevant metals. This area of research aims to approach high technology with the abilities of fundamental science. Researchers hope to enable progress in several different technological areas by the use of SAMs on these substrates [35].

Titanium, which is today commonly used for medical implants because it fulfills the necessary mechanical requirements and because it can be embedded in a "living" environment without irritating or poisoning the patient [36], is an example of such an advance. Its aptness for the fabrication of implants could be further enhanced by an ultrathin coating.

One disadvantage of bare titanium oxide is a high surface energy (e.g. water contact angle $\leq 10^\circ$ [25]) which makes its surface very sensitive to adventitious contamination. A methyl-terminated SAM could potentially lower the surface energy substantially. We deem it as particularly advantageous, that SAMs can be established on (possibly complicatedly formed) workpieces by a simple dipping process and that the bulk properties are retained after the coating.

Another group of technical devices which could benefit from a well-established SAM-technology on metal oxide substrates, are adsorption sensors based on the optical principle of total internal reflection. This phenomenon occurs at the interface between two phases with different refractive indices and the critical angle of incidence below which light is not refracted into the other phase, depends on the step in the refractive index. If something adsorbs onto such an interface (e.g. the adsorption sensor) then this discontinuity generally changes, so that adsorption processes can be monitored by an optical experiment. Via the help of a SAM, the surface chemistry of the sensor could be flexibly altered to control the adsorption (e.g. specific adsorption of one species) while the sensitivity of the sensor itself remains unchanged ($\lambda_{\text{light}} \approx 300\text{nm}$, $\text{thickness}_{\text{SAM}} < 3\text{nm}$). This (variably) controlled selectivity combined with an optical readout technology form the basis of such adsorption sensors. SAMs also intrinsically bring the potential to miniaturise such sensors, thereby enabling the integration of multiple sensors into one detector or in situ measuring devices. In both these cases, the aim is hence to establish (ultra-)thin films with a very exactly defined surface chemistry that can additionally be flexibly varied for sensor applications, two qualities which are proven strengths of SAMs. In order to solve this challenge with "common" SAM-technology, four issues need to be solved. A headgroup, that strongly binds to the substrate, has to be found, if possible, one which can be used on various metal-oxides. In a next step, this needs to be connected to a molecular spacer (e.g. normally an alkane chain $C_{11}H_{22}$–$C_{21}H_{42}$) which will adopt an ordered conformation in dense films and to the end of which functional endgroups can be attached (e.g. -CH_3 or -OH). Finally, one has to clarify the preparative procedure with which highly ordered films can repeatedly be produced and which complies with other possible requirements for the workpieces (e.g. contamination or environmental issues).

We already know that phosphate-based methyl-terminated molecules (e.g. $O_3H_2POC_{18}H_{37}$)

adsorb onto diverse metal-oxide surfaces (e.g. Al_2O_3, Ta_2O_5, Nb_2O_5, ZrO_2 and Ti_2) and form films with a similar degree of order as in alkanethiol SAMs on gold [37]. The following experiments built on the knowledge from the above-mentioned study and tried to answer different questions. We addressed different three questions — the first one being whether molecules binding to the substrate via phosphonic acid (O_3P-) can also establish films of a similar or possibly even better quality. In a next step, the ammonium salts of the free acids were synthesized to investigate a preparation from aqueous solutions and finally hydroxyl-terminated as well as mixed films with both hydroxyl and methyl endgroups were studied.

The change to ammonium salts is motivated by the potential to replace organic solvents by water. For surfaces which are embedded into biological environments, (especially implants where subsequent changes may necessitate an additional operation) the general practise is to use as few harmful compounds as possible in the production process so that the inflected damage to living areas is minimised. It is not self-evident that SAMs can be established on titanium oxide from aqueous solutions because water and hydroxyl ions can also strongly bind to the substrate [36].

The shorter chain length is connected to the change in the solvent. Alkane phosphates are intrinsically amphiphilic (i.e. also the reason why they are widespread detergents [38]) and therefore the dangers of micelle formation and poor solubility exist. Because SAMs are preferably prepared from solutions below the critical micelle concentration (CMC) [39], a reduction of the hydrophobic groups and associated increase of the CMC potentially simplifies the film formation (see section 6 for a more detailed discussion). It is also generally easier to synthesize shorter-chained molecules, an advantage especially for an alternative end-functionalisation. The length of the alkane spacer influences the successful formation of ordered films so that it is not clear whether the dodecyl chain is long enough. Equally long alkanethiols form ordered SAMs on gold but because our titanium substrates are far less regular (see section 3.2) it is possible that 12 methyl(ene) units are insufficient for a highly ordered film.

Experiments with hydroxyl-functionalised and mixed films were mainly pursued with regard to the potential opportunities in sensors. For such applications, success crucially depends on the versatility of the SAM technique. Again in contrast to alkanethiols on

gold, an end-functionalisation may prove to be infeasible, because the hydroxyl-groups can strongly interact with the solvent so that the film formation is altered.
This chapter has been published in some parts [40] and the discussion of the (OH)DDPO$_4$-ammonium salts as well as of the influence of substrate on the order in films follows this publication. If the published NEXAFS tilt angles of methyl-terminated dodecylphosphate are slightly different from those presented in this chapter, then this stems from the fact, that we have measured additional samples of this surfactant since then thereby increasing the data set.

3.2 Experimental

Substrate preparation. The substrates were prepared by sputtering a thin layer (20nm or 100nm) of titanium onto silicon wafers (Powatec, GmbH, Cham, Switzerland) using reactive magnetron sputtering [41]. Prior to the coating process, the samples were cleaned ultrasonically in a toluene(uvasol, Merck, Dietikon, Switzerland) bath for 15 minutes and subsequently dried in a nitrogen stream.
In the course of this chapter, the thinner layers will be called "oxidic"and the thicker ones will be referred to as "metallic". The chemical shift of the Ti 2p peak is sufficient to discriminate different oxidation states of titanium with XPS. For the thinner layer, only one species is found, which corresponds to the most stable oxide (oxidation number 4), while the thicker layer additionally exhibits a second resonance characteristic for the metallic form of titanium (oxidation number 0) [36]. This latter kind of chemical composition is that of a metallic sample which is covered by a natural oxide layer. The "metallic" coating is substantially rougher (R_a=1.32±0.07nm) than the thin "oxidic" one (R_a=0.44±0.02nm), which only minutely adds to the roughness of the silicon substrate. [25] This increase is probably due to the onset of recrystallization in the 100nm thick layer [42].
AFM and XPS measurements were performed to characterise the bare substrates and confirm their chemical integrity. Apart from a minor (hydrocarbon) contamination, which is inevitable for substrates with such a high surface energy which were exposed to air, the chemical composition matched the theoretical structure [25].
Synthesis of the adsorbates. The synthesis of the various compounds are discussed in

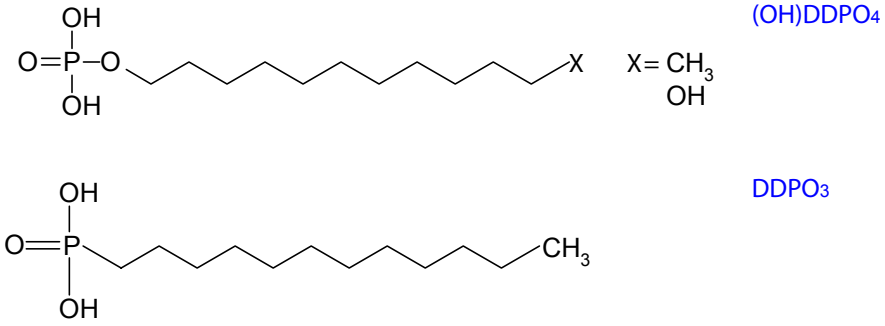

Figure 3.1: The structures of $DDPO_4$ and $DDPO_3$ which were used in this work.

detail in a dedicated study [43] and will only be presented briefly at this point. All the free acids where obtained from external sources. Dodecylphosphate ($DDPO_4$) is commercially available and was bought from Aldrich (technical quality). Prof. H.-J.Adler (Institut für Makromol. Chemie u. Textilchemie, University of Dresden, Germany) kindly supplied us with dodecylphosphonate ($DDPO_3$) as well as the hydroxylterminated phosphate ($OHDDPO_4$) which was synthesised in his laboratory. The different molecular structures are depicted in figure 3.1.

The free acids served as precursors for the synthesis of the corresponding ammonium salts in our laboratory in Zurich. After dissolution in 2-propanol (UVASOL quality, Merck, Dietikon, Switzerland) the starting materials were then mixed with ammonia (p.a., Merck). A white powder precipitated, which was separated, cleaned and dried. Quantitative yields (approx. 70-75%) were achieved with this route of synthesis. Before using the products, the stoichiometry of all compounds was determined with NMR to verify the success of the synthesis and proved to match the predicted structure (With a slightly low contribution of the nitrogen signal in $OHDDPO_4$ as the only exception) [25].

Film Preparation In order to prevent any disturbance due to contamination, we cleaned all the glassware with piranha solution (H_2SO_4 + 30% H_2O_2 in approx. 3:1 proportion). All the solutions had a constant phosphorus concentration of 0.5mM. In the case of the mixed solution, with both $DDPO_4$ and $OHDDPO_4$, an equimolar (i.e. 0.25mM per surfactant) mixture was prepared. High-purity water (HPLC, Fluka, Buchs, Switzerland) was used as solvent for aqueous solutions, while organic solutions consisted of an n-heptane/

	Energy range	time per step[ms]	number of sweeps
C1s	280–300	50	20
O1s	525–545	50	50
P2p	127–147	50	30
P2s	185–205	50	30
Ti2p	453–478	50	30

Table 3.1: Experimental parameters for the detail scans of the individual energy ranges.

2-propanol (both spectroscopic quality Uvasol from MERCK) mixture in a 100/0.4 volumetric ratio. These concentrations were significantly below the CMC (e.g. $1.6{\cdot}10^{-2}$M for $DDPO_4^{2-}Na_2^+$ [44])

Titanium coated substrates were cleaned in an oxygen plasma and immediately afterwards immersed into the solutions, where they stayed for 48 hours. Then they were extracted and carefully rinsed with the pure solvents in order to remove any excess of adsorbates and finally dried in a nitrogen stream.

Contact angle measurements. In contrast to the other measurements in this thesis, S.Tosatti used a computer automated measurement system (Contact Angle Measuring System G2/G40 2.05-D, Krüss GmbH, Hamburg, Germany) to measure water contact angles. All the reported values are the average of advancing contact angles at 6 different spots per sample and of 2–4 samples.

XPS. All the XPS-results that are presented in this chapter were acquired under standard conditions at a take-off angle of 45° and 0.1eV energy step size in 3 cycles. Before the data analysis, the spectra were energy calibrated to account of charging with the alkane peak ($C1s_{alkane} \equiv$ 285.0eV) Table 3.1 shows the experimental setup that was used for the individual detail scans.

NEXAFS measurements were carried out under standard conditions (see chapter 1). The electron flood gun had to be used in order to compensate a slight charging of the samples. As always, we took all the necessary precautions to ensure that the neutralising electrons did not oversaturate the channeltron or damage the samples.

	Oxidic Substrate	Metallic Substrate
$DDPO_3$	111(1)°	117(1)°
$DDPO_4$	111(1)°	116(1)°
50%$DDPO_4$/50%$OHDDPO_4$	70(1)°	76(1)°
OH-$DDPO_4$	55(1)°	60(1)°

Table 3.2: Advancing water contact angles of the various phosporic- and phosphonic acids on titanium oxide substrates.

3.3 Results

Advancing contact angles S. Tosatti extensively investigated phosphorus-based SAMs on titanium oxide substrates with contact angles [25, 41]. At this point I present a subset of his results in order to complete the discussion of the NEXAFS measurements. Contact angles (see chapter 2) are expected to be highly informative for these systems since the reference values of the different chemical groups significantly differ (i.e. water for CH_3 111-115° / CH_2 102–103° / OH 0° / [24] TiO_2 <10°)

Table 3.2 concludes these water contact angles. The contact angles of methyl-terminated films indicates that the topmost layer is mainly composed of methyl groups and consequently indicates a high degree of order in these films. In the case of hydroxyl-functionalized films, the experimental values however strongly deviate from the reference values. Contact angles for $OHDDPO_4$ films are much too high for a supposedly hydroxyl terminated film and indeed approach the reference value for a methylene-bearing surface. As expected, the contact angles of mixed films lies between those of the two pure films, yet still below that of a completely methylene-terminated surface. On the basis of the values for the pure films, the fraction of methylterminated molecules on the surface can be calculated using a model for the contact angle of a heterogeneous surface. Cassie derived an expression (equation 3.1) for the macroscopical contact angles in the case of microscopical heterogeneities [45] while Israelachvili and Gee performed similar calculations for surfaces which are anisotropic on the atomic- or nanometer-scale [46] (equation 3.2). The average tilt angles in these two models are given by the following equations:

$$\cos\theta_{\text{Mixture}} = f_{\text{DDPO}_4}\cos\theta_{\text{DDPO}_4} + f_{\text{OHDDPO}_4}\cos\theta_{\text{DDPO}_4} \quad (3.1)$$

$$(1+\cos\theta_{\text{Mixture}})^2 = f_{\text{DDPO}_4}(1+\cos\theta_{\text{DDPO}_4})^2 + f_{\text{OHDDPO}_4}(1+\cos\theta_{\text{OHDDPO}_4})^2 \quad (3.2)$$

Where $\theta_{\text{Mixture, DDPO4, OHDDPO4}}$ denote the different experimental contact angles and f_{DDPO4} respectively $f_{\text{OHDDPO4}} = 1-f_{\text{DDPO4}}$ are the fractions of the individual species within the film. In these models, the films obtained from competitive adsorption out of an equimolar solution consist of 26% for Cassie's model (respectively 33% for the model of Israelachvili & Gee) methyl-terminated species and 74% (respectively 67%) hydroxyl-functionalised molecules.

XPS spectra reveal the oxidation states and relative fractions of the different atomic species (see chapter 2.2). We performed XPS measurements on the SAMs with the aim of finding differences between $DDPO_3$ and $DDPO_4$. Primarily we were interested in the binding mechanism, which may be fundamentally different to SAMs on gold, or the binding-strength. Changes in these parameters, so we hoped, would be reflected in the binding energies as a chemical shift. Other points of interest included the detection and quantification of any unintentional contamination or an estimation of the amount of water (respectively hydroxyl ions) which remained bound to the substrate [36]. For the longer chained octadecylphosphoric acid (ODP) on tantalum oxide, Rossi and coworkers established an elaborate model of the different peaks in the oxygen and carbon region [47]. Later, Hofer adapted this model for the case of ODP on titanium oxide [43] and this modified version remains valid for $DDPO_4$ and was used as a reference for the analysis of our spectra. Unfortunately an analogous reference measurement of the pure adsorbent is missing until now for $DDPO_3$ so that its analysis is more complicated. Nevertheless I analysed the spectra according to the same model and then checked whether it is still valid for $DDPO_3$ or whether it needs to be adapted. This approach is practicable because we are mainly interested in systematic differences between the two adsorbents. Table 3.3 shows how the carbon and oxygen regions were decomposed into individual peaks in this study.

Phosphorus regions At first, the 2s (185-205eV) respectively 2p(127-147) regions were investigated for both $DDPO_3$ and $DDPO_4$. Figure 3.2 shows examples of such spectra and table 3.4 summarizes the experimental energy centroid and width (for the 2s peak).

		Attribution	Energy[eV]	FWHM [eV]
C	1	Alkane	285	1.55
	2	**C**-O-P	286.5	1.75
O	1	Ti**O**$_2$	530.1	1.55
	2	Ti-**O**-H, Ti-**O**-P, P=**O**	531.1	1.7
	3	P-**O**-R, P-**OH**	532.6	1.7

Table 3.3: Components in the carbon 1s and oxygen 1s regions of ODP on TiO_2 as proposed by Rossi et al. and later adapted to titanium oxide.

	2s		2p	
	Energy[eV]	FWHM [eV]	Energy[eV]	FWHM [eV]
$DDPO_3$	190.8	2.4	132.9	1.7
$DDPO_4$	191.5	2.6	133.7	1.8

Table 3.4: Experimental parameters for the 2s and 2p regions of phosphorus. The energetic differences between $DDPO_3$ and $DDPO_4$ can clearly be detected.

These results are encouraging for a further study because the chemical environment of at least the phosphorus atoms is sufficiently different that it can be picked up with XPS. A measurement of free $DDPO_3$ that is not bound to the substrate could bring clarity into the bond strength of $DDPO_3$ relative to that of $DDPO_4$

Carbon regions. The model for alkane phosphates contains two components in the carbon region, the parameters of which were established by Rossi et al. and are shown in table 3.3. One of them (i.e. C1) refers to atoms bonded to two other carbon atoms and two hydrogen atoms while the second component (i.e. C2) arises from the carbon atom that is closest to the phosphorus. There is no reason why the form or energy of the alkane peak should be different in $DDPO_3$ compared to that in $DDPO_4$. The second peak, on the other hand may be subject to a substantial change, as illustrated by the different electronegativities (En_P=2.19, En_O=3.44, En_C=2.55). From the comparison of the electronegativities, we expect the binding energy of the electron from the carbon atom which

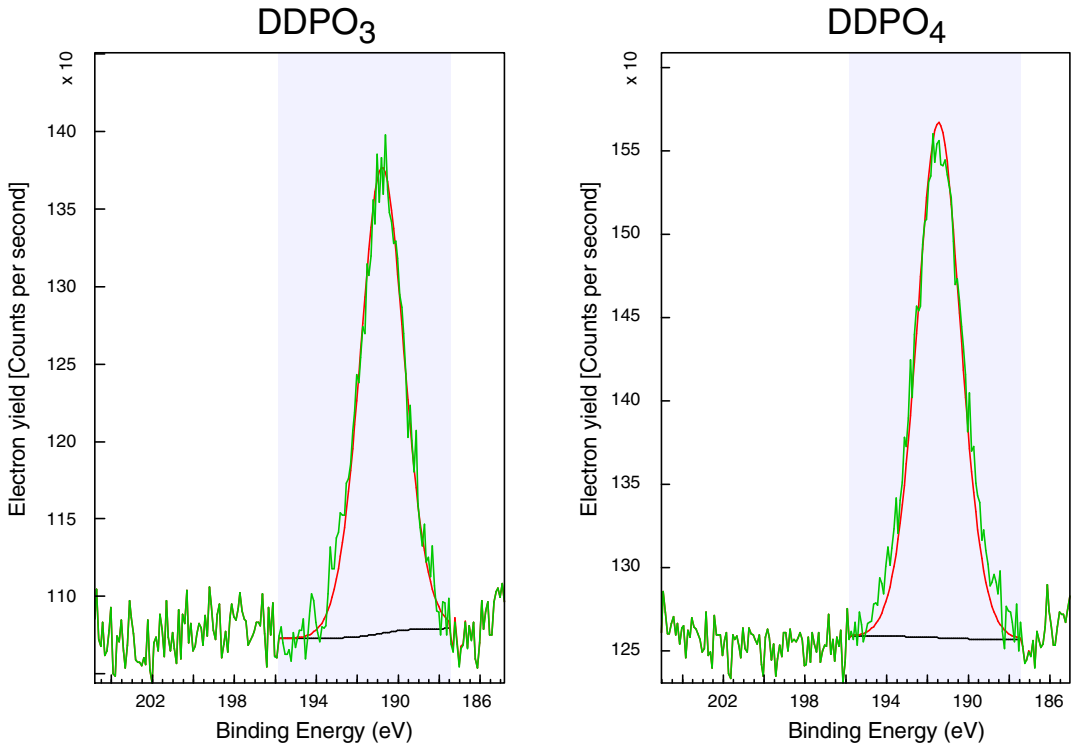

Figure 3.2: The energies of the 2s peaks in phosphorus spectra of $DDPO_3$ and $DDPO_4$ show, that the oxidation states of the phosphorus atoms are different.

is directly bound to the phosphorus atom in $DDPO_3$ to resemble that of the alkane peak (see section 2.2) and hence be significantly lower than the corresponding phosphorus atom in $DDPO_4$ which is connected to a more electronegative oxygen atom.

Table 3.5 shows how big the relative fractions of the two carbon species compared to the total carbon signal are, under the assumption that Rossi's model is valid for $DDPO_3$. As predicted, the C2-peak is substantially lower for $DDPO_3$ than for $DDPO_4$. The prognosis based on the electronegativities proves to be correct. In the unchanged model, the second carbon peak completely vanishes. Indeed the RMS, a gauge for the quality of a fit, only minutely increases if this component is omitted in a fitting procedure and an analysis which allows the form and position of this peak to vary, fails to find a stable solution for such a feature.

Oxygen analysis. Table 3.3 shows the decomposition of the oxygen region into three

	$DDPO_3$	$DDPO_4$
C1	100%	93%
C2	0%	7%

Table 3.5: Decomposition of the carbon 1s region into the two components in Rossi's model for ODP. The C2 peak is absent for $DDPO_3$, in complete agreement with the predictions.

	$DDPO_3$	$DDPO_4$
O1	72(1)%	61(9)%
O2	25(2)%	25(5)%
O3	3(1)%	14(3)%

Table 3.6: In a first step, the oxygen 1s regions of both $DDPO_3$ and $DDPO_4$ were deconvoluted into the three components from the ODP model and their fractions of the total signal were calculated.

components. It corresponds to the established model for ODP with the difference that the substrate peak had to be moved when changing from Ta to Ti. Peak 1, the substrate related oxygen resonance, is not expected to change (see section 3.3) with the adsorbents. Peak 2 is more difficult to predict but potentially the most interesting feature, since it contains the strength of the interaction between adsorbent and substrate. It contains a substrate-related component from Ti-**O**-H which will probably not change in energy or width. The other oxygen atoms that contribute to this resonance (Ti-**O**-P and **O**=P) might however change their attributes, so that it would separate into several new peaks. Finally, the last peak (Peak 3, P-**O**-R and P-**O**-H) will only contain P-**O**-H contributions, which can, in turn, be slightly influenced by the different oxidation state of the phosphorus atom. Table 3.6 shows the fractions of the different oxygen species in the ODP model. Again $DDPO_3$ and $DDPO_4$ significantly differ from each other.

Hofer et al. investigated the way in which a phosphate headgroup binds to a titanium oxide substrate [47]. According to these authors, two mechanisms for this are possible: mono- respectively bidentate, after the number of oxygen atoms of one phosphate group which are involved in the bond. In the case of ODP, the molecules appeared to bind to the substrate in both ways and none of the two mechanisms was clearly favoured. The

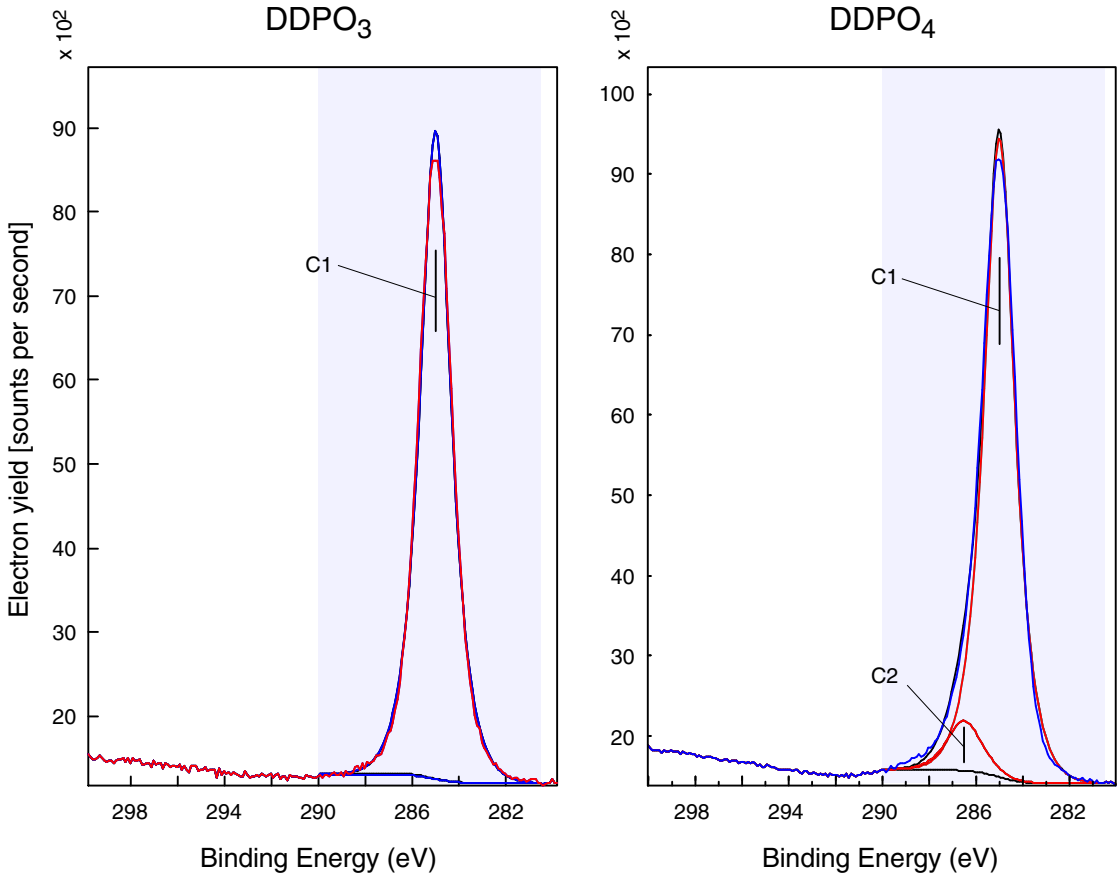

Figure 3.3: Carbon 1s spectra for $DDPO_3$ and $DDPO_4$. The best fits to experimental data are also shown and clearly reveal the disappearance of the C2 component.

more complex and diverse binding mechanism in combination with an at best short-range regular substrate structure is an interesting facet of SAMs on metal oxides. Both these features intuitively hinder the formation of highly ordered films.

If the attribution of the different species is correct, then the third oxygen peak (O3) is affected by the fraction of monodentate- respectively bidentate-bound molecules. Figure 3.4 shows the two mechanisms for $DDPO_3$ and $DDPO_4$ and illustrates (i.e. highlighted in red), how many oxygen atoms contribute to the O3-peak. The ratios of the O3-peak intensities (V) between $DDPO_3$ and $DDPO_4$ can be used to quantify the fraction of molecules that are bound by the monodentate principle (x) under the assumption that the fractions of monodentate bound molecules are the same for $DDPO_3$ and $DDPO_4$.

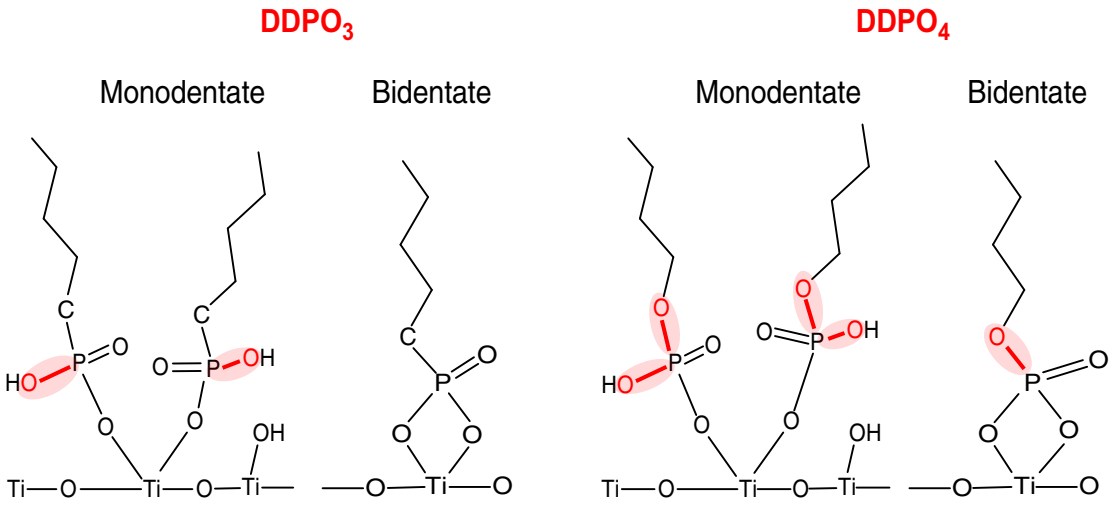

Figure 3.4: Illustration of the mono- respectively bidentate binding mechanisms. The number of atoms (i.e. highlighted in red) which contribute to the oxygen O3-Peak varies for $DDPO_3$ and $DDPO_4$.

$$x = \frac{V}{1 - V} \tag{3.3}$$

This predicts 25–42% of the phosphate/ phosphonate groups to bind in the monodentate arrangement.

An accurate decomposition of the oxygen region into the constituents cannot be achieved without supplementary information about the forms and energies of the different resonances. In the previous work the researchers obtained this by measuring the XPS spectra of the adsorbate and substrate alone. We however lack such an energy reference for $DDPO_3$ until now, so that we can at best make an educated guess on the changes in the model upon switching the headgroup. All attempts to refine the ODP model for $DDPO_3$ without such a powder reference failed — most notably because the number of free parameters did not render any stable fits. Considering that a reliable decomposition has the potential to bring clarity into the relative binding strengths and possibly about the water content in the films, makes the acquisition of a powder reference an imperative task for the near future.

Titanium 2p region The titanium 2p region (453–478eV) probably does not reveal any differences between the two different adsorbent species, since the substrate remains

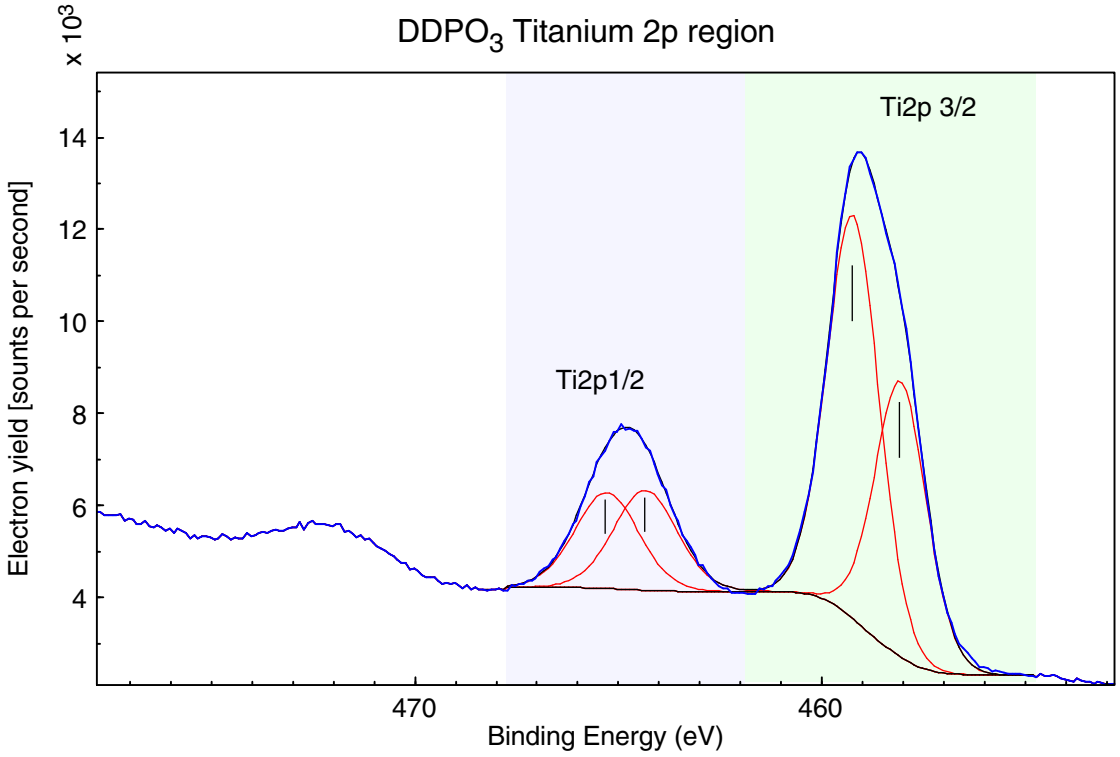

Figure 3.5: An example of a detail spectrum taken for the Ti 2p region of $DDPO_3$ on 100nm of titanium ("metallic"). Apart from the two angular momentum states ($2p\frac{1}{2}$, $2p\frac{3}{2}$), there also appear to exist two chemically different kinds of titanium atoms in the probed layer as indicated by the shoulder of the $2p\frac{3}{2}$ peak.

unchanged by a change in headgroup. Figure 3.3 is one example of these spectra. The experimental centroids consistently lay at 464.8eV for Ti2p3/2 and at 459.1eV for Ti2p1/2. Especially the lower peak led us to believe that there were actually two different chemical species of titanium contributing to the signal — the deconvolution of which is also shown in figure 3.3. We used the total titanium signal as a quantitative reference for the composition of the interfacial layer. The fractions of the individual elements normalized to the titanium signal are concluded in table 3.7. Note that no absolute calibration to the sensitivity factors or the exact transmission function were performed so that this table does not quantify the absolute fractions of the different elements but reveals systematic differences between the different adsorbents.

NEXAFS

	$DDPO_3$	$DDPO_4$
$C1s_{exp}$	0.42	0.59
$P2p_{exp}$	0.034	0.043
$P2s_{exp}$	0.026	0.035
$O1s_{exp}$	1.13	1.29

Table 3.7: The intensities of the different elements, normalized to the substrate Ti 2p peak reveal quantitative differences between $DDPO_3$ and $DDPO_4$.

Chemical composition. As in every NEXAFS investigation, the first step was to deconvolute the different spectral features, attribute them to specific electronic transitions and identify the chemical species which are present at the surface.

Carbon. A carbon spectrum of $OHDDPO_4$ (see figure 3.6 as an example) shows the features in the carbon 1s region. The slight rise in the spectrum at 280–285eV probably stems from higher-order photons which also pass the monochromator and excite transitions in oxygen (E_{1s}=530eV) or titanium (E_{2s}=560.9eV) atoms. At 287.6(2)eV the first pronounced feature (1) appears with an intensity that varies with the angle of photon incidence. It is associated with transitions into molecular orbitals which are linear combinations of atomic orbitals belonging to a carbon and its neighbouring hydrogen atoms. High-resolution NEXAFS experiments [48] reveal that transitions into several different final states contribute to this resonance. In addition to their NEXAFS experiments, the same researchers also performed molecular-dynamics calculations on the corresponding surfactants (long-chained alkanethiols) and were able to unambiguously associate the resonances with concrete end states. They discovered that at least one of these components had a strong Rydberg character [48]. For our NEXAFS instrument, the energy resolution is insufficient to discriminate the individual features, so that we observed them blurred to a single resonance with a TDM perpendicular to the alkane chain axis. The allocation to a single molecular endstate (e.g. σ(C-H)) is however not correct and we reflect this in abbreviation "R*".

The first resonance is partially obscured by the ionisation step, which was found to lie at 288.1eV [49]. Our experimental results are consistent with this reference value although

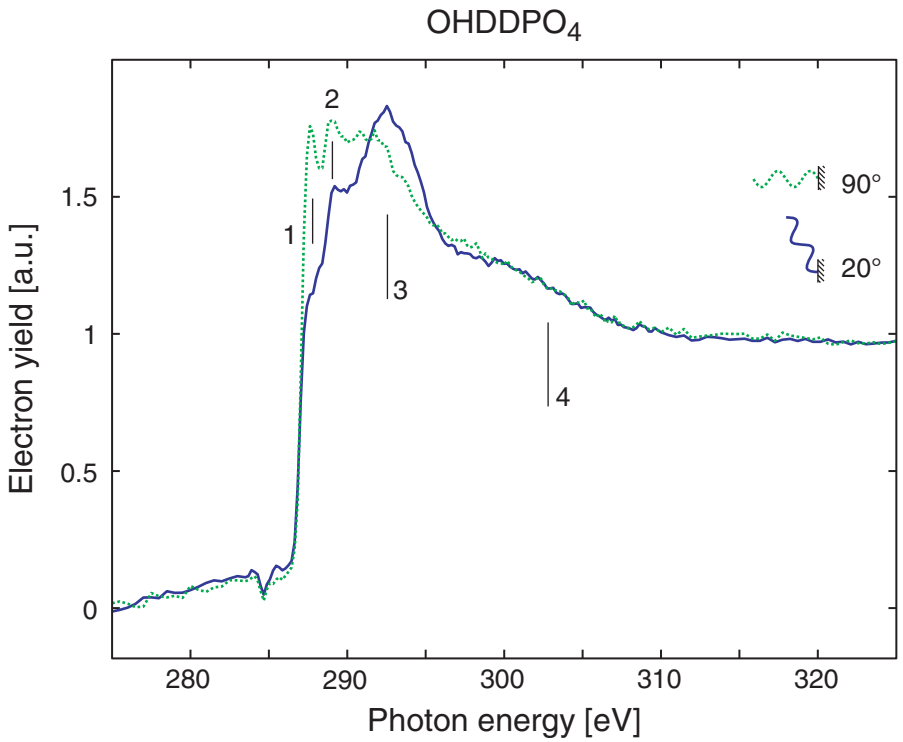

Figure 3.6: A NEXAFS spectrum of $OHDDPO_4$ on the "oxidic" titanium surface shows the different spectral features. Their number and properties match the theoretical prediction.

the spectral resolution again does not allow a more precise determination of its energy. Multiple steps as a consequence of chemical shift for carbon atoms in different chemical environments are not likely to be detectable because the alkane species is by far the predominant one (see XPS section 3.3).

At 289.25(20)eV a next resonance (2), which is attributed to final orbitals of the type σ(C-O) [49] is found. Again, it cannot be visually separated from the R* resonance in the spectra due to the energy resolution and the density of spectral features in this energy region, but appears distinctively in difference spectra (see figures 3.8 or 3.9). Its contribution is stronger for the hydroxylterminated films, where the number of contributing atoms is relatively higher (i.e. twice as high omitting any electron attenuation). In the course of an analysis via the method of difference spectra, this feature was inevitably included in the integration of the R* resonance, which strictly speaking renders this procedure unusable. We however still performed such an analysis because we expected the

disturbance to be minor considering the small number of C-O bonds (i.e. 0 for $DDPO_3$, 1 for $DDPO_4$, 2 for $OHDDPO_4$).

Another angle-dependent resonance appears centered at 292.5(5)eV and stems from final σ^*(C-O/ CC) orbitals [49]. Just as for the R* resonance, its angle dependence is much more pronounced in the methyl-terminated films. Here an inclusion of the C-O resonance in the integration of the intensity does not present a danger for the outcome of an analysis with difference spectra, since this resonance exhibits exactly the same angular behavior as the C-C resonance. We expect a final resonance of the type σ^*(CO/ CC) at 302eV [50] which shows the same angle dependence as the resonance at 292.5eV but this is indistinguishable on top of the total signal.

The number of features as well as their concrete energy positions exactly fits the prediction for the specific surfactant molecules.

Chemical composition — oxygen. An interpretation of absorption spectra at the oxygen edge was more complicated and revealed less information than the carbon region. Several factors explain why this analysis was more problematic than that the for the carbon edge. A first obstacle is the lack of a suitable energy reference. In combination with a broad scattering of literature values for the different transitions, this made an exact mapping of the individual features virtually impossible [51]. All the spectra (see figure 3.7) show a diffuse broad peak at 530(1.5)eV which appears to consist of two (or more) different resonances (i.e. approx. 529eV (1) and 531.5eV (2)). At least one of these constituents lies below the energy of the absorption edge and is likely to be associated with a $\pi*$(P=O) orbital as final state.

In contrast to the carbon edge, oxygen spectra probably exhibit three (see the XPS-section 3.3) absorption steps, which are distinctively separated in their energy positions, two of which are expected to make quantitative contributions. We also know from XPS spectra, that the predominant oxygen species is that of the substrate-related titanium dioxide. We hence expect to observe a multi-step structure. The lack of an energy reference as well an uncertainty about the number of resonances makes it impossible to meaningfully decompose the spectrum into its constituents and identify the exact energy positions of the different steps.

Well above the absorption edge(s) a second broad resonance is situated (centered at

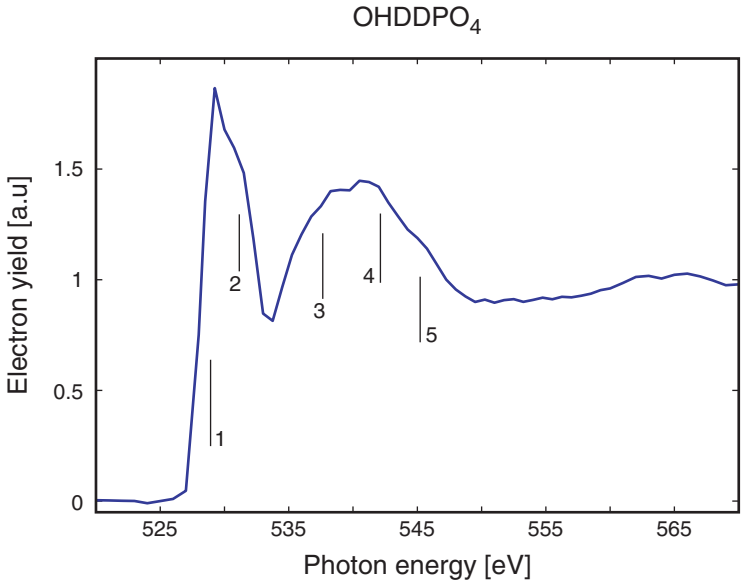

Figure 3.7: A NEXAFS spectrum in the oxygen 1s region of $OHDDPO_4$ on the "oxidic" titanium surface exemplarily shows the different spectral features. All the samples yielded identical, angle-independent spectra.

approx 541eV) which again consists of at least 2 or 3 individual transitions (approx. energy positions: 538eV (3), 542eV (4) and 545eV (5)). Following the general scheme of orbital energies [2] these probably match final states of the kind σ^*(Ti-O, C-O, P-O or H-O) for the different types of oxygen atoms.

All our samples produced indistinguishable oxygen spectra within the statistical significance under all angles of photon incidence. This insensitivity towards the adsorption of an adlayer, the different headgroups or an additional oxygen-bearing endgroup strongly reduced the value of oxygen spectra for the characterisation of the organic films. We attribute this situation to the overwhelming proportion of oxygen in the substrate.

Average tilt angles. The angle dependent features in the carbon spectra indicate that the films are at least partially ordered so that we applied the method of difference spectra investigate this in more detail. A hexadecanethiol SAM on gold was used as reference system for the machine parameter (see chapter 1) of the R*(287.6eV) and σ^*(CC/CO) 292.5eV resonances. Table 3.8 summarises the tilt angles obtained in this way.

A number of trends can be recognized in this table. For every choice of surfactant or

	Metallic Substrate		Oxidic Substrate	
	R*	CC	R*	CC
$DDPO_3$ (free Acid)	39(2)°	40.5(20)°	33.9(17)°	32.7(18)°
$DDPO_3$ (ammonium salt)			31.0(24)°	30.3(28)°
$DDPO_4$ (free Acid)			37.1(36)°	38.5(26)°
$DDPO_4$ (ammonium salt)	43(1)°	42.5(30)°	38.6(15)°	37.7(12)°
50%$DDPO_4$	48(1)°	46(1)°	43(2)°	45.5(2)°
50%OH-$DDPO_4$				
OH-$DDPO_4$	49(1)°	50(1)°	44(1)°	51(1)°

Table 3.8: Chain tilt angles as calculated for the R* and CC resonances using the method of difference spectra.

resonance, the tilt angle is always higher on the thicker, metallic, titanium films than on the thin (20nm) films. Similarly the introduction of hydroxyl-functionalised surfactants systematically increases the average tilt angle towards the magic angle of a disordered system while not reaching this. Finally, the tilt angle also varies upon a change in headgroup so that $DDPO_3$ films persistently posses a lower tilt angle than $DDPO_4$. The type of preparation did not systematically influence the tilt angle. For both $DDPO_3$ and $DDPO_4$ the experimental tilt angles of the ammonium salts equal those from the free acids within the experimental accuracy.

The lowest tilt angles for $DDPO_3$ on the oxidic substrates resemble those of the ODP with a longer chain or those of a hexadecanethiol layer on gold which forms notably well ordered films [52].

As in the case of the contact angles, the results of the mixed films lie between those for the pure layers and again the average tilt angle ($\theta_{\mathrm{Mixture}}$) can be interpreted as an average between the two isolated values (θ_{DDPO4}, $\theta_{\mathrm{OHDDPO4}}$) weighted by their relative fractions (f_{DDPO4}, f_{OHDDPO4}) in the total layer. Under this assumption, the NEXAFS tilt angle gives another estimation of the proportions of the two species on the surface according to the following equation:

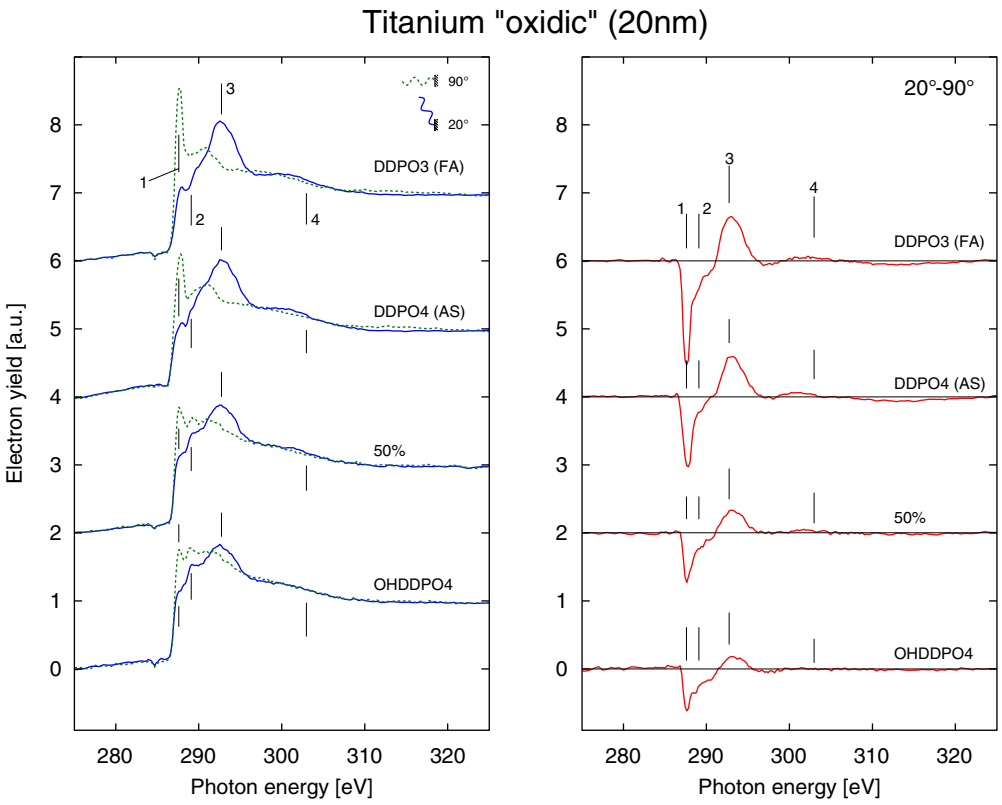

Figure 3.8: All adsorbents exhibit different angle-dependent resonances in the carbon spectra. Difference spectra reveal an additional C-O resonance, which is hardly detectable in the total spectra.

$$\cos^2\theta_{Mixture} = f_{DDPO4}\cos^2\theta DDPO4 + f_{OHDDPO4}\cos^2\theta_{OHDDPO4} \tag{3.4}$$

This predicts the mixed films to consist of 23% methyl-terminated molecules for the "oxidic" and 35% for the "metallic" substrates, which is in good agreement with the prediction from water contact angles (see section 3.3).

Our interpretation of the tilt angle uses the results of $DDPO_3$ as a starting point. Since its water contact angle suggests that the topmost layer of this film mainly consists of methyl groups and its NEXAFS tilt angle is nearly identical to that of the well ordered ODP [53], it is considered to correspond to a perfectly ordered SAM. We hence consider the tilt angle which $DDPO_3$ based films establish on the smooth oxide substrate as the "ideal" angle that alkane chains adopt in the densest packed, best ordered films on titanium oxide. De-

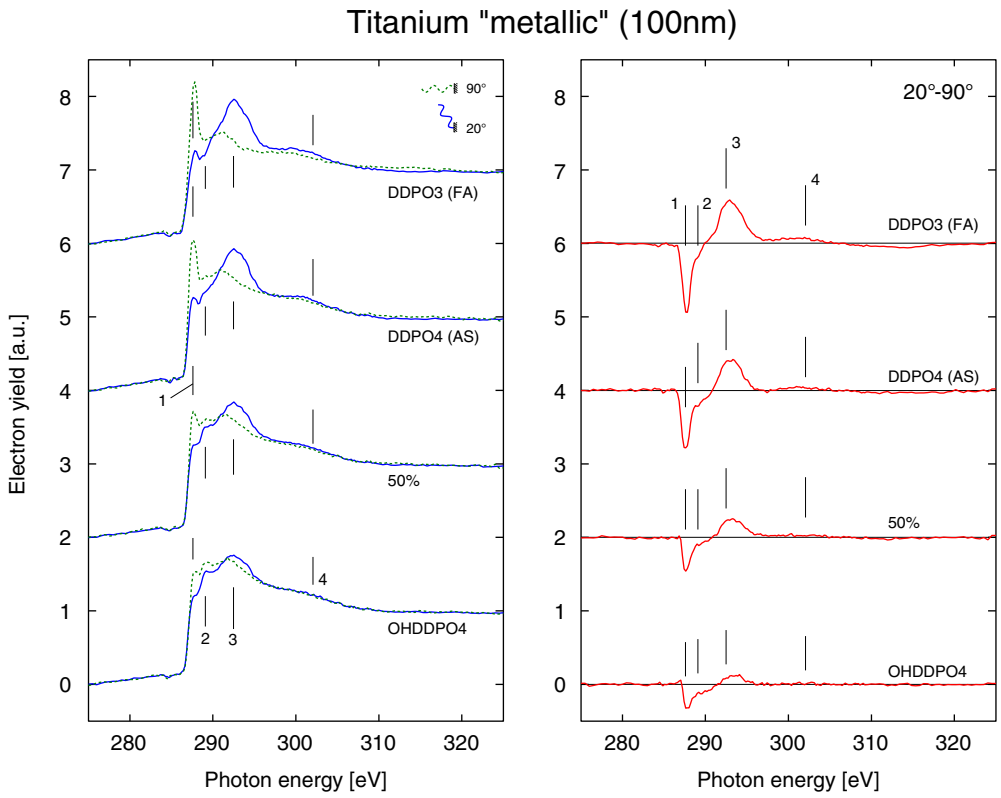

Figure 3.9: For the "metallic" substrates the (difference) spectra are qualitatively similar to those on the thinner "oxidic" samples but show a less pronounced angle dependence.

viations from this reference towards higher tilt angles are logically explained by a loss of order in the films and an associated approach towards the "magic angle" of a disordered system.

3.4 Discussion

General Both $DDPO_3$ and $DDPO_4$-based surfactants form dense layers with a high degree of order, as proven by their angle-dependent resonances and water contact angles. The chemical information from XPS and NEXAFS measurements suggest that their consistence equals the theoretical prediction. A reduction of the chain-length as well as a preparation from aqueous solutions at least in principle do not prevent the formation of SAMs on titanium oxide substrates. All the XPS results, noticeably the extensive series

for $DDPO_4$ by S. Tosatti [41] point towards quantitatively very similar packing densities in all the films.

Influence of substrate roughness. Films which were established on the rougher ("metallic") substrates consistently showed less order than their equivalent counterparts on the smoother("oxidic") substrates. This difference can be explained by two effects: The substrate structure only possesses a short range order which extends over a few nanometers or is even amorphous [42]. Molecules which adsorb onto the substrate at the border of two domains or onto an irregular site are impeded from adapting a regular conformation. Their effective conformation is always a compromise between the influences from the two unharmonized neighbouring domains. Domain boundaries are hence regions with an increased probability for perturbed molecular conformations. Because the rougher substrates tendentiously posses an even higher number of disturbed sites (i.e. is even less structured), the proportion of disordered molecules will also increase, which explains the higher tilt angle.

The second phenomenon is not related to the shrinkage of the average domain size but rather to the effective physical quantity that we are measuring. Because the beam spot is macroscopic, we measure the average tilt angle of TDMs with respect to the mean sample plane. On rough substrates, the individual subsurfaces (i.e. average size $\leq 100\ \mathrm{nm}^2 \Leftrightarrow 10^{10}$ subsurfaces within the beam spot) are however tilted from the substrate plane especially if as in this case a partial recrystallisation has occurred [54]. Since SAM formation is a molecular process, dominated by short-range next-neighbour interactions, molecules in a SAM are tilted by an "ideal SAM-angle" with respect to the local plane. With respect to the macroscopic plane, the tilt angle of a subsurface can hence vary from the ideal value simply because the subsurface itself is tilted from the "mean" plane. If multiple subsurfaces with different tilt angles but all with the same "SAM-tilt angle" are analysed together, then the overall angle dependence decreases, so that the apparent order on a macroscopic scale is always lower or at best equal to that on a microscopic scale. This is most plausibly illustrated by the example of a perfectly ordered SAM on a sample which consists of) equally distributed (i.e. polar tilt angle subsurfaces pointing in every direction. A NEXAFS experiment could not detect any directional preference and conceive the sample in the same way as one without any internal order.

Similar considerations have been performed for contact angles where the influence of topography is more complicated (e.g. lotus-effect, see chapter 2) [23]. We indeed attribute the higher contact angle of $DDPO_3$ and $DDPO_4$ on the "metallic" than on the "oxidic" substrates to such topographical effects and not to a change in order so that these values are not in contradiction to the NEXAFS tilt angles. Indeed the water contact angles for methylterminated phosphates/ phosphonates on "metallic" substrates are actually even slightly higher than the expectation for a flat, completely methyl-terminated film [24].
It is not a new discovery that the substrate structure influences the quality of ultrathin films [54, 55, 56] and it would indeed appear as a surprise if the arrangement of molecules would not depend on the two-dimensional periodicity of the substrate. The confirmation of this effect on titanium oxide may however present a severe drawback for the plans to functionalize medical implants with SAMs if the full potential of SAMs is required because stringent specifications for the surface roughness would have to be met on macroscopic, machined parts in order for this technique to work.

Hydroxyl-functionalization/ Mixed films

One of the main advantages of the SAM method is the possibility to flexibly adjust the surface chemistry independently of that in the bulk [49]. This potential is further enhanced if multiple endgroups can be used and ideally mixed films containing more than one kind of endgroups can be established. Sensor applications would especially benefit strongly from this capacity. Unfortunately this goal is not yet reached with $DDPO_4$-based molecules. Both in the hydroxyl-terminated, as well as the mixed films, the NEXAFS tilt angles are substantially higher than for the methyl-terminated ones. Due to this loss of order, the positional constraints of the functional endgroup is lost, which manifests itself for example in the water contact angle of $>50^\circ$ for the hydroxyl-terminated molecules.
Nevertheless, the order does not completely vanish so that the films are not completely disordered. The NEXAFS tilt angles are not equal to the "magic angle" of a disordered film (54.7°) and also the water contact angle is also still significantly below that of a methylene terminated surface (102-103° [24]) These results suggest that the films are slightly less dense and hence less well ordered [32]. The ordering of molecules in a monomolecular film only starts at a coverage of about 90% of a complete monolayer [32] so that small differences in the degree of coverage could lead to the experimentally observed

deviations. The degree of coverage that was measured with XPS does not change for the hydroxyl-functionalised or mixed films, which fits this view. The sensitivity of the XPS technique and especially of the used instrument is not sufficient to allow the detection of such subtle differences so that the films appear identical [25]. Folkers et al. investigated differently functionalised alkanethiols on a range of metal substrates and measured similar water contact angles for the hydroxyl-terminated species. They attributed these results to a lower degree of coverage and proved this by measuring slightly lower film thicknesses for these films [57].

I have already mentioned that it is not a priori clear whether $OHDDPO_4$ can actually form highly ordered films as well. The polar endgroup will increase the mutual interactions between surfactant molecules and hence energetically promote SAM formation. This trend has been observed for other systems [49]. In the case of adsorption onto titanium-oxide from aqueous solutions, two effects can change or impede the film formation. On the one hand the hydroxyl-groups can now also interact with the substrate to produce an end-on adsorption or a flat orientation in which both the head- and the endgroup are bound to the surface [58]. Based on the identical XPS coverages, we think that these effects only play a minor role. A flat adsorption would be accompanied by a significant reduction of the number of molecules on the substrate which XPS measurements could detect in the form of a reduced attenuation of the substrate peaks. An adsorption by the endgroups, where the phosphate group is located at the top of the films, would be picked up by angle-dependent XPS measurements. Secondly, the endgroup can strongly interact with the polar solvent so that the kinetics may change or solvent molecules may be incorporated in the resulting films, which could disrupt these or reduce the coverage. The influence of solvent molecules on polar endgroups has been studied with STM and computer simulation, where it showed to play a decisive role in the ordering of the topmost chemical groups [59]. As apparent from the XPS studies [25] the kinetics only changed slightly, so that no change in the chemical composition is detectable with XPS after 48 hours of immersion.

We are unable to quantify the amount of water that is integrated in the films or on the substrate. Of the three techniques we used, XPS is the most suitable for such an investigation but the characteristic peaks (i.e. O2 Ti-**OH**, O3P-**O**)) also contain contributions from atoms which belong to the adsorbate and the quantitative sensitivity is not high

enough to draw any significant conclusions.

After the analysis of the two pure films, the interpretation of the mixed ones is relatively analogous. Both the contact angle and the NEXAFS tilt angles lie between the two pure values. The estimations about the fractions of the two species, yield the same values for the three complementary techniques (within the experimental accuracy [25]). Both species appear to be present on the surface and the surface coverage of carbon and of phosphorus (as measured by XPS) indicates the formation of a mixed but similarly dense film.

It is possible that highly ordered methylterminated molecules coexist next to comparatively disordered hydroxyl-terminated phosphates. This hypothesis is especially enforced by the NEXAFS experiment in which the order in mixed films is explained by the order in the pure films weighted by their relative fractions (i.e. obtained with XPS) A phase-separation and the formation of demixed islands on surface could plausibly explain that we calculated the same fractions of the individual species with three complementary methods. We do not attribute the differences in order between the differently end-functionalized or mixed films to a fundamental physical limitation but are rather inclined to think that they are induced by the preparation. A change of the preparative conditions (e.g. temperature, pH, concentration, post-treatment), might in our opinion lead to hydroxyl-terminated films which are just as ordered as the methylterminated films.

Head group Molecules with a O_3P- headgroup (phosphonic acid) consistently formed films with a higher degree of order than those with an O_3PO- headgroup (phosphoric acid). It is again not unambiguously clear, whether a fundamental difference between these films exists. The experimental differences do not necessarily arise from differences in the interactions of surfactant and substrate but can also be induced by the preparative procedures. XPS spectra show differences in the oxygen and phosphorus regions but these are not sufficient to unravel the influence of the headgroup on the quality of the resulting films. Indeed more work in this direction is needed, most notably the establishment of an XPS reference for the free adsorbent. Temperature-programmed desorption (TPD) experiments will resolve the question, whether one or the other kind of surfactant establishes a stronger binding to the oxide surface, and these are also planned in the near future.

Free acid vs. Ammonium salts $\Leftrightarrow$ organic vs. aqueous solvents

For the quality of the resulting films it did not play a (statistically) significant role, whe-

ther these were prepared from aqueous or organic solvents. The change to water as a solvent meant replacing the free acids by the corresponding ammonium salts, which however completely dissolve into free anions in the solutions if the concentration is below the CMC [38, 44]. As a conclusion of these results the binding mechanism of the surfactants is the same for both their ionic and covalent versions. We also interpret this discovery in such a way, that water does indeed not enter the lower parts of the films in high quantities or even takes part in the binding of the headgroups to the substrate. If this were true, then packing density or order would most certainly be affected by using water as the solvent. The binding mechanism of alkanephosphates and -phosphonates is hence determined by the substrate and the adsorbents just as in other SAMs [19] and only weakly by solvent constituents. An apparent influence of the solvent (e.g. slightly better ordered films of $DDPO_3NH_4$ compared to the free acid form $DDPO_3$) is as in the case of the hydroxyl-functionalization, caused by a particular preparative parameter (e.g. temperature) and could be avoided, which again underlines the importance of finding the "ideal" conditions.

3.5 Conclusions and outlook

Titanium oxide surfaces can be covered by a dense, monomolecular film of alkanephosphate or -phosphonate molecules. Methyl-terminated adsorbents establish highly ordered monolayers out of both aqueous and organic solvents. In this context $DDPO_3$-based layers possess more internal order than their $DDPO_4$ analogues. Hydroxyl-functionalised molecules fail to form equally well-ordered films and also induce disorder into mixed films. Despite all our experiments we have not yet discovered a fundamental explanation of how the differences in the film quality are connected with the change in head- and endgroup. This uncertainty continues because the number of parameters that can influence the film formation — most notably related to the preparation — is too high to suggest a unique phenomenon.

Our inability to produce well-defined monolayers with a highly variable chemical endgroup in turn means that chemical sensors based on functionalized dodecylphosphate SAMs remains out of reach for the time being. An application of $DDPO_4$-SAMs for medical implants is strongly affected by the dependence of order on the roughness of the

substrate. It indeed presents a difficult challenge to control the topography of machined or macroscopically coated workpieces on the nanometer scale. Whenever the full potential of the SAM method is imperative to the success of a coating, our system of preparation and the adsorbates fall short of fulfilling the task. Nevertheless, a strong reduction of the surface energy and hence a reduced sensitivity to contamination was very successfully achieved and also proves to work for very rough substrates [25]. If this is the main goal of the coating, then these monomolecular films of $DDPO_3$/ $DDPO_4$ can be used under the condition that they meet all the other requirements, such as mechanical stability.

Adsorption of phosphorus-based surfactants is a highly interesting but complicated process. After these studies a lot of details of these systems still remain unresolved and await to be addressed. The results of this study lift two issues into the focus of future experiments. A next step must be to unambiguously pin down those determinant factors during the film preparation, which influence the outcome most. Owing to the large set of possible parameters, this is likely to be tiresome but SAMs are known to be disturbed if crucial procedures are not strictly adhered to, especially in the case of more sophisticated systems, where the constituents of the substrate, surfactant and solvent can interact with each other in numerous ways. Further efforts should then be directed to measuring the binding strengths of $DDPO_3$ and $DDPO_4$ (TPD, XPS powder reference for $DDPO_3$). I believe that supplementary knowledge about these molecular mechanisms will significantly enhance the practical value of this class of SAMs. Indeed, none of the originally intended aims has been shown to be unreachable because of fundamental reasons but all of them might be achieved if the proper preparative procedures are found and applied.

Chapter 4

Oligo(Ethylene glycol) functionalised Alkanethiols on Gold

4.1 Motivation/ Introduction

One of the outstanding properties of SAMs, is that a comparatively simple preparative procedure can be used to reproducibly establish very well-defined films with a designated chemical functionality on a substrate. The growing field of life science needs such coatings. Biomedicine and -technology for instance often needs surfaces that can resist the non-specific adsorption of proteins. These macromolecules are generally understood as "building blocks" of life, fulfilling such vital tasks as the localisation of chemical reactions [60], mechanical stabilisation (e.g collagen) or material transport (e.g. Haemoglobin) [61, 62] in organisms. In accordance with their importance for life, the scientific interest in proteins is enormous. An understanding of their functionality will not only benefit fundamental biology but can also offer numerous technical and economical opportunities to people who can make these principles work in their favour. Prominent examples are improved medical implants, protein sensors for medical diagnosis and research purposes or advanced drugs with a higher efficiency.

This explains the importance of surfaces which interact with proteins in a special way.

Oligo(ethylene glycol(EG)) (OEG) functionalised monolayers are another example for ultrathin layers, which are interesting because of their relevance for biological applications. OEG terminated alkanethiols on gold were the first SAMs to be discovered, which were able to resist protein adsorption [63].

Poly(ethylene glycol)(PEG) coated substrates are well known to fulfill the task of blocking protein adsorption [64] but SAMs of shorter oligomers bring the advantage of a higher conformational definition, the potential to tailor the chemical endgroup to some extent as well as their ease of preparation. With regard to modern technology, their low thickness renders them suitable for miniaturised devices, a property which could be highly useful for solving complex biological problems (e.g. in genomics). A protein adsorbing onto these polymer coated surfaces greatly reduces the conformational freedom of the polymer molecules and expels water out of the films. PEG films are in summary protein resistant because of entropic constraints — a mechanism which is widely known as "steric repulsion" [64]. In contrast to polymer-coated surfaces, the non-fouling nature of OEG-SAMs is until now not restlessly understood and remains the focus of numerous scientific works. For the explanation of this effect, it is mandatory to study the chemistry and the molecular structure of these films in detail.

In the first publication which dealt with EG films on gold and in which their protein resistance was discovered, ellipsometry measurements of the film thickness were presented. In comparison to the well-known, highly ordered alkanethiols in a tilted all-trans conformation, EG-terminated films were too thin for the molecular chain lengths which the authors interpreted as an indication of a low degree of internal ordering. The next study devoted to the conformation of OEG-SAMs, came from Harder et al. [65] and was a milestone in the search for an explanation of protein resistance in ultrathin films. Their Fourier Transform infra-red (FTIR) results showed systematic differences between protein resistant films on gold and their analogues on silver, which do not repel proteins. For OEG-SAMs on gold, they observed additional vibrational modes which also occur in crystalline [66, 67] yet not in amorphous [68] PEG. This correlation led the researchers to believe that the EG units in the SAMs adopt the same conformation as PEG in its crystalline form, namely a 7/2 helix [66]. On silver, these vibrational modes were missing, because the EG units allegedly had to adapt a stretched, more linear conformation due to

the (slightly) higher packing density. In the eyes of Harder and his coworkers, water can interact much stronger with the helical EG units than with the linear molecules and hence a "protective" layer is formed on the SAMs, which prevents the adsorption of proteins. In the course of this work, a number of mainly theoretical studies corroborated Harder's model [69, 70, 71].

There are, however, also several arguments against this conception. It fails to explain, why mixed films consisting of EG-functionalised molecules as well as a fraction of up to 30% of bare, short-chained ($S(CH_2)_{11}OH$) alkanethiols are also protein resistant [72]. In such thinned films, the ordered well-defined conformation of the EG units is most likely distorted and significant amounts of molecules will probably lack a preferential order. Furthermore, 5–10 other surfactants have been found in the meantime, that also form protein resistant films [73]. A comparative study of all these molecules shifts the focus onto the charge distribution within the (overall neutral) SAMs and rules out the explicit molecular conformation as a general explanation for protein repellency [73]. Diverse AFM-based studies [74, 75, 76], in which the approach of a protein towards the OEG-SAMs was mimicked with the AFM tip and the force acting on it was analysed, suggest a similar explanation. All these experiments point towards "electrostatic" effects as a key component for protein repellency while the exact conformation of the molecules only plays a minor part [74].

Until now only two fundamental statements about the internal orientation of OEG-terminated films on gold can be made. The molecules are not in a stretched (all-trans like) conformation [63] and partially adopt the energetically favourable helical crystal structure of PEG [65]. None of the sets of experiments, however, allowed a quantification of the fraction of these helical moieties and no method has ever gauged, which percentage of the molecules is **not** in this conformation, for instance adsorbing in a random conformation. NEXAFS experiments yield quantitative information of molecular orbital tilt angles which can, by comparison with an "ideal value", be converted into a measure of the degree of order in films — thus filling this prominent vacancy of knowledge. Tetra(ethylene glycol)-hydroxyl-terminated alkanethiols on gold have already been studied with this technique [77] and showed no prominent angle-dependence in the electron yield, which is commonly interpreted as the sign of disordered films. We have investigated OEG termi-

nated films with a variable number of EG units and, in addition to the above-mentioned NEXAFS study, also simulated the "ideal" conformations (e.g helical EG units on top of tilted alkane chains) proposed by Harder et al. [65] and were thus able to test their conformational model.

4.2 Experimental

Surfactants. All surfactants structurally consist of an undecanethiol ($HS(CH_2)_{10}CH_3$), to the end of which a varying number of ethylene glycol (OCH_2CH_2) units is attached. Together with a chemical endgroup, this renders the following general molecular structure: $HS(CH_2)_{11}(OCH_2CH_2)_nR$. The synthesis of the adsorbates was carried out in the laboratory of Professor Grunze (Angewandte Physikalische Chemie, University of Heidelberg, Germany) according to procedures presented in literature [63, 72, 76], where the chemical composition of all products was also confirmed. We used the surfactants without any further purification. The abbreviations EG3 (n=3, R=OCH_3) and EG6 (n=6, R=OH) are derived from the number of ethylene glycol units, while EG350 (n=8–9, R=OCH_3) and PEG2000 (n=approx. 45, R=OCH_3) refer to the masses of the attached ethylene glycol blocks in atomic units.

SAM Preparation. Gold samples were prepared by thermally evaporating (Balzers BAE 370 coating system, pressure $\sim 5 \cdot 10^{-7}$mbar, deposition rate of 0.5–1nm/s) 80nm of polycrystalline gold (99.99%, Balzers Materials, Liechtenstein) onto silicon (100) wafers (MEMC Electronic Materials, Inc., St. Peters, MO). The bare substrates were immersed into a 2mM ethanolic (>99.8%, p.a., Merck, Switzerland) solution of the surfactant molecules immediately after coating and remained there for an extended period of time (typically 24h). Upon taking the samples out of the solutions, they were rinsed with the pure solvent and further cleaned in an ultrasonic bath of ethanol to remove loosely bound residual molecules, before and we finally dried them in a stream of nitrogen. In order to reduce degradation during transport, all samples were packed under an inert nitrogen atmosphere, out of which they were only taken immediately before the NEXAFS measurements.

NEXAFS measurements were performed under standard conditions (see section 1 for

more details). The samples did not discernibly charge up, so that we were able to conduct the experiments without using an electron floodgun. In accordance with the molecular structure, we measured spectra in the 1s regions of carbon (275–325eV) and oxygen (520–570eV).

Theoretical calculations. The aim of our NEXAFS experiments was to determine, whether OEG-terminated alkanethiols establish ordered films upon adsorption onto gold and if yes, whether the molecules adopt the proposed conformation of tilted alkane chains with vertically standing, helical EG-units on top of them.

A series of NEXAFS spectra at different angles of photon incidence yields the average tilt angles of the different kinds of bonds (i.e. more precisely: the associated TDMs). The individual bonds of a polyatomic molecule in a SAM do, however, not all have to point in the same direction. In such a case it is unfortunately impossible to calculate the individual angles backwards from the overall average tilt angle. Hence numerous different conformations of one molecule can lead to one and the same average angle-dependence. It is even possible to construct perfectly ordered structures which lack any angle-dependence even though no single TDM is actually tilted by the "magic angle" (54.7°).

Because of this averaging, it is fundamentally impossible to determine the effective conformation of the OEG molecules and no set of NEXAFS experiments can unambiguously confirm, that they adopt one unique conformation. Nevertheless, NEXAFS experiments are useful because they present a complementary test for Harder's model [65]. If the films actually favour this special conformation, then we are able to calculate the average tilt angles of the different TDMs. In order for the model structure to be eligible, the experimental tilt angles have to match the predicted ones. If they fail this test, then the proposed conformation can be excluded with certainty, while a match corroborates the hypothesis without positively identifying it as the only possibility.

The "ideal" tilt angles for this comparison were calculated according to the following algorithm. At first, coordinate files were created for the molecules. The alkane chain was considered as linear (i.e. the TDM of the transition 1s$\rightarrow \sigma$(CC) is parallel to the chain axis and the R*-TDM is perpendicular to it [78]) and we built the EG units with the help of the PEG crystal structure [66]. Wherever less than an entire unit cell (7 EG units) was required, we used the respective number of EG units from the "lower" parts of the unit cell

(see original reference for numbering of the atoms within the unit cell [79]). We assumed EG350, which is in practice a mixture of molecules with 8 and 9 EG units, to contain 9 EG units. The terminal endgroups (-OH respectively -OCH_3) were attached according to an educated guess but some uncertainty remains for their exact positions. In accordance with Harder's model, the alkane chain axis was assumed to be tilted from the surface normal by 33° [19] and was allowed to freely rotate around its longitudinal axis. This rotational degree of freedom was incorporated into the calculation by numerically averaging over the different chain positions and affected the theoretical prediction of the R*-resonance. The EG blocks were vertically erected and then the tilt angles of all the individual bonds (θ_i) were calculated. Because the TDMs of all the involved electronic transitions (i.e. R*, σ) point along the interatomic axis of the two involved atoms, this calculation was equivalent to calculating the tilt angle of the corresponding difference vectors between two atoms:

$$\cos\theta_i = \frac{\Delta z_i}{\sqrt{\Delta x_i^2 + \Delta y_i^2 + \Delta z_i^2}} \tag{4.1}$$

From the individual tilt angles, an average value ($\overline{\theta}$) was obtained according to the following equation:

$$\cos^2\overline{\theta} = \frac{\sum_{i=1}^{n}\cos^2\theta_i}{n} \tag{4.2}$$

This procedure is equivalent to breaking the molecule down into diatomic moieties, adding up their individual NEXAFS intensities and then calculating the angle dependence of this total signal (see chapter 1), a procedure which is also referred to as the "building block principle" [2]. For cases where more than one type of transitions contribute to a NEXAFS resonance (see section 4.3), the same principle was applied to combine them. Differences in the absorption cross-sections can be accounted for, by weighting the different transitions by their oscillator strengths, the same fashion in which the attenuation of the signal from lower parts of the films is also incorporated. In practice, we assumed a two-layer model consisting of the (unattenuated) EG-units and the alkane chain which was exponentially attenuated with a mean-free length of 2nm (i.e. the increase of the mean-free path in NEXAFS compared to XPS experiments [28] stems from the larger fraction of electrons, which are accepted by the channeltron [80]). All the calculations were carried out with MATLAB [81] programs, which had undergone an extensive testing before being applied to the systems.

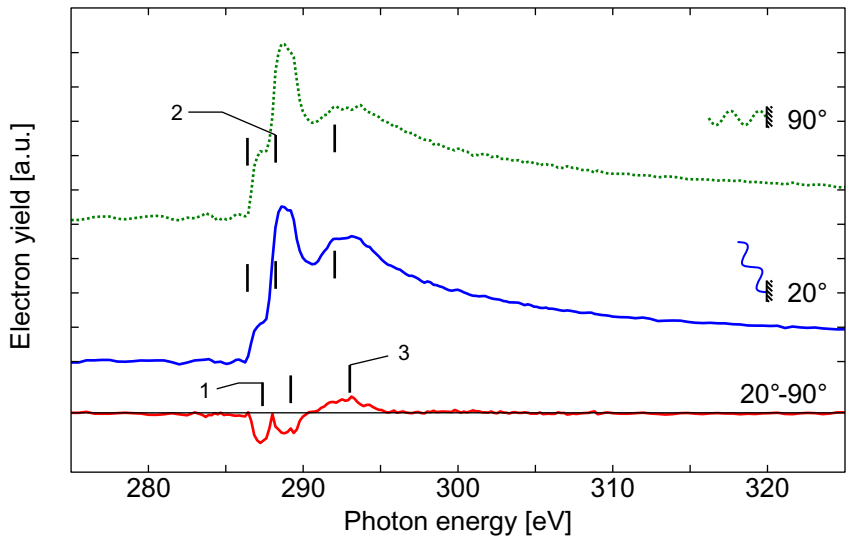

Figure 4.1: A carbon spectrum of EG3 exemplarily shows the different spectral features which were identified during the data analysis as well as their angle-dependence.

4.3 Results

Chemical composition. The first task during the data analysis of NEXAFS spectra, consists in the identification of all spectral features and their association with electronic transitions. In this stage, the chemical integrity is normally gauged and radiation damages can often be recognised [16].

Carbon range. Figure 4.1 exemplarily shows the carbon region of EG3. Pre-edge transitions of the kind C1s $\rightarrow \pi^*$ occur at a photon energy of 285.3(5)eV [16]. For both alkane chains and the EG units, this transition is symmetry-forbidden (see section 1), so that the presence of this resonance would indicate a carbon contamination or a damage to the films from the X-ray irradiation [82]. The lack of this feature in all the EG spectra hence confirmed the chemical integrity of the samples.

The energetically lowest resonance (1) is found at 287.6(5)eV. It arises from transitions into CH orbitals and is abbreviated as R* because of its Rydberg character [48] as discussed in details in the case of alkane-phosphates on titanium oxide (see chapter 3). For both EG3 and EG6 its intensity articulately varies with the angle of photon incidence.

We perceive a next resonance (2) at 289.0(5)eV which is attributed to transitions into σ(CO) orbitals [49] or possibly an additional CH orbital [51]. Its relative increase with the number of EG units implies that these transitions occur in the EG units. Between these two resonances lies the onset of ionisation. The density of spectral features and the experimental energy resolution render it impossible to fix the energy of this step precisely, but our spectra are in complete agreement with its reference value of 288.1eV from other studies [49].

Manifestly above this first set of features, a next peak (3), that appears to consist of two peaks in some spectra, is found at 292.75(50)eV. It originates from transitions into σ^*(CC/ CO) orbitals [51] [50] and again exhibits an angle dependence for EG3 and EG6. We did not observe the further σ^* (CC/ CO) resonance predicted at approximately 303(1)eV by other studies [50], in any of our spectra. It either misses completely or more likely disappears in the experimental noise because of a comparatively low oscillator strength.

Oxygen region. All oxygen spectra are shown in figure 4.2 and visually consist of a broad, peak-like feature and the absorption step. The "peak" in practice consists of two, possibly three, individual resonances which all have the same symmetry properties (most likely transitions into σ(**O**C) respectively σ^*(**O**C) orbitals). We deconvoluted the signal into one gaussian peak and a step (error function) using a least squares fitting procedure to quantify the intensity of the resonances. This may be a physically inappropriate description of the spectra but due to the limited amount of reference data [51], no better model could be established. Even without such, we are however still able to investigate the tilt angle of the CO-bonds because all the included transitions posses the same symmetry so that they can be summed up and treated as one resonance. The fitting of the signals relied on the energy difference between the resonance (1) and the ionisation step (2), which was available from ISEELS measurements of the chemically similar diethyl ether ($E_{Resonance}$=538eV, E_{Step}=538.1eV) [51]. Because the spectra were not absolutely energy calibrated, a constant offset was allowed to vary during the fitting procedure. The width of the ionisation step did not noticeably influence the outcome of the analysis but was fixed to 1.75eV. In order to optimally quantify the intensity of the resonance, we allowed the fitting routine to freely adjust the height and width of the gaussian peak. Although the number of free parameters appears high, the fit routine consistently found the same

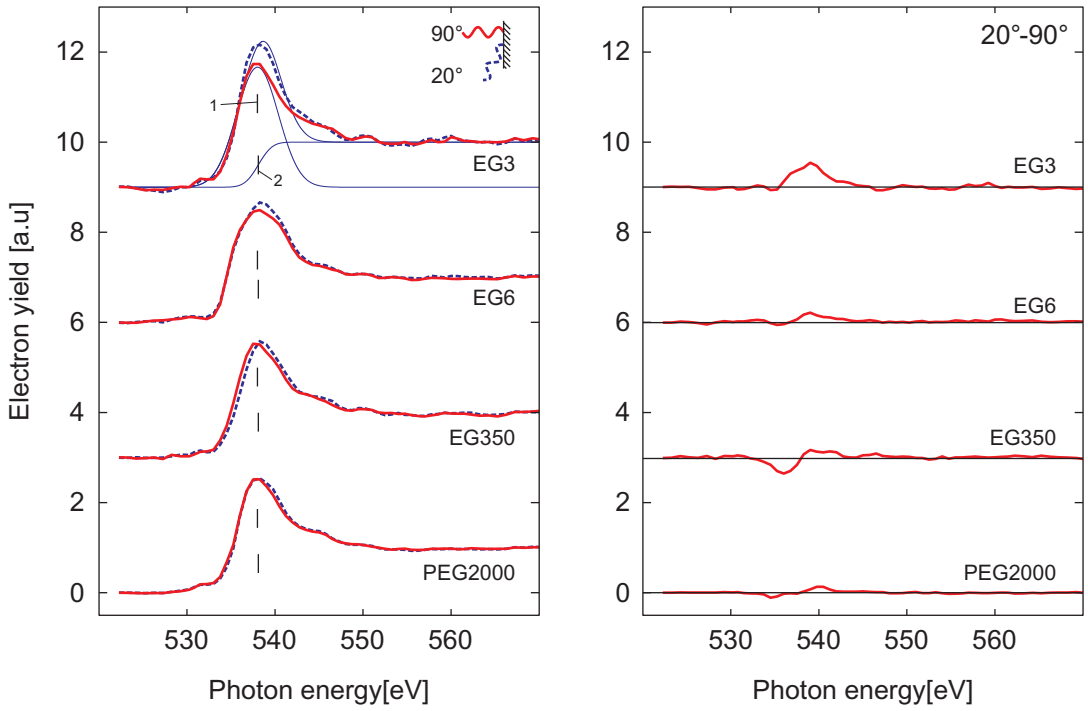

Figure 4.2: The oxygen spectra consist of a broad peak and only show an angle-dependence for EG3

optimal fit parameters independently of which starting values we chose, so that the fit can be regarded as stable and meaningful.

Average tilt angles. The angle dependent features in the NEXAFS spectra of EG3 and EG6 unambiguously prove, that these molecules form at least partially ordered films on gold (see also figure 4.3). In a next step, we hence calculated the mean tilt angles of the different transition dipole moments. For this analysis, the method of "difference spectra" was applied to determine the tilts of transitions at the carbon 1s edge. In the case of the oxygen spectra, tilt angles were calculated from ratios of the peak intensities at different angles of photon incidence assuming a degree of linear polarisation of 85% and a relative uncertainty of 10% for the intensity. Table 4.1 summarises the tilt angles which resulted from this analysis.

All transition dipole moments in all the PEG2000 spectra show a tilt by the "magic angle" (within the experimental accuracy). We interpreted these results as a proof of disorder and not as a particular molecular conformation which renders exactly this tilt angle.

	R*	σ^* (CC CO)	σ/σ^* (OC)
EG3	45.5(17)°	50.3(4)°	50.5(20)°
EG6	51.0(20)°	52.5(3)°	53.6(30)°
EG350	54.9(3)°	55.5(18)°	54.7(30)°
PEG2000	53.8(10)°	56.6(14)°	54.9(30)°

Table 4.1: Tilt angles for the different TDMs. The values for the R* and the σ^* (CC/ CO) resonance were determined with the method of "difference spectra" and hence describe the tilt angle of an alkane chain.

	R*	σ^* (CC CO)	σ/σ^* (OC)
EG3	59.9(10)°	50.3(4)°	50.5(20)°
EG6	56.8(10)°	52.5(3)°	53.6(30)°
EG350	54.8(2)°	55.5(15)°	54.7(30)°

Table 4.2: Effective tilt angles for the different TDMs. The transformation of the R^*-resonance was necessary because of the normalisation of the machine factor when using the method of "difference spectra".

This interpretation is strengthened by the length of the molecules and the polymer length distribution which makes a dense, highly ordered structure in the probed part of the films unlikely (see also section 4.4 for a more detailed discussion). For this reason, we refrained from any further calculations for these films.

The normalisation of the slope for difference spectra was such, that the analysis of the carbon resonances yields average tilt angles of an alkane chain. In order to compare the experimental results with theoretical predictions, the "chain tilt angle" of the R* now had to be converted into a more meaningful effective "TDM tilt angles". For this purpose the same algorithm, used to predict the tilt angles of EG functionalised alkanethiols, was applied to unfunctionalised alkane chains again averaging over rotations around the longitudinal axis. The tilt angle of the σ^*-resonance remains unchanged because its TDM points along the alkane chain axis and hence does not change direction upon rotation around this. Because the oxygen spectra were analysed without such a normalisation, they directly yielded the orbital tilt angles. Table 4.2 concludes the average tilt angles for the different resonances.

Theoretical calculations. The algorithm, which predicts orbital tilt angles for model

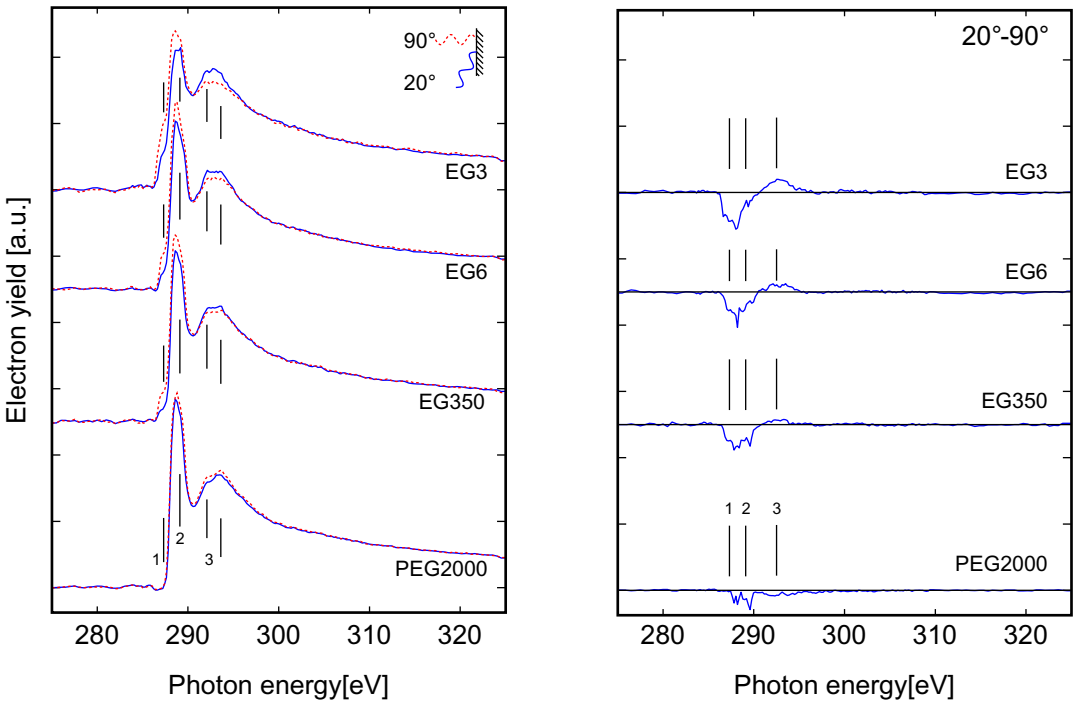

Figure 4.3: A comparative graph of all the EG samples shows the trends for the orbital tilts — most notably a decrease in angle-dependence with higher numbers of EG units.

conformations of the EG-molecules was presented in detail in the experimental section (see section 4.2). At this point it is noteworthy, that the effective mean-free lengths for electrons is longer in NEXAFS experiments (approx. 2nm compared to approx. 1nm for electron energies 200-600eV) than standard reference values [80]. This does not imply, that electrons undergo less inelastic scatterings but is a consequence of the retarding voltage (typically -150V) which can also be overcome by (Auger) electrons that have already lost a substantial amount of energy in inelastic scatterings so that these will also be collected by the channeltron (see experimental section 1.6). Because some uncertainty remains to how much the electron signal is attenuated in NEXAFS measurements, we performed the calculations with and without the application of a double layer model. In both cases, the CH and CO tilts were additionally combined (with the same oscillator strength) to accommodate the possibility of a mixed R* region (286.5–290eV) and for the higher σ^* resonance (291–296eV) we also averaged over transitions into both CC and CO orbitals.

Table 4.3 shows all these calculated tilt angles.

Without electron attenuation					
	R*=CH	R*=CH+CO	σ^*=CC	σ^*=CC+CO	OC
EG3	64.5°	61.6°	44.3°	46.4°	49.7°
EG6	63.4°	60.5°	45.1°	47.9°	51.4°
EG350	62.6°	59.8°	45.1°	48.6°	52.0°
With electron attenuation					
	R*=CH	R*=CH+CO	σ^*=CC	σ^*=CC+CO	OC
EG3	62.8°	59.5°	44.7°	47.7°	50.4°
EG6	60.9°	58.1°	46.4°	49.9°	52.1°
EG350	60.4°	57.7°	46.3°	50.4°	52.4°

Table 4.3: Theoretical predictions for the tilt angles with and without the application of a double layer model.

4.4 Discussion

On the basis of the NEXAFS spectra we can deduce, that the chemical composition of all the samples qualitatively conforms to the theoretical expectation. EG3 and EG6 both form ordered and hence dense films during their adsorption onto gold, a direct and undisputable consequence of their angle dependent spectra. We did however not discover any evidence of order in the (sub-)monolayers of EG350 and PEG2000.

PEG2000 films are probably disordered in the probed part of the layer. NEXAFS is only sensitive to the topmost 3nm of a sample [80]. The "natural" length distribution of the PEG2000 molecules is, however, so broad (i.e. 45±11 units [83]), that this top part of the PEG layer is either significantly distorted or completely amorphous. Any ordering of the EG units in the parts below this, cannot be detected because of the escape depth of the electrons, so that the NEXAFS experiments are not in contradiction with the IR studies [65, 83], which distinctively detect helical EG units even in these films [83]. Indeed there are still some questions concerning the order in PEG films. These are to our knowledge the only molecules with such a considerable length (approx. 12nm correspon-

ding to a chain length of 130 atoms) which spontaneously form ordered structures upon adsorption without any external impulse such as is the case for polymer chains aligned by rubbing [84,85]. The degree of coverage (50 –90% [86,83]) is barely sufficient for the lowest alkane chains to adopt the tilted all-trans conformation known from common SAMs [19] yet the Harder's FTIR results also observe them to be well ordered. Additionally, the topmost 2–3nm of the molecules do not contribute to the energy gain from ordering but still hinder the kinetics of film formation.

For the thinner EG350, an interpretation of the results is not as easy. Other molecules with a similar chain length, which form highly ordered SAMs, have been found [48] and according to AFM measurements [75], the force, which is exerted on a protein approaching EG350 films, is qualitatively similar to those on EG3- and EG6-terminated surfaces. For these reasons, EG350 was included in the comparison between the experimental results and theoretical predictions for the helical model, even though there was no direct evidence of any order in these films.

As pointed out in the experimental section (see section 4.2) the "magic angle" of an isotropic system does not necessarily imply a complete lack of order but can also arise from a particular molecular conformation. Indeed the calculated tilt angles of the R* and σ^*(OC) resonances were not far away from the "magic angle". Our predictions for the tilt angles, that resulted from the theoretical calculations (see table 4.3), however differed from the experimental values (see table 4.2) with statistical significance for all three surfactants (i.e. EG3, EG6 and EG350).

We subsequently expanded the model by assuming the films to be a binary system, consisting of ideally arranged molecules and such which were completely disordered, with the aim to estimate the **maximal fraction of ordered molecules** in the films. The fraction of disordered (f) and ordered (1-f) molecules as well as the experimental tilt angle (θ_{exp}) and the according values for an ideally ordered (θ_{ideal}) respectively a completely disordered film (θ_{magic}=54.7°) are connected via:

$$f = \frac{cos^2\theta_{\text{exp}} - cos^2\theta_{\text{ideal}}}{cos^2\theta_{\text{magic}} - cos^2\theta_{\text{ideal}}} \tag{4.3}$$

Table 4.4 shows the fraction of disordered molecules by which the real films are distorted from the model structure.

Without attenuation of the electron signal					
	R*=CH	R*=CH& CO	σ*=CC	σ*=CC& CO	σ OC
EG3	45(11)%	23(16)%	80(3)%	75(3)%	16(50)%
EG6	74(15)%	63(23)%	90(11)%	86(4)%	67(112)%
EG350	99(3)%	98(5)%	—	—	100(130)%
With attenuation of the electron signal					
	R*=CH	R*=CH& CO	σ*=CC	σ*=CC& CO	σ OC
EG3	34(14)%	8(16)%	80(3)%	71(4)%	2(61)%
EG6	65(20)%	38(23)%	88(3)%	80(6)%	58(143)%
EG350	98(5)%	97(8)%	—	—	100(175)%

Table 4.4: Estimation of the fraction of disordered molecules in a binary film in which the only two possible molecular conformations are that proposed by Harder and a completely disordered one.

Despite a large scatter, two trends can consistently be observed. None of the films exactly matches Harders model and the quantification of disorder suggests that substantial fractions of molecules to be in an amorphous conformation. This fraction systematically increases with the number of ethylene glycol units to reach its maximum in EG350-terminated films where it accounts for the entire film. This increase implies, that the amorphous moieties are not just located in the topmost endgroups but must range into the middle part of the films. With a growing molecular length, the relative contribution of the topmost groups decreases until the lowest atoms are not probed anymore. This is however not yet the case for EG350. The confidence interval of the fraction of "disorder" is all the higher, the closer the ideal tilt angle and the "magic angle" lie together. For the σ*(CC/ CO) resonance of EG350, this gap is for instance so small, that the experimental value is not in this interval anymore (i.e. possible by the experimental accuracy and necessarily because of a systematic deviation) so that the deviation can not be quantified.

These results only contradict those from IR measurements at first view because we do not claim to positively identify a concrete conformation for these films (see section 4.2) so that film structures which comply with both studies can be imagined. Apart from theoretical calculations [69, 70], no method can unambiguously detect the conformation of the

EG-terminated alkanethiols on gold and FTIR spectra are notoriously difficult to quantify.

4.5 Conclusions and outlook

We have measured NEXAFS spectra of OEG-terminated alkanethiols on gold with a variable number of EG units. For the two shorter surfactants EG3 and EG6 a (pronounced) angle-dependence of the spectra indicates, that these molecules adsorb to form dense and at least partially self-assembled films. The longer two surfactants EG350 (8–9 EG units) and PEG2000 (approx. 45 EG units) do however not show this quality — thus giving no positive proof of self-organisation.

It is fundamentally impossible to detect order in the lower parts of PEG2000 films because of their thickness ($\geq$12nm). The topmost parts (approx. 3nm) of these layers are most certainly completely disordered because of the chain length distribution of the molecules (i.e. 45$\pm$11 EG units) and the lower parts of the films are attenuated too strongly.

The interpretation of NEXAFS tilt angles is more complicated than for linear chains (e.g. alkanethiols on gold) because the proposed conformation with upright standing helical EG units on top of alkane chains which are tilted by 33° like methyl-terminated alkanethiols. In such a conformation, not all TDMs of one kind are tilted by the same angle, so that the overall tilt angle is an average of the individual TDMs and does not hold any direct conformational information. In order to understand the experimental results in more detail, we calculated the tilt angles of the "ideal" model conformation proposed by Harder et al. and were, with the help of these theoretical predictions, able to test, whether the films arrange in exactly this orientation.

This comparison revealed significant deviations between the "ideal" and the experimental tilt angle for all the surfactants, resonances and the different ways of calculating the tilt angles. Our NEXAFS experiments hence confirm, that the actual film structure cannot be that of molecules which all perfectly adopt the proposed conformation. Because all the individual TDMs are averaged out to a mean tilt angle, it is however not possible to replace Harder's model by a more appropriate alternative. Instead, we quantified the fraction of molecules in an amorphous conformation required to explain the observed NEXAFS discrepancies between the experimental results and the theoretical predictions. Under this

assumption, significant fractions of disordered molecules were obtained for all the monolayers. The amount of disorder is directly correlated with the number of EG units and reaches its maximum in EG350 where the "ideal" conformation completely vanishes and the entire film appears amorphous.

The diverse IR studies are not necessarily in complete contradiction with this discovery. Conformations, with some fraction of helical EG units can be imagined, which would not match Harder's model and would still render the observed tilt angles. Because of the remaining ambiguities, we propose a study of the analog films on silver, because the EG units allegedly obtain a stretched conformation on this substrate. In that case, an analysis of the NEXAFS results would be significantly easier because the observed orbital tilt angles of the proposed structure would correspond to the tilt of alkane chains in unfunctionalised alkanethiols on silver.

Part III

Self-assembly in ion-exchanged films on muscovite mica

Chapter 5

General

5.1 Introduction

In this part of my thesis, various aspects of SAMs on muscovite mica are presented. The first chapter contains background information to the investigations such as the motivations for this project, scientific gaps as well as chemical fundamentals of the substrate and the surfactants. It is followed by a chapter that focusses on effects influencing the film structure such as the solvent, which all need to be understood in order to deposit well-defined and highly ordered monolayers on mica. The two subsequent chapters each contain a study of conformational order in a monolayer on mica, first in function of the symmetric chain length of dialkylammonium ions and the second in pyridinium-based ions.

Two fields would strongly profit from a SAM technology on muscovite mica. The first is fundamental surface science, in which muscovite mica is often used as a model substrate because of its nearly perfect flatness (see chapter 5.2 for more information) and the second are polymer composites containing muscovite mica particles (approx. 10μm·10μm·100nm [1]) [87]. With respect to fundamental surface science, the possibility to produce well-defined layers of tunable chemical functionality via a simple dipping process, while retaining the flatness of the substrate, would add to the importance of muscovite mica as a substrate.

"Composite" materials are distinguished by the fact, that certain properties of a form-giving matrix are specifically enhanced by the addition of a second component, without

[1] W. Caseri, IfP, ETHZ private communication

losing its advantages. This modular approach to designing a material allows the targeted tuning of macroscopic properties, so that a material can be selectively optimised for its field of application (e.g. costs, mechanical or thermal stability). Polymers are typical representators of such matrix materials. They have low materials and fabrication costs, possess a low density and an excellent processability but fall short in aspects like stiffness or the mechanical, respectively thermal stability in comparison to other classes of materials like metals or ceramics, which makes them unsuitable for numerous applications. "Improved" polymers, in which the advantages are mostly retained, while the disadvantages are eradicated with a proportionate effort, hence have many prospective fields of applications and represent a common goal in the science of functional materials. Today, polymer composites are already wide-spread. Fiber reinforced polymer matrices are, for instance, often used in modern aerospace machines because of their unrivaled specific stability. Instead of fibers, the materials properties of polymer matrices can also be improved by the addition of particles. The reasons, for using such enhancing agents, lie more in the achieved effect per cost and the retained processability than in the total enhancement.

Muscovite mica possesses excellent mechanical properties along its twodimensional layers (see section 5.2) and has a high dielectric constant [88]. In comparison to other layered silicates, the mechanical properties are better in muscovite mica, because no intercalation (i.e. ion exchange into the intermediate layers) and swelling in solution are observed [89]. The abundance of natural muscovite mica is high and it can easily be mined and processed to flakes so that muscovite mica is available in large quantities and at a low price. Due to the combination of excellent materials properties and low costs, muscovite mica is hence a valuable filler for polymer matrices, with which functional composites have already been designed [87]. In section 5.2, the physical properties and their molecular origin of muscovite mica are revisited again in more detail.

Generally, the behaviour of a composite material is determined by three distinct factors, namely the bulk properties of the two continua as well as the interaction between them. Despite its low volumetric fraction, the "intercomponent" contribution can strongly influence the macroscopic properties of a composite material. Mechanical properties, for instance, are only improved by a modifier if the interaction between the two components reaches a certain strength so that stress within the matrix can partially be transferred to the modifier.

The same component also determines, whether two components can be intermixed. Unfunctionalised muscovite particles are incompatible with poly(tetrafloroethylene)(PTFE) because the mutual surface energies vary too much, so that the components demix into two phases. Because of its significance for the properties of the resulting material, control over the interface between the components is desirable in the design of novel composite materials, which and can be obtained in different ways:

- Modification of the polymer e.g. by the incorporation of chemical groups.
- Addition of a third, adhesion-promoting, agent into the matrix.
- Chemical modification of the particle surfaces.

Surface scientific studies have provided a numerous types of targeted chemical surface functionalisations. The concrete problem of modifying small mica particles could elegantly be solved with ultrathin, self-assembled monolayers (SAMs). This approach to controlling matrix-filler interactions, offers the advantage of a maximised efficiency, because the chemical modification is introduced directly at the targeted spot and because monomolecular films alter the stoichiometry by the smallest degree possible. SAMs can be deposited on numerous samples by a spontaneous adsorption from solution. In this way, highly ordered films can reproducibly be established in a simple preparative procedure, which is relatively insensitive against weak perturbations, such as a contamination of the solution. Because of the robustness and the ease of such a functionalisation, this principle could also be adapted for large-scale industrial applications.

Similar to composite materials, the chemical functionality of a SAM is also modular. The three blocks of a SAM-forming molecules – head-, spacer- and end-group – can be exchanged quite independently of each other, to establish similar films on a novel substrate by changing the headgroup or to alter the surface chemistry by replacing the endgroup. Owing to this modularity, SAMs offer a simple and flexible route to chemically modifying surfaces. With the help of SAMs, macroscopic properties such as the wettability of a substrate can substantially be changed, flexibly tuned and understood on a molecular level [90].

For a controlled and targeted modification of mica surfaces with SAMs, suitable surfactants and experimental procedures must be found. A success of the method requires, that

highly ordered monomolecular films can be routinely deposited. Extensive studies on the molecular mechanisms and structures of such films are hence necessary, before the technique is ready for use. Numerous surface analytic methods for the investigation of ultrathin films on macroscopic samples and, to some extent, on samples in powder form, exist [91]. XPS can be used to obtain the chemical composition of a surface region, verify its chemical integrity or to measure the degree of coverage reached by an adlayer (see chapter 2.2). Conformational order of the intermediate spacer-groups, the fundamental feature upon which the positional guarantee of the functional endgroups depends and on which the chemical modification via the SAM method is based, can be detected and quantified using NEXAFS (or FTIR [92]). We decided to start our studies on macroscopic samples in order to apply theses experimental techniques and to take care, that all the preparative steps could be transferred to mica particles later on.

The task of establishing a flexible SAM-technology suitable for mica particles as sheets alike, can be divided into several distinct subtasks. In a first step, SAM-forming surfactants must be found and internal order must be proven. This contains the identification of a suitable headgroup, which binds to mica, and the search for spacer-groups that will arrange in a regular conformation at high coverage. Closely related to the adsorbents, is the search for preparative methods, which also have to be suitable for a surface modification of mica particles. In a next stage, the existing protocols need to be extended differently endfunctionalised molecules in order to establish the desired chemical flexibility. Apart from the acquisition, respectively synthesis of novel surfactants, the preparative procedures or the choice of spacer-blocks may have to be adapted, since the chemical endgroup can influence film formation [49, 40]. Despite the prospect of lowering the surface energy of the modified mica by producing methyl-terminated films, the full potential of SAMs only unfolds, if SAMs with a variety of different endgroups can be deposited on the surface. After these two stages, we will be able to produce highly ordered monomolecular films with variable chemical functionality on muscovite mica, using protocols that are applicable to mica particles as well as mica sheets. This is sufficient to use such mica samples as model substrates for further surface scientific experiments but more work is needed for the successful fabrication of mica reinforced polymers.

Equipped with the detailed knowledge about the thin films, polymers must now be mixed

with mica particles that were modified according to the same protocols so that the effect of the surface modification on the macroscopic properties of the composite materials can be studied. Such experiments are complimentary to those on the thin films but the two data sets will correlate with each other, if the interface between the particles and the polymer matrix influences the composite properties and is controlled by the SAMs. If such a correlation is found, then the mechanism of matrix enhancement can be understood on a molecular level under the condition that the two bulks are thoroughly studied. After these experiments on the particle composites, the previous steps may have to be repeated until the interaction between matrix and filler can finally be specifically tuned by a SAM.

This part of my thesis documents the first step of the project to establish the full SAM-technique on mica such that it can be used for the tailoring of mica particle composites, namely the search for suitable surfactants, experimental conditions and the proof of order. Ultrathin films on muscovite mica have already been studied by other research groups, so that we could build upon existing experience. The largest scientific effort was previously put into monomolecular films of quaternary ammonium salts, to which one or more alkane chains were attached. These ions are well-known tensids and are commercially available in numerous variations. At the surface of freshly cleaved muscovite mica, cations (i.e. potassium) are located, which can be exchanged by other ions (e.g. ammonium) from a solution [93]. Thin films of alkylammoniumions on muscovite mica should resemble SAMs of alkanethiols on gold in many aspects such as force components or resulting structures (see section 5.3 for detailed information on the surfactants). The possibility to profit from the experience with these surfactants were believed to prove helpful in the course of this project, so that we decided to start our experiments with them. Despite the existing publications, of which several already report the formation of self-organised films from these molecules [94, 95, 96, 97], their thin films still needed to be investigated with surface analytical methods. The mechanism, via which the surfactants bind to the substrate, is, for instance, not unambiguously clear for all experimental conditions and may be unsuitable for the functionalisation of mica particles (see chapter 6). Additionally, a high probability existed, that fundamentally different types of films can form depending on the exact preparation and that again several preparative protocols were not applicable for mica particles.

5.2 The structure of muscovite mica.

Muscovite mica is a layered silicate like other clay minerals such as vermiculite or montmorillonite. Its crystal structure (see figure 5.1) is a succession of negatively charged two-dimensional layers held together by (potassium) cations. Due to the difference in bonding strength, between the "ionic" interlayer and the covalent intralayer forces, muscovite mica preferentially cleaves between two layers. This anisotropy is so pronounced, that the atomically flat terraces of cleaved mica are substantially larger than for instance on silicon substrates. They are considered to extend over areas of about $1\mu m^2$ [98] but even larger terrace sizes of several square centimeters have been reported [39].

Nearly ideally flat mica surfaces can be produced via a simple cleaving process, which explains, why mica is a common model substrate for surface studies in which zero-roughness is required (e.g. AFM and the Surface Forces Apparatus, which also needs thin and transparent substrates and hence extensively relies on muscovite mica). It is even possible to transfer this flatness to thin gold [99] and silver [100] samples, thereby producing ultraflat metallic surfaces.

An individual layer of muscovite (shown in figure 5.1 b) is a symmetric sandwich of octahedrally coordinated aluminium atoms (see figure 5.1 a) between two layers of SiO_4-tetrahedrons. Three out of four of these tetragonally coordinated oxygen atoms lie on the outer side of the mica layers, where they form a planar hexagonal network (see figure 5.1 c), in which every apex oxygen atom is shared between two tetrahedrons. One quarter of all the silicon atoms is replaced by isomorphous aluminium (Al^-) anions, thus rendering the layers negatively charged. The unshared, inwards facing, oxygen atoms are bound to the central aluminium atoms and occupy half their octahedral binding sites – the other half is filled by hydroxyl groups (see figure 5.1 a).

In accordance with this description, the chemical formula of muscovite mica is $KAl_2(AlSi_3O_{10}(OH)_2)$. Depending on its place of formation, the chemical composition of natural mica can deviate from the ideal structure. Muscovite mica can, for instance, contain other metals (e.g. magnesium [88]) instead of aluminium and potassium and can also incorporate alien species (e.g. graphite) to some extent [101, 102]. The interlayer potassium ions are twelve-fold coordinated and lie in the indentations of the hexagons

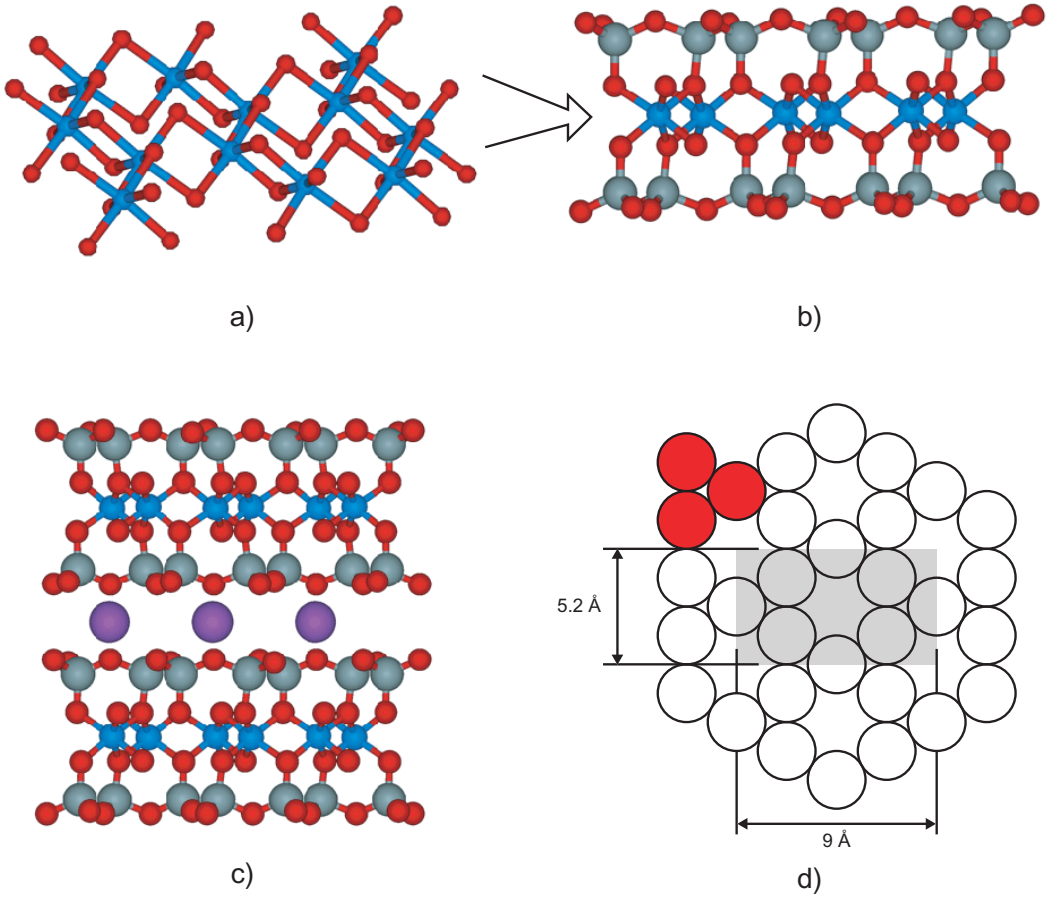

Figure 5.1: The crystal structure of muscovite mica. a) The inner octahedrons of aluminium atoms b) Side view of a single mica layer showing the silicon oxide tetrahedrons and the sandwich structures. c) Side view of two adjacent layers together with the interlayer cations that hold the layers together d) Top view of a mica layer, showing the hexagonal network of oxygen atoms. The three atoms coloured in red belong to one SiO_4 tetrahedron.

formed by the apecial oxygen atoms (see figure 5.1 c/d). After cleavage, approximately half of the potassium ions remain on each of the two newly formed surfaces, thereby occupying an average area of $48\mathring{A}^2$ which corresponds to $2.1{\cdot}10^{14}$ (or $3.5{\cdot}10^{-10}$Mol) ions per square centimeter [103]. The cations on the surface can be completely replaced by a number of ions in a solution, but apart from very small mica particles (i.e. partially delaminated) no intercalation occurs under standard conditions (e.g. temperature and

pressure) so that only the surface ions are exchanged.

5.3 Quaternary ammonium salts.

We started our investigations with quaternary alkylammonium ions because of the existing publications of their thin films on mica and their commercial availability. The quaternary ammonium group possesses four chemical docking sites, to one or more of which an alkane spacer can be attached, so that the spacer density can be changed in multiples (1–4) of the headgroup density. For ions with more than one spacer group, these can be individually endfunctionalised, so that films, which are chemically mixed on a molecular level and for which no danger of demixing and island formation exists (see chapter 3). Similarly, the spacers can also contain different numbers of methylene units to produce asymmetrically long surfactants. The ammonium headgroup is onefold positively charged, so that the density of such ions after a complete ion exchange, is given by the cation density of natural mica, which amounts to one cation per $48\mathring{A}^2$, a mean area per ions about twice as large as the area per thiol group on gold (i.e. $21\mathring{A}^2$ [19]). Using dialkylammonium ions (i.e. ammonium ions to which two alkane chains are attached) it is thus possible to reach a similar density of alkane spacers ($1/24\mathring{A}^2$) as in alkanethiol-SAMs on gold, the most studied SAM-forming system. From studies on these molecules [32,33], this density is known to be a decisive parameter for the formation of highly ordered films. Even at full coverage, films of single-chained alkylammonium ions would thus not be dense enough, for the interchain VdW forces to reach the necessary strength so that no conformational ordering would be induced into the chains (compare with [90]). Preceding studies of Brovelli et al. [104] confirmed this dependence of conformational order on the number of spacers per headgroup. Based on this argument, our studies focussed on doublechained dialkylammonium ions. Monomolecular films of dialkylammonium ions formed on mica resemble alkanethiols on gold and other SAM-forming molecules in various respects. The molecules are also strongly bound to the substrate by a specific headgroup and the two-dimensional arrangement of the headgroups is templated by the regular structure of the substrate. Additionally, a density of alkane spacers close to that in many other SAMs can be reached. From all these parallels, it can be expected, that structurally similar organic adlayers are formed, in

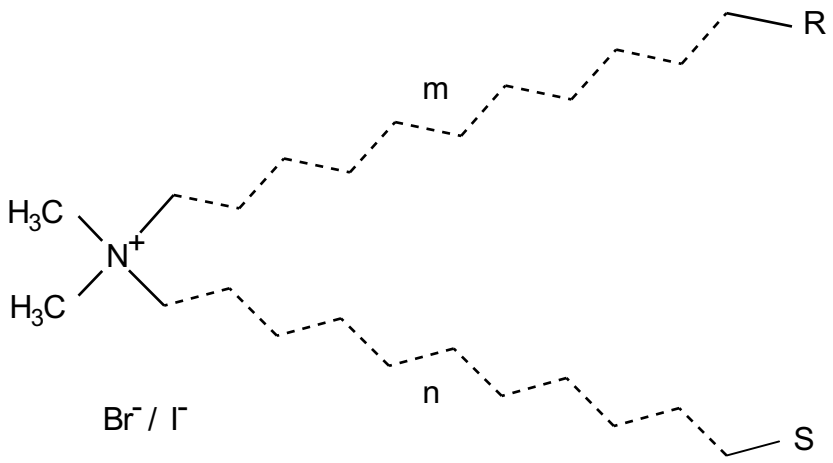

Figure 5.2: The general structure of a dialkylammonium ion, our initial choice for SAM deposition on muscovite mica.

which the alkane spacers also obtain a tilted all-trans conformation. Apart from being fundamentally similar to alkanethiols, there also exist two important differences to the latter. On the one hand, two alkane spacers are united at one single headgroup, in the proximity of which, they will mutually obstruct each other in adopting the ideal conformation. The lowermost part of the films will hence likely be distorted, respectively adapt another conformation than the tilted chains in the upper parts of the film. In this case, the methylene units closest to the headgroup may not contribute to the energy gain as strongly as the upper parts, so that longer alkane chains will be required for order to start (see chapter 7). The general structure for the investigated cations is: $(CH_3)_2N^+(CH_2)_mR(CH_2)_nS$ and is shown in figure 5.2. Most of our surfactants had bromide as the counterion but in some cases we also used an iodide salt. For an ion exchange of free ions out of solution, the counterion is, in first approximation, not expected to affect the film structure, so that the films can be compared with each other, regardless of the counterion.

Throughout the thesis, we will refer to the salts and the free cation by the same name for simplicity, wherever this distinction is clear from the context. Using the notations in figure 5.2 we abbreviated the compounds according to the following scheme: CnCm if R=S=CH_3

Abbreviation	Full structure	Source
C8C8	$(CH_3)_2N^+(CH_2)_7CH_3(CH_2)_7CH_3$ I^-	Caseri/ Ranieri [105]
C12C12	$(CH_3)_2N^+(CH_2)_{11}CH_3(CH_2)_{11}CH_3$ I^-	Fluka
C14C14	$(CH_3)_2N^+(CH_2)_{13}CH_3(CH_2)_{13}CH_3$ Br^-	Fluka
C16C16	$(CH_3)_2N^+(CH_2)_{15}CH_3(CH_2)_{16}CH_3$ Br^-	Fluka
C18C18	$(CH_3)_2N^+(CH_2)_7CH_3(CH_2)_{17}CH_3$ Br^-	Fluka
C8C8C8	$(CH_3)N^+\{(CH_2)_7CH_3\}_3$ Br^-	Aldrich

Table 5.1: Summary of all the different di-alkylammonium ions used in this thesis

and Cm if R=CH_3 n=0 S≠CH_3. All commercially available compounds were bought from commercial suppliers in analysis quality (p.a.≥98%). Some surfactants, however, had to be synthesised specifically for these experiments. W. Caseri (with the help of G. Ranieri, both IfP, ETHZ) carried out all these syntheses according to procedures presented in literature (see for instance [105]), recrystallised the products and performed an elemental analysis to confirm the chemical composition. We used all surfactants without any further cleaning. Table 5.1 summarises the chemical structures, supplier (respectively name of the chemist who synthesised the compound as well as reference to the synthetic procedure) and the abbreviation of the compound.

We chose to use the same working concentrations as Seimiya et al. [94] because of various reasons, which simplify the interpretation of the experiments. All the salts are soluble in these concentrations in warm and cold water as well as in all the other solvents used in this thesis (see chapter 5.4). Additionally, they all lie below the critical micelle concentration (CMC), the concentration above which the ions stop being present as free ions but form supermolecular structures in order to reduce hydrophobic interactions. The absence of micelles is proven by the fact, that the ions are soluble in this concentrations at temperatures below the "Krafft"-temperature, the temperature at which the solubility equals the CMC [106], tabulated reference values [107] and test measurements of the specific resistivity in function of the concentration. Micelles may drastically alter film formation (see chapter 6) so that their absence helps exclude several film structures. Finally, the volumes of our pill glasses (5ml) contain a high excess of free ions at these concentrations, so that

complete ion exchange is not limited by the concentration. A complete ion exchange will hence occur as long as this is energetically favoured and that there are no kinetic barriers preventing SAM formation.

5.4 Experimental

5.4.1 Materials

Muscovite mica. We bought muscovite mica in sheet form from Provac (Product number P-OTS-06027 T, BALZERS, Liechtenstein). Samples were cleaved on both sides using adhesive tape immediately before use (e.g. ion exchange) in order to minimise contamination of the extremely high energy surfaces [108]. As mentioned above, the chemical composition of natural muscovite mica can deviate from the ideal one, for instance through the incorporation of alien materials (e.g. graphite). We indeed detected traces of carbon in some batches of muscovite, which we believe to stem from the bulk rather than from the surface region (see chapter 8).

Lithium chloride ($\geq$98%) was obtained from (Fluka,Buchs, Switzerland) and used without any purification. Lithium cations are well-known to exchange all the potassium ions on the surface planes of muscovite and have been shown to increase the rate and/ or the maximal surface coverage of a subsequent ion exchange [109]. The reason for the advantageous role of LiCl is thought to lie in its smaller ionic radius. Ion exchange in contrast to covalent adsorption, always necessitates one species to desorb (nearly) simultaneously to the adsorption of the replacing surfactant. In denser films, this two-particle process can effectively be limited by the steric restrictions imposed by the entering and the leaving species so that ions with a lower ionic radius will be replaced faster and easier. We hence exchanged the potassium ions by lithium ions before the actual ion exchange, where not explicitly stated otherwise. For this initial exchange, we used aqueous lithium chloride solutions with a large excess of lithium in solution (i.e. concentration 0.5–1M) and immersed the samples for at least 3 days before any subsequent use. In XPS measurements (not shown), the potassium signal reaches its minimum after $\leq$1 day so that a complete ion exchange is guaranteed after this time, while the associated increase of the lithium signal cannot not be detected because of a low elemental sensitivity factor (see chapter

2.2). After this intermediate ion exchange, all the samples were taken out of the LiCl solutions and thoroughly rinsed with clean water in order to remove any loosely bound lithium still present on the surface. Very rarely, control XPS spectra of such samples revealed traces of lithium on the mica, in which case the counter-ion (chlorine) was also detected. This indicated, that some salt, which was loosely bound to the mica had not been washed off during the cleaning procedure and such samples were discarded from any further treatment.

Solvents. During the experiments, various solvents were used. In the majority of the experiments, we prepared the films from aqueous solutions but more recently the focus has shifted towards a number of organic solvents and their mixtures with water (see chapter 6 for more details). As water, only fresh ultrapure water (Easypure, Barnstead, $\geq$18.2MΩ cm^{-1}) was used in any stage of sample preparation. Organic solvents included cyclohexanol ($C_6H_{11}OH$), methanol, ethanol and chloroform, which we bought from Fluka (Buchs, Switzerland) in analysis quality (p.a. $\geq$98%) and used without any further purification.

Cleaning of glassware. Any glassware used in the process of preparing solutions, exchanging the surface ions on mica or rinsing a sample, was carefully cleaned to minimise an effect of contamination. First, all glassware was extensively washed with water and soap to remove any loosely bound material. After rinsing with deionised water, the samples were then immersed (24h) into a cleaning solution of RBS-50 (Fluka, Buchs, Switzerland), in which organic contaminants were dissolved and subsequently rinsed with deionised water again. Traces of ions on the glass surfaces were removed by immersion into a bath of sulfuric acid (4%, 24h) rinsing with ultrapure water and immersion of freshly prepared aqueous (ultrapure water) solutions of nitric acid (30% nitric acid, 24h). Finally, the samples were thoroughly rinsed with ultrapure water and dried in an oven. During the time (less than one month) drying and use, the glassware was stored in a sealed condition.

Film preparation always consisted of an immersion of mica sheets into solutions of the ammonium ions. Usually, the apex ions were exchanged by lithium ions first, in order to accelerate a subsequent ion exchange and to increase the final coverage [109]. In some cases we however refrained from this measure for experimental reasons (see

chapter 6). Investigations on non-lithium exchanged mica will be specifically denoted and substrates will be differentiated by the surface cation present before the ion exchange with ammonium ions (i.e. K- respectively Li-mica). The study of non-lithium exchanged K-mica helps to reveal an influence of the lithium pretreatment and makes it possible to follow the ion exchange with XPS via the decrease of the potassium signal. This is not possible with lithium-exchanged mica because of the low elemental sensitivity factor of lithium (see chapter 2.2). All the solutions except cyclohexanol (which freezes) were stored in the refrigerator (approx 5±3°), again abiding the preparative procedure of Seimiya et al. [94]. The standard time of immersion was three days after which no changes in the film structure were found to occur. After this time, the samples were taken out of the solutions, thoroughly rinsed with water and stirred in pure water for 30 seconds and finally blow-dried under a stream of nitrogen.

5.4.2 Methods

Contact angle measurements. Advancing water contact angle measurements were performed under standard conditions (see chapter 2). All the experimental values are the average of four samples, on each of which two drops were measured. Occasionally, water contact angles were substantially lower on one spot of a substrate or the drop obtained an irregular borderline on the substrate. Such exceptions are suspected to be connected with a partial exfoliation in the solution and the data of such samples were discarded before any further analysis. We will discuss the interpretation of the contact angles in the following chapters and mention, that this is not completely clear just like the results of other research groups. In summary (see chapters 6 and 7), the experimental values lie below the expected reference data and are apparently in contradiction to the results from other techniques.

Islands of the surfactant molecules on the substrate or molecules adsorbed in an end-on conformation were proposed as models, with which the unexpectedly low contact angles could be explained (again see chapter 6). In both of these extensions to the simple SAM model, a strong dependence of the experimental water contact angles on any contact of the samples with water after the extraction must be expected, so that the specific

procedure of measuring this angle may influence the outcome of such experiments. Also, because these films bring the danger of a facilitated dissolution of the molecules with them, the contact angles will notably not be "equilibrium" quantities any more but rather decrease over time. All the data presented in this part of the thesis, were measured in air, after about 30($\pm$10) seconds of exposure to air and immediately after the deposition of the water drop. Ambient humidity was not measured and the drying of the samples under the nitrogen typically took about 20–30s.

XPS measurements were performed under standard conditions (see chapter 2.2 for the operational parameters). Before any detail spectra were taken, the chemical integrity of the sample was confirmed by a survey spectrum and an eventual presence of the counterion (i.e. bromide) was detected. Such was only occasionally found and always accompanied by a manifold increase of the ammonium ions, which we interpreted as a sign of insufficient rinsing and loosely bound salt on the mica. Such samples were discarded from further analysis. In accordance with the expected chemical composition of the surface region, detail spectra of the following spectral regions were subsequently measured:

A severe charging (approx. 4eV) of the samples occurs upon irradiation of muscovite mica with X-rays because it is strongly insulating. This was corrected in the data analysis by shifting the spectra with respect to the reference energy (285.0eV See chapter 2.2 and [110]) of the aliphatic C1s peak. In order to obtain quantitative information about the chemical composition of the surface region, the area below the photo-electric peaks in the spectra were numerically integrated. A background from non-element-specific electrons was subtracted using a standard model (see chapter 2.2). The instrumental transmission function was not taken into account, so that it is impossible to deduce quantitative ratios between the different elements. Assuming a temporally constant transmission function, the quantitative amounts of one element can, however, be compared between different samples. Test experiments on freshly cleaved mica from a single batch showed, that no changes of the transmission function occurred over the time of experiments (approx. 1 month) within the accuracy of the instrument.

The degree of coverage can be monitored by normalising the signals of nitrogen (and potassium for K-mica) to that of oxygen if a reference of given coverage is available. In this case, the amount of oxygen remains constant during ion-exchange and is attenuated

Region	Energy region [eV]	Number of scans
C 1s	280–307	90–120
K 2p	280-307	90–120
K 2s	372–392	90
N 1s	394–414	300
O 1s	525–545	15
Al 2s	113–133	60
Si 2p	95–115	90
Si 2s	145–165	90
Li 1s	47–67	90
Br 3p	178–198	30

Table 5.2: Regions for which detail spectra were acquired with XPS. Note that some regions uniquely belong to the substrate (e.g. K, Al, Oxygen) while others are only found in the surfactant (e.g. N, C in the absence of contamination).

by the overlayer in the same degree as all the other substrate peaks and the nitrogen peak from the bonding ammonium headgroup, if the nitrogen is located directly at the mica surface.

NEXAFS. All the NEXAFS spectra were acquired under standard conditions (see chapter 1). Because of the severe charging due to X-ray irradiation, the use of a neutralising electron floodgun was necessary for all the films on mica (see section 1.6). All the necessary care was taken to minimise and to judge any influence of the low energy electron current on the integrity of the samples, especially on the organic adlayers. Experiments, in which a particular angle of photon incidence was measured twice after different times of exposition to both the X-ray beam and the neutralising electrons on the same sample, never suggested any dependence on time and the typical sign of radiation damage, the growth of a pre-edge π^*-resonance [82] was never observed either. In accordance with the molecular structure of the surfactants, we measured NEXAFS spectra at the 1s edges of carbon (275–325eV) and nitrogen (380–430eV).

Chemical composition – carbon. Figure 5.3 exemplarily shows the NEXAFS spectrum

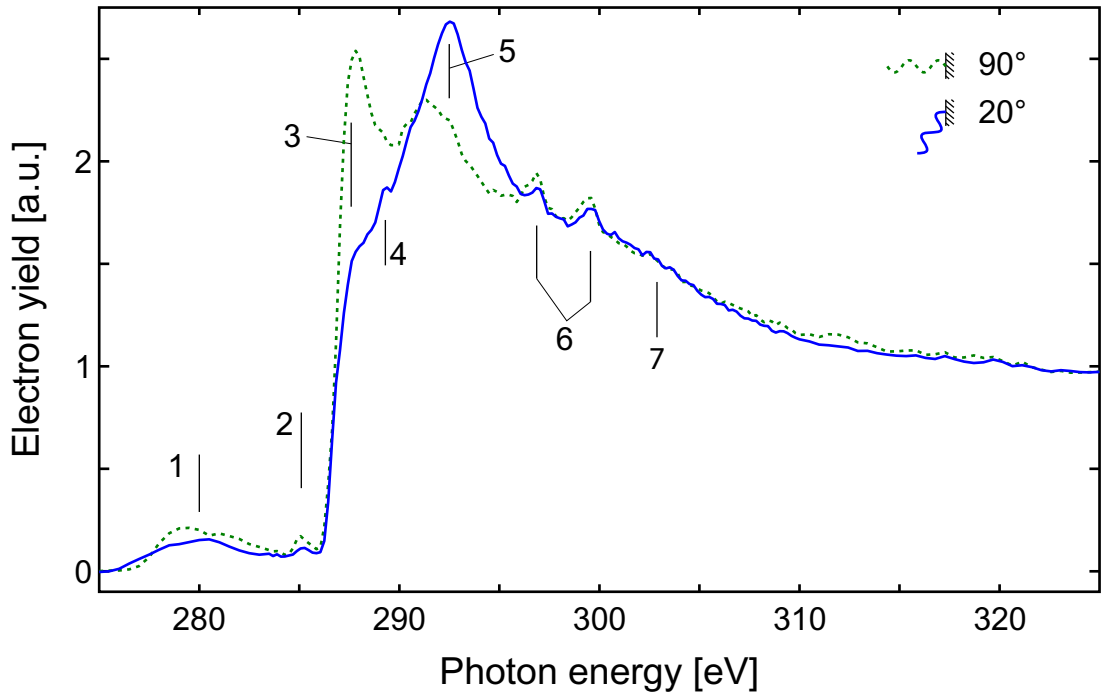

Figure 5.3: NEXAFS spectrum in the C1s region of C14C14

of C14C14 adsorbed onto muscovite mica from an alcohol/ water mixture (see chapter 7 for more details) at grazing (20°) and normal (90°) angle of photon incidence. The carbon spectra of all the (di-)alkylammonium ions on mica all showed the same features with varying relative intensities. At 280(1)eV a first broad resonance (1) is found, which stems from second order photons inducing electron transitions from the 1s orbital of oxygen atoms in the bulk (see chapter 1.6). We sometimes observed a next resonance (2) at 285(0.5)eV, which is attributed to transitions into orbitals with a π^*-symmetry (C1s $\rightarrow \pi^*$). This transition is symmetry-forbidden (see chapter 1.3) for alkane chains, so that the presence of this resonance implies a further carbon species other than the surfactant in the surface region. Muscovite mica can incorporate carbon (e.g. graphite [101,102]) during its formation so that the exact location of this additional species within the surface region is not clear and can also lie within the mica bulk itself. We believe, that this resonance may indeed stem from incorporated carbon, as it was consistently observed or absent for mica samples from a particular batch, while no correlation with the choice of surfactant

or other experimental parameters was found. This hypothesis was further strengthened by NEXAFS experiments of freshly cleaved mica from such a batch, in which the same resonance was also observed (see figure 8.3 in chapter 8).

The next spectral feature (3) lies at 287.6(2)eV. It is observed in all alkane-based SAMs and stems from transitions into final states which are a mixture of atomic orbitals of both carbon an hydrogen. As discussed in details at another place in this thesis (see chapter 3), this resonance is a superposition of several electronic transitions that cannot be separated due to the limited energy resolution and hence appear as one transition with a TDM perpendicular to the alkane chains [48]. Directly above this resonance, the 1s absorption edge of carbon with a reference energy of 288.1(5)eV [49] follows. No decomposition of this spectral region into all the individual constituents was performed, so that no exact estimation the steps energy position is possible, but our experiments are in full agreement with the reference value. The origin of the small peak (4) at 289.0(5)eV is not clear and this feature may also be an artefact from the correction of the spectral transmission function (see chapter 1.7). We only observe it in some spectra and propose its attribution to a transition into a σ^* orbital (i.e. C1s$\rightarrow$ σ^*(CN [111]/ CO [49]) which does not exist in for methylterminated alkanethiols on gold.

At higher photon energies, a second alkane related resonance (5) is found centered at 292.5(5)eV. It is present in all NEXAFS spectra of alkane-based surfactants and stems from transitions of the kind C1s $\rightarrow$ σ^*(CC). The next two transitions (6) arise from electronic transitions in the interlayer potassium ions of mica (K2p$\rightarrow$3d [112]). They gradually vanish with increasing thickness of the adlayer. For C18C18 films, they are nearly completely missing, while they clearly protrude out of C8C8 spectra (see figure 7.1 for both these spectra). Finally, a further transition (7) into an orbital with σ^*(CC) symmetry is sometimes discernible at 302(1)eV. It has a low oscillator strength and hence appears very weakly or is lost in the experimental noise. Table 5.3 presents all the NEXAFS features in the carbon 1s region for alkylammonium ions on mica.

Only the alkane-related R* (2) and σ^*(CC/ CO) (5) resonances showed an angular dependence in some cases, while the intensity of all the other features in the carbon region remained unaffected by a change in the incidence angle as expected. The angular variations of these two resonances give insight into the conformation of the alkane chains,

Number	Energy [eV]	Transition
1	280(1)	Oxygen
2	285	C1s→ π^*
3	287.6	R^*
4	289	C1s→ σ (CN/ CO)
5	292.5	C1s→ σ^* (CC)
6	297.2 & 300.0	K2p→3d
7	303	C1s→ σ^*
1	401(1)eV	unknown, possibly N1s→ π^3 (NC)
2	407(1)eV	unknown

Table 5.3: NEXAFS resonances in the carbon and nitrogen 1s regions for alkylammonium ions.

indicates a regular arrangement and can be used to quantify the degree of conformational order in the organic films. From the peak intensities at different angles of photon incidence, we calculated the average tilt angles of the corresponding TDMs using the method of "difference spectra" [10], using films of alkanethiols on gold were as reference for the machine factor (see chapter 1).

NEXAFS – nitrogen. All the NEXAFS spectra of dialkylammonium ions in the nitrogen region exhibit a low signal-to-noise ratio. This is demonstrated in figure 5.4, which exemplarily shows the NEXAFS spectrum of C16C16 adsorbed onto mica from an alcohol/ water-mixture. Because of this low statistical significance, the underlying slope, which is a relict from the correction of the transmission function (see chapter 1.7) could not be successfully be subtracted from the spectra in all cases. In contrast to the carbon edge, we did not have an energy reference sample so that the energy calibration was performed by means of the features in the spectra themselves. The adjustment was made difficult by the lack of any sharp and prominent features, with which an energy correction would be simplified, and because no NEXAFS data for chemically equivalent species were available.

Three spectral features can be found in the nitrogen region, of which only two are always present. These include the absorption edge, which was measured to lie at 407(1)eV and

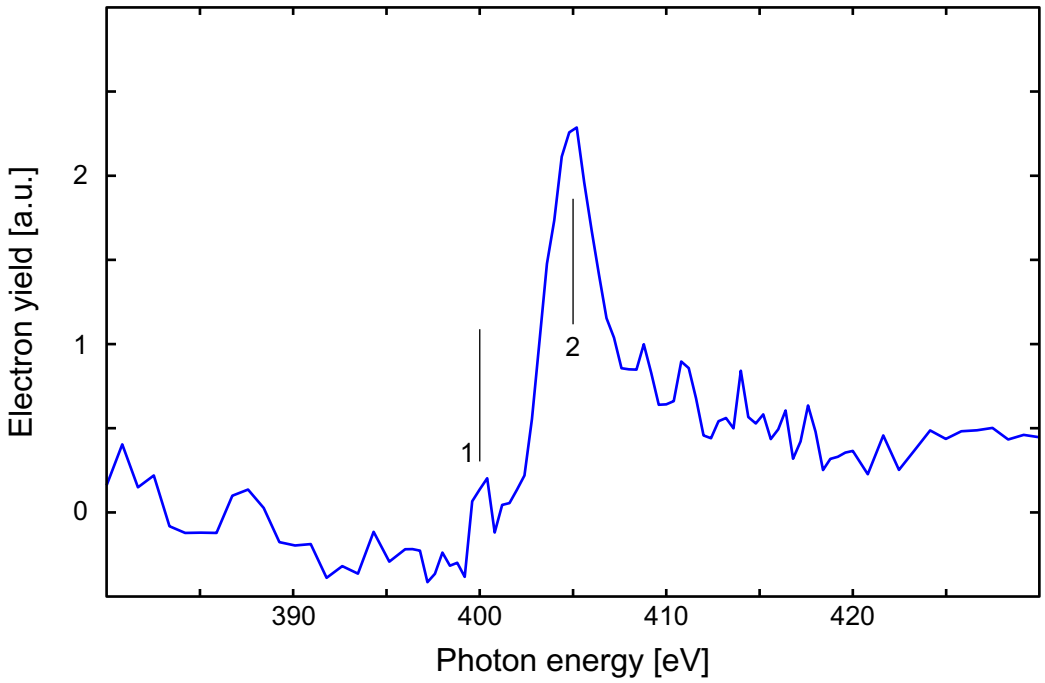

Figure 5.4: NEXAFS spectrum in the N1s region of C16C16. All the spectra showed a high amount of noise and one (possibly two) resonances

a broad resonance (2) situated above the step and centered at 408(1)eV (all [113]). In analogy with other NEXAFS experiments [2], we attribute it to transitions into a final orbital with σ^* symmetry (i.e. C1s$\rightarrow \sigma^*$(NC)). A third feature (1) lying below the absorption edge at 401(1)eV was sometimes observed. We did not find any correlation between its presence in the spectra and a particular experimental parameter (e.g. surfactant). Its energy position in respect to the absorption edge makes transitions of the kind N1s$\rightarrow \pi^*$ the most probable origin of this resonance. Its genuineness is, however, not confirmed and it may also stem from the data normalisation. For the tetragonal ammonium group, a π^*-resonance would be symmetry forbidden and nitrogen-containing contaminants are not often observed, so that the origin of such a peak is not be understood. No feature in the nitrogen 1s region ever showed any dependence on the angle of photon incidence, which is expected for a tetragonal structure like the ammonium group. The signal-to-noise ratio is explained by the low fraction of nitrogen present on the surface and would make the detection of weak angle-dependencies impossible.

Chapter 6

Solvent dependence of conformational order and film formation.

6.1 Introduction

The formation of SAMs is a complicated process, in which the different participating building blocks (i.e. substrate, solvent, head- and endgroup or spacer) are interacting with each other at every stage and with different types of forces. Due to the complexity of such the systems, it is hence usually impossible to understand SAM formation in all details. Fortunately, simplified models are often sufficient to explain the resulting film structures. In the most basic view, the adsorption of the surfactants is dominated by the, usually well-understood, attraction of the headgroup and the substrate – thereby determining the surfactant density at complete coverage. Depending on the strength of interspacer forces and forces between neighbouring endgroups in this arrangement, conformational ordering will take place or not. This simplified model, however breaks down if the film formation is complicated by secondary effects, for instance if solvent constituents can also bind to the substrate, the adsorbates interact with the solvent in a special manner or if the endgroup is repelled by the solvent, so that a full ordering, which brings the endgroups into contact with the solvent, is energetically hindered. In the case of ion exchange, it will also be

necessary for the surfacial ions to dissolve, an effect that can normally be neglected for samples with a low surface area, since the quantities of ions are so low, that solubility is not a limiting factor.

In the numerous studies, that were already performed for (di-)alkylammonium ions on mica, the most commonly used solvent was water. Unfortunately, water brings some of the above-mentioned complications with it. It is polar and thus attracted to the charged mica surface [114, 108] – as demonstrated by the vanishing water contact angle of mica. Due to autoprotolysis, water also contains free protons and hydroxyl ions, which can influence the film formation of ammonium ions by competitive ion exchange (H^+) or by an incorporation of anions. At normal pH values, their concentrations are substantially lower than those of the surfactant ions, so that they will only play a role if the adsorption of the surfactants is hindered in some way. Strongly repulsive hydrophobic interactions are acting between the alkane spacers of the surfactants and water molecules in solution. This force component accounts for the low solubility of (di-)alkylammonium ions in water, which becomes worse with increasing alkane chainlength and is much lower than in other polar and apolar solvents [105]). Similarly to other amphiphilic surfactants, (di-)alkylammonium ions strive to minimise the strength of these interactions in water and can, in the course, form various types of agglomerates, in which the exposure of the spacers to water is reduced [115]. Langmuir layers [24, 91], monolayers of increased ion density at the water/ air interface, and micelles represent examples of such agglomerates.

Monolayer structures can also form from solutions, in which the surfactants are agglomerated but the kinetics are qualitatively different from those of free ions adsorbing onto a substrate, because the agglomerates adsorb intact and then unfold on the surface [95]. During this phase, numerous rearrangements have to take part, which complicate the adsorption process and hence slow it down in comparison to the adsorption of free ions.

For the success of this project, it is vital to understand the influence of the solvent on the resulting layers, and the binding mechanism of the surfactants to the substrate. A substantial amount of work has already been carried out on these systems but most groups used different experimental conditions, analytical methods and solvents. If some publications hence apparently contradict each other, then the origin of these disagreements is not unambiguously clear, so that they may stem from the different conditions rather than

experimental or interpretative mistakes. For the desired functionalisation of mica particles for polymer composites, a strong bond between the organic adlayer and the mica is mandatory for the transfer of loads between matrix and filler. Additionally, the entire working principle of a SAM is based on the location of the functional endgroups in the topmost region of the film. This is, however, only fixed if the molecules adsorb onto the substrate with the headgroups facing the substrate. In order to exclude end-on adsorption, a direct binding of the headgroup to the substrate hence represents a necessary condition, without which the SAM method cannot work.

Apart from ion exchange, other film forming mechanisms out of aqueous solutions exist, some of which have already been observed. Surfactant ions can, for instance, agglomerate directly on the mica substrate to form islands, in which hydrophobic interactions are reduced in comparison to the free ions in solution [115]. In this case, the headgroup could, however, also be facing the solution. In fact, no ion exchange has to take place in this mechanism, if the positive charge of the surfactants is compensated by incorporated anions and island formation has already been observed with octadecylphosphonic acid [116], which carries the opposite sign of charge, so that a direct ionic bond is impossible. Similarly, micellar structures (i.e. "hemimicelles" [117]) can grow on the substrates – especially above the CMC [118]. If micelles are present in the solution, then they can also adsorb and remain intact or unfold to form multilayer structures [115]. Finally, a "Langmuir-Blodgett"(LB)-type of film can also be deposited when the sample passes through the water/ air interface (in both directions, see [91] pages 2317–2344).

All these types of films fail to fulfill the requirements of the designated chemical functionalisation of mica. They lack a strong bond to the substrate, especially because their energetic basis is partially eradicated when the surrounding water is removed. Consequently, they fall short in terms of mechanical stability, so that loads could not be transferred from polymer matrices to the embedded mica particles. Because the conformation of the molecules within these types of films is less well-defined, the positional restriction for the functional endgroups falls away, so that, apart from the stability, the chemical functionality may also be lost. Furthermore, if the interaction between the surfactant and the solvent plays a crucial role for the molecular structures in the resulting films, then a change of the chemical endgroup can result in qualitatively different films, because the latter molecular

block also interacts with solvent constituents. As a consequence, the method would loose its modular flexibility and new preparative procedures might have to be identified upon every change of functional chemical endgroup. Finally, a later transfer of the experimental procedures to microscopic mica particles is no longer guaranteed if parameters like the surfactant density on the water surface or the speed, at which these are pulled through the interface, strongly influence the film formation (i.e. LB-deposition).

As outlined in the previous chapter (see chapter 5), the initial stage of establishing a SAM technique suitable for macroscopic mica samples as well as mica particles alike, consists of finding suitable surfactants and preparative procedures. In the case of dialkylammonium ions, this includes the proof of ion exchange because a strong bond between the headgroup and the substrate – a crucial requirement for the success of the SAM method – can only be established with this binding mechanism. Due to the paths of interactions between the solvent (especially water) and the surfactants and substrate, its choice must a priori be assumed to strongly influence the ease of preparation as well as the resulting film structure. Experiments of Brovelli et al. [104], upon which these experiments build, have shown, that it is, in principle, possible to obtain well-ordered films from an aqueous solution but this experimental protocol was associated with a problematic dissolution and brings the danger of agglomeration within the solvent (especially if it should become necessary to switch to higher concentrations), with it. We hence investigated, if more highly-ordered films can be prepared or if the preparative procedure could be simplified, by changing the solvent. Finally, understanding the binding mechanism and the solvent dependence, will also help to clarify the comparison between our results and those from other experimental groups. A substantial number of publications on thin films on mica already exists, which seem to contradict each other in some cases (see for instance [95] and [104]). By identifying the influence of the solvent, it may become possible to subsequently profit from this experience and thus accelerate our further progress.

6.2 Experimental

Samples were investigated with water contact angle experiments, XPS as well as NEXAFS according to the procedures presented in the introductory chapter (see chapter 5). We were

interested in two questions, namely the fundamental route, by which films form, as well as the degree of conformational order in dependence of the solvent. Several fundamentally different ways of film formation may exist, of which not all are suitable for the designated functionalisation. Especially from aqueous solutions it is not clear, which force component dominates, so that investigations of the binding mechanism were necessary, before it was possible to direct the attention towards novel surfactants with different chemical endgroups.

As explained in the introduction of this chapter, we depend on a film formation by ion exchange, because this fixes the location of the endgroup and a ensures sufficient binding strength. In principle, the proof of ion exchange consists of showing the removal of the initially present ions, complete coverage with ammonium ions as well as the absence of any counterions. For Li-mica, it is however experimentally impossible to quantify the amount of lithium on the surface of a low surface-area mica sheet with XPS, even at full coverage, because of its low elemental sensitivity factor. Depending on the predominating force components, the resulting films can differ in three ways. If no ion exchange takes place, counterions will be present in the films. This may, for instance, be the case for apolar solvents, in which the surfactants are dissolved as ion pairs. Secondly, large differences in the coverage may occur, depending on the energy gain due to the adsorption. Both of these effects can be observed with XPS and the second one also with contact angle measurements, our two laboratory-based techniques.

Finally, even ion-exchanged films with a quantitatively similar surfactant density can exhibit large differences in their degree of conformational order. Conformational order, the prerequisite for the SAM-method, will only begin to establish during the final phase of adsorption, when the density of adsorbed molecules is close to its maximum and internal rearrangements take place [90, 32, 33]. Even second-order effects can decisively affect this final stage of the film formation and thus change the degree of internal order that is finally reached. XPS is not sensitive to such small differences in coverage. On the basis of the experimental water contact angles, such quantifications are in principle possible (see chapter 2). However, previous studies (see for instance [119]) have revealed unexpectedly low contact angles for these films, which cannot be interpreted entirely in terms of alkanechain ordering. Because of these discoveries, we used NEXAFS, with which conformational order

	N(1s)/ O(1s)	Contact angle
freshly cleaved	$\equiv 0$	$<10°$
10 seconds	0.0061(19)	59(7)°
1 minute	0.0093(30)	64(9)°
10 minutes	0.0130(15)	85(4)°
3 days	0.0120(30)	89(2)°

Table 6.1: Amount of nitrogen on the surface (no calibration of the experimental transmission function) and the advancing contact angle of mica samples immersed into an aqueous solution of C18C18 for varying lengths of time.

within the adlayer is directly probed and the spectra of which are easier to interpret in terms of conformational order.

6.3 Results

Proof of an adsorption in solution. In a first step, we investigated, whether an adsorption takes place in solutions or whether LB-type of film deposition occurs. Because hydrophobic interactions play an important role for aqueous solutions of C18C18, as manifested by the low solubility [105] and CMC [107], a Langmuir film can be expected at the water/ air interface so that a deposition of molecules during the transfer through this is possible. Table 6.1 shows the water contact angle as well as the nitrogen (N1s) to oxygen (O1s) ratio for samples of Li-mica, which were immersed into an aqueous solution of C18C18 for different lengths of time ranging from 10s to 3 days.

A clear increase in contact angle and nitrogen content can be recognised during the first 10 minutes of immersion. Such would not be observed for LB-films, since the only important parameters in that case are the density of molecules at the water interface as well as the speed at which the sample is transferred through the interface [24], both of which were not changed during these experiments. If an adsorption takes place in the solvent itself, then the resulting coverage will increase as a function of time and equilibrium will only eventually be reached. Fortunately, at the standard concentrations, the rate of adsorption lies on the same time scale as the one on which we measured, but rate constants can be

	K(2s)/ O(1s)	K(2p)/ O(1s)	N(1s)/ O(1s)
freshly cleaved	0.051(2)	0.118(5)	$\equiv 0$
LiCl	0.037(3)	0.089(8)	$\equiv 0$
C18C18 on K-mica	0.034(4)	0.080(11)	0.014(1)
C18C18 on Li-mica	0.039(3)	0.087(8)	0.016(1)

Table 6.2: Amount of nitrogen and potassium (no calibration of the experimental transmission function) and the advancing contact angle on mica surfaces, which were immersed into an aqueous solution of C18C18 for varying lengths of time.

changed, if necessary, by adjusting the surfactant concentration, so that the evolution of an adsorption in solution could be monitored in any case. The observed time dependence shows, that an adsorption takes place in the solution – thus excluding the possibility of an LB-type of film under these conditions.

Binding mechanism. After the confirmation, that an adsorption of the dialkylammonium ions onto mica takes place in the solution, an identification of the binding mechanism, followed. The chemical functionality of a SAM depends on the location of the headgroup at the substrate (which in turn would be guaranteed by the ionic bond between the ammonium group and the substrate) and a film density, which is equivalent to a mean area per alkane spacer of approximately 21Å^2(i.e. the chain density of alkanethiols on gold [19]). Because the replacement of lithium ions cannot be monitored with XPS, we used K-mica immersed into C18C18 for three days instead. In this setup, the height of the potassium signal can be used to quantify the amount of exchanged ions. Potassium is present both in on the surface as well as in the bulk of mica, so that this signal does not decrease to zero even after complete exchange of the surface ions. Lithium is well-known to exchange all the surface ions of mica [109]. We immersed freshly cleaved mica substrates into concentrated (i.e. 1M) solutions of LiCl for a prolonged time (i.e. more than 2 days). This treatment ensured all surface potassium ions to be replaced, so that the potassium signal from these samples could be used as a reference for complete ion exchange, to which the potassium signal of the C18C18 samples could be compared.

Table 6.2 shows the amounts of potassium and nitrogen normalised to the substrate oxy-

gen peak – thus compensating for an attenuation due to the organic adlayer, so that they can be compared to each other. In comparison to freshly cleaved mica, the potassium signal decreased as 1:0.72 during the replacement with lithium. This is in good agreement with a theoretical prediction, which assumes half of the potassium ions to belong to each of the newly formed surfaces during cleavage, an electron attenuation length of 2nm [28, 29] and the electron take-off angle of 45° (see chapter 2.2).

After the standard immersion time of K-mica into an aqueous solution of C18C18, the potassium signal decreased to the same level, as the one after an exchange with lithium ions, suggesting that a complete ion exchange had also taken place with C18C18. The possibility of a competitive coadsorption of protons from the water in principle exists, so that these XPS data, while proving ion-exchange, do not necessarily imply, that all the ion sites were filled exclusively with ammonium ions. The experimental sensitivity of the XPS machine, which does not allow the discrimination between 90% and 100% ion exchange must also be borne in mind. For mica samples, where the surface potassium ions were exchanged with lithium ions prior to the C18C18 treatment, no information on the coverage with ammonium ions can be deduced from the potassium signal. As expected, it also lies on the level according to no surface potassium, but this level was of course already reached after the pretreatment and remained unaffected during the adsorption of ammonium ions. The amount of nitrogen on the surface is the same as without the lithium treatment, so that the quantitative surface coverage of ammonium ions is close to the one without the lithium pretreatment. No sign of the most prominent counterion in the solution (i.e. Br^-), was found in any of the spectra. While this is again not a proof of the absence of anions on the surface (OH^{-1} ions cannot be detected), it shows that the surfactants adsorb onto muscovite mica as free ions.

The contact angles of 90(2)° for both Li- and K-mica lie below the reference value of a methyl terminated surface (110°) and surprisingly also below that of a surface covered by methylene groups (103°) [24]. It is hence not possible to obtain structural information from these values and the model of a homogeneous, completely methyl(ene)-covered surface must be extended in order to be consistent with the experimental data. Several explanations, which are compatible with the NEXAFS experiments of Brovelli et al. (who observed similar water contact angles [104]) and the experimental contact angles, exist

including an incomplete coverage with densely packed islands [116, 120, 97] or a fraction of molecules adsorbed in "flip-flop" conformation [95]. For an adsorption out of aqueous solutions, film growth at the border of dense islands is likely to occur. because the hydrophobic interactions of the alkanechains are strongly reduced within the islands of maximal density, so that islands represent an energetically favourable pre-cursor to the complete film. An adsorption in the "flip-flop" arrangement is not the ground state for the adsorption of the surfactants , since the ionic headgroup is separated from the surface by about 2 nm. If, however, hydrophobic interactions reach a substantial strength, then end-on adsorption can be energetically favoured because the endgroups are shielded from the solvent and subsequent dissolution, followed a head-on adsorption, will be strongly kinetically hindered.

For both island formation and "flip-flop" mechanism, it is possible to calculate the fraction of molecules in the "ideal" arrangement from the experimental contact angle by assuming, that this arises from a mixture of "ideal" and "perturbed" fractions according to the Cassies equation [45] (see chapter 3):

$$f \cdot \cos\theta_{\text{ideal}} + (1 - f) \cdot \cos\theta_{\text{perturbed}} = \cos\overline{\theta}_{\text{experimental}} \tag{6.1}$$

Where f denotes the fraction of molecules in the ideal arrangement and $\theta_{\text{perturbed}}$ respectively $\theta_{\text{perturbed}}$ are reference values for the two species, which have to be known from literature. This results in 73(3)% respectively 80(3)% of the films to be in the "ideal" conformation of methyl- or methylene terminated surfaces are assumed for the ideal structures. For $\theta_{\text{perturbed}}$ a value of 0° was assumed. Suter et al. [92, 121] estimate a degree of ion-exchange amounting to 70–80% for ion exchange onto partially delaminated mica particles, which is in excellent agreement with these estimations and strengthens the hypothesis of islands.

Solvent dependence. The solvent dependence was investigated with the aim of improving experimental procedures, obtaining films of a higher degree of internal order and understanding, the apparent contradictions in existing publications by eradicating one free parameter. We prepared films of C12C12 from methanol, water, chloroform, cyclohexanol (C_6OH_{12}) and a 1:1 volumetric mixture of methanol and water in analogy to published preparative methods [121, 95, 96, 97, 119]. Grainger and his colleagues prepared films from

	K(2s)/ O(1s) $\cdot 10^{-2}$	K(2p)/ O(1s) $\cdot 10^{-2}$	N(1s)/ O(1s) $\cdot 10^{-3}$	contact angle
Cyclohexanol	3.3(3)	8.2(7)	8(1)	52(7)°
Chloroform	3.4(3)	8.3 (10)	9(1)	77(5)°
Methanol	3.3(3)	8.1(6)	10(3)	91(1)°
Methanol/ water	3.4(1)	8.4(2)	12(2)	90(1)°
Water	3.1(1)	7.6(2)	8(1)	88(4)°

Table 6.3: Advancing water contact angles and the amount of the two most prominent cations (nitrogen and potassium) in films of C12C12 prepared from different solvents.

cyclohexane [96]. In preliminary experiments, serious problems concerning solubility of our standard concentrations occurred and only very sparse films (water contact angle $\leq$ 45°) could be established. In order to reduce these problems, we chose the slightly more polar [122] cyclohexanol instead.

C12C12 was chosen, because earlier NEXAFS experiments had shown weak signs of internal order in such films, when prepared from aqueous solutions. With such a surfactant it would hence be possible to detect both films with a lower coverage as well as such with a higher degree of internal order than those prepared from aqueous solutions.

From the preparative point of view, all the solutions containing polar non-aqueous solvents (i.e. methanol, methanol/ water, chloroform) exceeded water and the apolar cyclohexanol. In contrast to the latter, a short ultrasonic bath at room temperature was sufficient to completely dissolve the salts in the standard concentrations. For water and cylcolhexanol, this was only possible after a prolonged heating (approx. 50° / approx. 6 hours) and stirring and these solutions both showed the tendency to become unclear again or even for salts to precipitate (i.e. days). Ralston et al. had already demonstrated, that dialkylammoniumions are nearly insoluble in water but can be dissolved in quantitative amounts in polar and apolar organic solvents [105].

Table 6.3 shows the water contact angle as well as the nitrogen (N1s) and potassium (K2s, 2p) signals, normalised to the bulk oxygen signal, of C12C12 after three days of immersion. The solution with cyclohexanol was not stored in the refrigerator, because

	Cyclohexanol	Chloroform	Methanol	Methanol/ water	Water
CH_3	0.29(7)	0.58(6)	0.76(2)	0.75(2)	0.72(5)
CH_2	0.31(8)	0.63(7)	0.83(2)	0.82(2)	0.79(6)

Table 6.4: Calculated fractions of the mica surfaces, covered with the ideal SAM-chemistry.

it freezes. Again no signs of the counterion (Br^-) were found. In contrast to water, the danger of additional ions from the solvent is strongly reduced for methanol, chloroform or cyclohexanol, so that the absence of bromide can, in these cases, be interpreted as an ion exchange [122]. The amounts of nitrogen on the surface are similar for all the solvents with the exception of cyclohexanol and water, which show slightly less nitrogen on the surface. The difference is, however, in both cases not higher than the experimental tolerance, so that little can be said about the coverage of these films.

More pronounced differences exist in the water contact angles, which are very similar for water, the water/ methanol mixture and methanol, but substantially lower for cyclohexanol and chloroform. This can be explained by a lower coverage respectively a higher number of molecules adsorbing in the "flip-flop" arrangement with the headgroup facing upwards. Since hydrophobic interactions are strongly reduced in comparison to water, the second hypothesis does not appear logical, considering electric neutrality and the absence of counterions. Similar as in the experiments on the binding mechanism, the experimental contact angles can again be transformed into a surface fraction covered by ideal film patches and fractions, in which where the contact angle amounts to 0° , such as bare mica or molecules in "flip-flop" arrangement. This estimation was again performed using the Cassie equation (equation 6.1) and the results are shown in table 6.4. It is not clear, whether the films from cyclohexanol and chloroform are in equilibrium or if higher coverages could be reached after a longer time of immersion. Since other research groups used shorter immersion times, and since the time, required for the establishment of a highly-ordered SAM, represents a vital quality in the assessment of solvents for their suitability with respect to the functionalisation of mica particles for industrial applications, we refrained from analysing samples, which were immersed into these solvents for longer times.

Methanol, water and a 1:1 volumetric mixture of the two, rendered films of the same den-

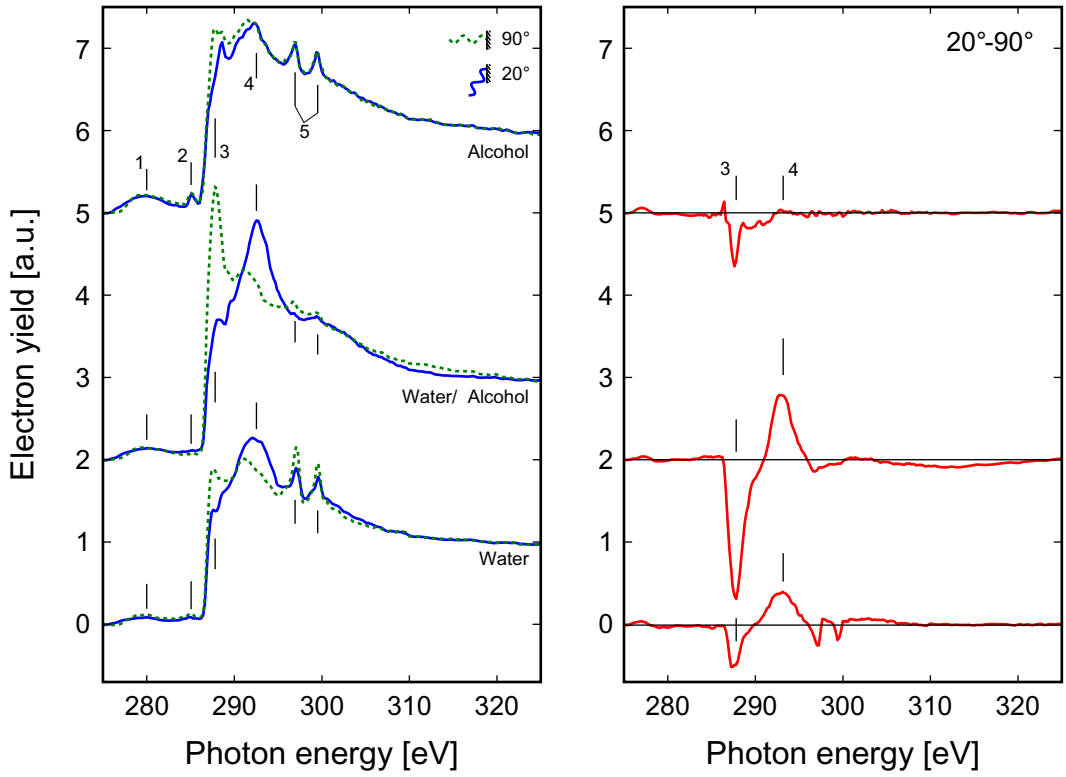

Figure 6.1: NEXAFS spectrum for C16C16 monolayers prepared from water, alcohol and a 1:1 water/ alcohol volumetric mixture.

sity within the experimental sensitivity of XPS and the contact angles. This equality does not imply, that the same degree of conformational order is also present in these films for reasons, previously explained. For the detection of differences in the degree of internal order, experiments, in which the regular conformation of the alkanechains could be directly proven and quantified, had to be performed. NEXAFS experiments were carried out on films of C16C16, which had previously shown a mediocre degree of internal order from aqueous solutions. Figure 6.1 shows spectra at the carbon 1s edge, which qualitatively all match the description given in chapter 5. On the left side, spectra at grazing (20°) and normal (90°) incidence are plotted above each other, while the right plot shows the differences between these two angles of incidence.

For all three solvents, the spectra exhibit some angle dependence, which was clearly maximised for the alcohol/ water mixture. Since only one sample was measured from the

aqueous solution and it was not possible to calibrate the machine factor during that beamtime, we refrain from presenting average tilt angles (see chapter 7 for the orbital tilt angle from the water/ alcohol mixture). Such values would not add to the qualitative information of the difference plots in significance as long as no detailed investigation of conformational order in function of the relative fractions, is undertaken.

6.4 Discussion

The experiments on the formation, influence of the solvent and the binding mechanism provide valuable insight into the structure of monomolecular films of dialkylammonium ions on mica. Under the chosen conditions, film formation takes place in the solution itself and the adlayer is not deposited during the transfer through the water/ air interface. A LB-type of film formation can be excluded, so that our method of preparation remains transferrable to mica particles.

During the adsorption, the surface potassium ions are nearly completely replaced. This was shown by samples without the lithium pretreatment, for which the potassium level can be used as an measure of the exchanged ions. Bromide, the anion of highest abundance in solution was never found in the XPS spectra. For aqueous solutions, the possibility exists, that protons competitively coadsorb or that hydroxylions are incorporated in the films so that complete ion exchange does not strictly imply a mean area of 48$Å^2$ per ammonium headgroup. Both of these ions from water cannot be detected because of their lack of electrons (i.e. H^+) respectively the amount of oxygen in the mica substrate (i.e. OH^-). No differences were found for a change of solvent to alcohol, where autoprotolysis can be neglected or is at least weaker by several orders of magnitude, or for a change of the initially present surface ions (i.e. K- respectively Li-mica), so that the the possibility of a strong concurrence from protons from water appears unlikely. Considering the experimental limitations of the XPS technique, our results are consistent with experiments performed on high surface area mica particles under similar conditions. These allow a more precise quantification of the amount of exchanged surface ions and showed the a degree of ion exchange with dialkaylammonium ions of about 80% [123].

The choice of solvent significantly influences the the ease of preparation. In chloroform,

methanol and the methanol/ water mixture the standard concentrations could, for instance, be readily dissolved during a short ultrasonic bath, while water and cyclohexanol required prolonged heating and showed the tendency to become unclear or for the precipitation of salt over time Dialkylammonium ions were shown to have a substantially higher solubility in polar organic solvents and even in the apolar hexane than in water because of the strong hydrophobicity of the alkane chains.

On the basis of their water contact angles, the solvents, investigated by us, split into two groups. Within these, chloroform and cyclohexanol show substantially lower contact angles than water, methanol and a 1:1 volumetric mixture of the latter. In the already established model of a "two-component" film, these differences can be explained by a changing match with the simple view of an ideal SAM. Fundamental differences can result from a different coverage, or a higher fraction of molecules in the "flip-flop" conformation. It is interesting, that the amount of nitrogen on mica surfaces did not change as strongly as the degrees of coverage by the contact angle would suggest. Alcohol and water as well as a 1:1 volumetric mixture of the two, cannot be discriminated on the basis of their water contact angles, so that structurally similar films are formed during the adsorption. NEXAFS experiments, which reveal the degree of conformational order and hence focus on the final stage of SAM formation, prove that the alkanespacers start adapting a regular conformation for all three of these solvents. However, the extent, to which they do so, varies between them, with a clear maximum in the 1:1 mixture. Because a mixture of water and alcohol had proven superior in terms of the resulting degree of internal order and successful in the ease of the experimental procedure, we decided to use this mixture as the solvent for future experiments. Suter et al., who have also reported the formation of highly ordered monomolecular films of dialkylammonium ions on/in mica particles used the same solvent for their preparation [92], so that a direct transfer to particles is guaranteed.

In contrast to the NEXAFS experiments on C18C18 [104] or C16C6, which indicated highly-ordered films, the experimental water contact angle never lay between the reference values of a methylene- and a methylterminated surface as expected, regardless of the solvent, time of immersion or the surfactant (i.e. C18C18 or C12C12). This eradicates the model of completely covering and partially ordered monolayers and necessitates an exten-

sion of the (over-)simplified model, in order to explain the coexistence of conformational order and the observed contact angles. Two possible explanations are the formation of ordered islands next to uncovered mica [116, 97], or an end-on adsorption in the so-called "flip-flop" conformation [95]. Under both of these hypotheses, the experimentally observed contact angle values are the result of a mixture of (ordered) alkane chains and strongly hydrophilic patches. The relative fractions of these two fractions can be calculated. Under the chosen experimental conditions, for which Brovelli et al. had already shown a high degree of conformational order, films form which resemble the "ideal" model to 75–80%. This is the same value, Suter et al. determined as the degree of ion exchange [123] for doublechained alkylammonium ions, so that the contact angles appear to confirm the concept of island formation. The measured contact angles are far from being equilibrium values for dialkylammonium ions on mica and decrease by approximately 20° in the course of a few minutes. We believe, that this is related to desorption and dissolution of originally bound ions into the water drop, which would be expected for both islands and molecules in "flip-flop" conformation.

Chen et al. [95], who proposed the "flip-flop" mechanism, were the only group, who measured water contact angles according to a methylterminated film (i.e. 110° [24]) after a prolonged drying process under a nitrogen atmosphere, during which they claimed the "flip-flop" molecules were removed from the surface. It is however not clear, why the reference values of methylterminated films would be reached, after approximately 20% of all the molecules had been removed, simultaneously lowering the degree of conformational order [95, 33].

All the experimental data fit well with a partial ion exchange in solution. In this view, the reduced contact angle of the films prepared in cyclohexanolic solutions can be understood. It is less polar than water and alcohol [122], so that the ammonium salts are not primarily present as free ions but rather in the form of cation/ anion-pairs. Nevertheless, ion exchange is also possible from apolar solvents but occurs via more complicated routes. Instead of a (nearly simultaneous [95]) adsorption and dissolution of two cations, an ion-pair is transformed directly at the binding site of the surface ion with the two cations being exchanged. Based on the different kinetics, such an ion exchange is either slower than for free ions or the equilibrium coverage is lower. A logical explanation within this

model for the enhanced order from an alcohol/ water mixture in comparison to the purely aqueous solution, also exists. Amphiphilic molecules are known to agglomerate to oligomeric blocks even below the CMC (i.e. in the absence of micelles) [115]. The addition of alcohol in quantitative amounts can help preventing such agglomerates, thus increasing the number of free ions in solution, opening simpler adsorption paths, increasing rate constants or leading to a higher equilibrium coverage.

It is not entirely clear, why the conformational order decreases again in the pure alcoholic solutions. Possibly, the highly polar solvent molecules can strongly bind to the substrate, so that ion exchange is hindered [124]. Additionally, the energy gain is reduced in comparison to water. The overall energy gain from an ion exchange is lower than for covalent adsorption because one ionic bond is formed, while one is, at the same time, broken. In alcohol, the dissolution of lithium may impose an energy barrier (as exemplified by the solubility of lithium in alcohol [122]) and hence change the relative ion-surface affinities and thereby the equilibrium coverage even though the solubility of lithium in ethanol would not as such forbid a complete exchange for low surface-area mica samples. Aside of the reduced energy gain from the headgroup, hydrophobic interactions fall away in alcohol, so that another force component in favour of densely packed structures is missing. For chloroform, similar arguments may be valid and the total effect is even more pronounced than in methanol. In principle the relative amounts of water and alcohol in the binary solution could be optimised, but such an investigation on mica sheets would necessitate exhaustive NEXAFS studies, which are avoided if possible because of the limited machine-time that is usually available. Equally highly-ordered films can probably form over a fairly broad range of mixtures, as long as no agglomeration of the surfactant molecules and quantitative fractions of both constituents are present, so that differences in the resulting order of the films are only expected to occur at the border to the pure solvents. We hence refrained from such experiments on the influence of the solvent until this current-best solvent proves unsuitable, for instance after a change in chemical endgroup. Because it allows the deposition of well-ordered films in an easy preparation and meets all the other requirements for the designated functionalisation, we decided to use this solvent, for which Suter [92] and his group had already proven that it is also suitable for mica particles.

The most simple view of a SAM considers the headgroup-substrate interaction to govern the film density and the interspacer VdW to determine, whether conformational order is established. Applied to the system of dialkylammonium ions, this would predict a complete ion exchange in which the ammonium groups are located at the mica surface plains and alkane chains, which are ordered or not depending on, whether the area of 24Å^2 is sufficient to induce the regular arrangements. However, films of these surfactants, as prepared under our standard concentrations, temperature and immersion time, cannot be explained completely by this oversimplified model, while resembling it to a large extent (75–80%). The observed deviations can consistently be explained by a reduced significance of headgroup-substrate forces in comparison to other SAMs and by assuming, that other force-components, notably those of the alkanespacers, are in the course more important for film formation. In this way, the observed solvent dependencies would also arise as a logical consequence. Unfortunately water, the until now most commonly used solvent for exchanging the surface ions of mica with (di-)alkylammonium ions, complicates the understanding and preparation of internally ordered films because it contains ions of its own that can also replace surface ions (i.e. H^+) or be included in the films (i.e. OH^-) but cannot be detected with XPS. In addition, alkane spacers strongly interact with water molecules. Hydrophobic effects can lead to surfactant agglomerations in the solution [115], on the substrate [117] or at the interface to air, thereby opening new routes of film formation, so that the adsorption mechanisms become more diverse and changes in concentration, pH or the chemical endgroup may switch from one formation mechanism to another.

Despite its plausibility, the "extended" SAM-model remains an unproven working hypothesis. Based on our experimental results and their statistical significance, it is impossible to discriminate between the two proposed mechanisms (i.e. island formation or "flip-flop" molecules) accounting for the incommensurately low contact angle, to prove one of the them or even to exclude more exotic explanations like a simplified intrusion of water into the films due to the higher area per spacer group in comparison to alkanethiols on gold or the hydrophilic mica step edges. Schwartz et al. have followed film growth of octadecylphosphonic acid (where the ionic interaction is missing, because headgroup carries a negative charge) onto mica with imaging-AFM and indeed observed the formation and

growth of densely-packed islands [116, 120]. The main drawback of this model is, that, while being able to explain the results for dialkylammonium ions adsorbed onto mica from various solvents, our model predicts disordered films for singlechained alkylammonium ions on mica. Unless the mechanism of film formation is fundamentally different for ions with only one alkane spacer per headgroup, we expect an average area of 48Å^2 per alkane chain, which is, as such, too low to induce conformational ordering [32, 90]. In other alkane-based SAMs, spacer densities around 1/20Å^2 are usually reached and studies have revealed, that in films with a coverage of less than 90% of this nominal density, the order is strongly reduced and eventually lost [33]. Theoretical models and calculations locate the explanation of this loss of order in the interspacer VdW forces as well as headgroup-headgroup interactions. Their strength strongly depends on the next-neighbour distance and conformational order will only be favourable over entropic hindrances, if it exceeds a minimum. In this framework, a lower boundary for the alkane chain length (see next chapter 7) as well as an upper limit for the area per alkane spacer are predicted aside of which, the alkanechains will not be present in the tilted, all-trans conformation. For alkanethiols on gold, the most thoroughly studied SAM system, both of these predictions were successfully demonstrated [31, 32].

On mica, the experiments of Brovelli et al. [104], in which single- and doublechained alkylammonium ions were deposited under identical conditions and the conformational order was studied, no sign of a regular arrangement was found for C18 (i.e. $(CH)_3(CH_2)_{17}(CH_3)_3N^+Br^-$) in contrast to C18C18, which showed a degree of order similar to that in films of alkanethiols on gold. Suter et al. found singlechained ions in a regular conformation when investigating partially delaminated mica particles [121], where intercalation had occurred and the ordering was established because of a partial interleaving of alkanechains from the upper and the lower layer. Although the concept of interleaving has since then been abandoned (as seen in the images of [123]), the interlayer distances of mica intercalated with singlechained molecules were always measured [121, 92] respectively simulated [123] to be lower than those of doublechained surfactants. In these cases, we hence consider the "bilayer" structure, which cannot be present on macroscopic samples without intercalation, as the reason for ordered singlechained films, so that we are not in contradiction to these studies. Films on mica sheets with a headgroup

density, tailored by the number of cation sites on the mica plane, are incompatible with ordered films of singlechained alkylammonium ions on mica, within standard SAM theory. Especially for aqueous solutions, other routes of film formation of alkylammonium ions on mica surfaces may, however, exist, via which higher alkanechain densities can be reached even with singlechained ions so that they would also form ordered structures. Consequently, other force components, e.g. hydrophobic interactions of the alkane chains with the surrounding water, will dominate the formation of such films and, in order to ensure electric neutrality, anions will be attached to the films in some (unknown) way.

Seimiya et al. performed systematic experiments on thin films of single- and doublechained alkylammonium ions on mica [94]. They indeed found an about doubled amount of nitrogen on the surfaces coated with a monomolecular film of singlechained ions than on those with dialkylammonium ions on mica but no traces of the bromide counterion with XPS. Based on high-resolution imaging-AFM, ordered structures of both single- and doublechained ions were identified but the authors did not observe any islands or contrast, which would indicate molecules in "flip-flop" conformations, while measuring similar water contact angles like ours. This may be related to the length scales on which these two techniques operate but is interesting, considering, that the same degree of order was also found when measuring under water, where a dissolution of the adsorbed ions is expected from the time dependence of the water contact angles. Also, from the fraction of islands predicted on the basis of the water contact angles, the scanning probe should occasionally, by coincidence, be brought down onto a patch of bare mica or islands of molecules in "flip-flop" conformation if patch sizes would substantially exceed the dimensions of the imaged areas. It is not clear either, whether the scanning tip of the AFM influences the film structures – which gains in significance, since the presented images look identical for bare mica, mica covered with single- and doublechained molecules. Seimiya and his colleagues were fully aware of this problem and discriminated the three films on the basis of force-vs-distance curves. Unfortunately we do not know, whether such measurements were performed before and after the imaging. Schwartz [116] and Salmeron [97] both studied monomolecular films on mica with AFM and detected islands when acquiring images on larger length scales.

Chen et al. also studied thin films of C16 (i.e. $CH_3(CH_2)_{15}(CH_3)_3N^+Br^-$) adsorbed onto

mica from aqueous solutions [95]. In contrast to all the other experimental groups, they measured water contact angles, which are in agreement with the reference values for a methylterminated surface. In their publication, an area of 48Å^2 per alkylammonium ion is claimed on the basis of XPS measurements, but it appears to be deduced from the reached equilibrium and the fact, that the potassium signal does not decrease any further, which is as already discussed, not sufficient for a strict proof, especially when using water as solvent. Neither was a comparison between a single- and a doublechained ions shown, nor did the authors perform an extensive analysis of the quantitative chemical composition of the surface region, so that we do not consider their interpretations as strictly justified and draw the attention to the sensitivity of standard XPS machines, which makes quantitative statements with a relative uncertainty of less that than 10% extremely difficult [18]. In addition to XPS and contact angles measurements, the authors also performed SFA experiments and detected, that the mica surface remained close to electric neutrality at all times. Despite a possibly completely different film formation and headgroup density, the number of positive and negative charges is thus still (nearly) equal, so that an overcompensation of mica surface ions is neutralised by anions (e.g. OH^- or Cl^-). In contrast to us or Seimiya and his group, the films of Chen also contained the counterion (i.e. chloride).

The existence of fundamental differences between ordered films of singlechained ammonium ions and the films we prepared with doublechained ammonium ions, appears imperative. We believe that these can only be resolved by applying a technique, with which conformational order can directly be probed and quantified, to the first category of films.

6.5 Conclusions

With respect to the goal of establishing a way of chemically functionalising mica surfaces with SAMs under the restriction that the same procedure must be usable for mica-polymer composites, conformational order of the alkane spacers alone is not sufficient. Equally important restrictions are imposed on the binding mechanism, the location of the headgroup and the preparative method. Using standard concentrations and a 1:1 volumetric mixture

of water and alcohol, films which fulfill all these requirements can be established during an immersion for three days.

Contrary to the initial doubts, films are formed via an adsorption within the solutions, even in water, where other routes of formation, such as LB-type of films exist. All the experimental results are in agreement with the model of ion exchange. However, the simple model, in which the films are formed to a large extent on the basis of the headgroup-substrate interaction must be extended in order to explain the solvent dependence as well as the experimental contact angles.

The experiments directed to the influence of the solvent have brought valuable insight into the binding mechanism and the route of formation with them and have helped to simplify the preparation and to optimise the degree of conformational order in the films. From cyclohexanol and chloroform, films of inferior quality in terms of water contact angle and hence chemical functionality resulted, possibly because of a reduced coverage. The standard concentrations of the surfactants could be dissolved much more easily in the polar solvents except pure water, while water and cyclohexanol required tedious heating and stirring. From water, methanol and a 1:1 mixture of both, films of a quantitatively similar density and composition could be prepared, which, however, differed in respect to the degree of internal order. With the help of the order-sensitive NEXAFS technique, it was possible to identify the 1:1 water/ alcohol mixture as the optimal solvent in terms of ordering.Due to its ease of preparation, and the excellently ordered films, which are formed in these solutions, we changed our preparative procedures and from now on used mixtures of alcohol and water to prepare the SAMs.

Both of these observations suggest, that interactions of other molecular blocks such as the alkane spacers with solvent constituents, play a substantial role for the resulting films, which is higher than in other SAMs. Based on the water contact angle, the deviation of the real structures from the "idealised" model films can be calculated – revealing a high percentage of the film to comply but quantitative fractions, which cannot be brought into agreement with this. Possible molecular mechanisms, which can explain the simultaneous existence of the high degree of conformational order and the unproportionately low water contact angles have been proposed. Neither of the two most plausible candidates, namely island formation and an adsorption in "flip-flop" conformation, however gain any evi-

dence from our experiments. The combination of imaging AFM [116, 94], the incomplete ion-exchange reported by Suter et al. [121] and our results strengthens the hypothesis of island formation and an incomplete coverage due to the insufficient ion-exchange capacity. As expected, these studies have brought some light into the differences existing between films, which were published by other groups. It remains unclear, how singlechained alkylammonium ions can form ordered films on mica surfaces and these experiments suggest, that the dominating mechanisms and forces are fundamentally different to the ones in doublechained ions.

Chapter 7

Chain length dependence of order in dialkylammonium SAMs.

7.1 Introduction

In the previous chapter, the focus lay on the identification of suitable preparative methods, the route of film formation and the nature of the established bond to the substrate. During these experiments, experimental conditions could be identified, under which highly-ordered films can be deposited onto macroscopic samples as well as onto mica particles in a later stage. It was also possible to build up a model of the underlying molecular effects leading to these films, which works well and is able to explain the observed differences, such as the water contact angles, to the predictions from other models. In this chapter, the first part of establishing a SAMs on muscovite mica is rounded off, by an investigation of the conformational order in SAMs of symmetric dialkylammonium ions of varying alkane chainlength.

For the targeted chemical functionalisation of mica, these studies help to optimise the surfactants. A suitable surfactant must form highly-ordered films after a simple preparation and be easy to synthesise. The next stage of this project will consist of fabricating films with a variable chemical functionality on top of self-assembled molecular units (i.e. head- and spacergroups), so that the ease of synthesis will subsequently gain in importance, since many dialkylammonium ions are only commercially available in their methylterminated

version.

Three parameters of an alkaneterminated quaternary ammonium salt can, in principle, be changed, namely the counterion, the number of alkane chains per headgroup as well as the individual chainlengths. In the general perception, the choice of counterion only minutely affects the film formation, especially if the ions are present as free, non-agglomerated, ions in solution and the counterions are not incorporated into the films. Agglomeration of amphiphilic molecules in water, which may strongly be influenced by the counterions [125], is not expected to present a problem in the 1:1 mixture of water and methanol [126, 115] and no signs of bromide were detected with XPS (see previous chapter 6) either, so that no further attention was directed to the counterion. In the previous chapter the formation of ordered films with singlechained alkylammonium ions has already been discussed. While such films may in principle exist, they will probably be governed by different force components and form viy a different, yet unknown route, which may be unsuitable for the functionalisation of mica particles, intended as fillers for polymer matrices. Brovelli et al. have already shown, that films prepared in the same way from aqueous solutions are ordered for C18C18 ions, while lacking conformational order with the singlechained C18-ions (i.e. $(CH_2)_{17}CH_3N^+(CH_3)_3Br^-$ [104]. Changing to singlechained ions because it would have required the repetition off all the previous work, while not promising substantial improvement over the currently used surfactants [105], so that we refrained from this measure. Increasing the number of alkane chains to three or four would not present a viable alternative either, because preparation and synthesis would, if anything, become more complicated, film formation would be slowed down and it is not clear, whether the resulting area per alkane spacer (12 respectively 16Å^2) would allow for a complete coverage. The only parameter left, was thus the symmetrical alkane chainlength of dialkylammonium ions, which we varied between C8C8 and C18C18, thus keeping the fundamental principle of film formation but possibly affecting the ease of synthesis and film preparation. Out of all the investigated surfactants, we were interested in finding the shortest alkanechains (i.e. thus simplifying the synthesis), with which highly-ordered films can be produced so that the surface chemistry is determined by the functional endgroups.

Apart from optimising the surfactants with respect to SAM technology, this investigation also provides further insight into the fundamental molecular mechanics of this family of

ultrathin films. The previous chapter, like other contemporary publications [94, 95], has already shown some fundamental differences to exist in comparison to alkanethiols on gold or other SAMs on metal (oxide) substrates. It is, for instance, interesting to find water contact angles as low as 90° accompanied by a degree of conformational order comparable to that of alkanethiol SAMs on gold. One possible explanation lies in the relative strengths of the forces between participating molecular blocks being different than for alkanethiols adsorbing onto gold from ethanolic solutions. In the general perception, the formation of SAMs is crucially influenced by three force components, namely the headgroup-substrate, interchain and the endgroup-endgroup interactions [90]. Shortchained alkanethiols will accordingly not form ordered films, because the interchain VdW forces are too weak to induce favour the tilted all-trans conformation.

The mean density of spacers is generally presumed crucial for the strength of the VdW interactions between neighbouring spacers and the establishment of regularly ordered films. Even for doublechained alkylammonium ions, this remains 15% higher (i.e. 24Å^2 [103] in comparison to 21Å^2 on gold [19]) on mica, so that the VdW forces between the spacer groups are, even at full coverage, lower than on gold. Additionally, the relative contribution from headgroup-substrate interactions may be weaker, in the case ion-exchanged films on mica, so that the total strength of the VdW forces has to be higher for ordered structures to form on mica. As a consequence, the lower boundary for self-assembly is hence expected to be shifted towards longer alkane chains in comparison to alkanethiols on gold. Owing to the relatively high area per ionic headgroup, two alkanespacers are combined at one ammonium headgroup for SAMs on muscovite mica, in order to reach a comparable density of alkanespacers as in other alkanebased SAMS. In close proximity to the ammoniumgroup, the two molecular spacers can mutually hinder each other from adopting the tilted all-trans conformation. In the course, the energy gain is reduced in respect to comparable systems with only one alkane chain per headgroup, so that the lower limit of methylene units required for the onset of conformational order, is expected to shift even further towards longer alkane chains.

Because of the reunion of two spacers at one headgroup, the conformation of the alkanechains may vary from the tilted all-trans conformation in the proximity of the ammonium group even if the upper parts of the films are highly ordered. Based on the X-ray diffraction

experiments of Hirabayashi et al. [127], Suter and his colleagues for instance report [123], that one of the two chains leaves from the adsorbed headgroup in a kink to run parallel to the other chain from the third methylene unit onwards. For SAMs this might imply, that the "unkinked" chains will protrude out of the dense films and be disordered in this endpart, so that two up to four methylene units do not adopt the all-trans conformation even in perfectly ordered films. NEXAFS experiments would in this case always detect alkanechains, in the tilted all-trans conformation together with a (small) fraction in a different, irregular conformation. Assuming that the number of perturbed methylene groups remains constant, the experimentally determined degree of order, would thus gradually increase with chainlength even in the case of maximal ordering.

Finally, the experimental water contact angles, which are not completely understood until now, have already been the subject of our discussion (see chapter 6 and speculations about their origin were made. If they can also be explained by the altered significance of interspacer VdW forces, then their experimental values would correlate with the alkane chainlength.

By changing the chainlength, the contribution of the alkanespacers is varied relative to the other force components so that the existing model, which partially explains the differences between dialkylammonium ions on mica and alkanethiols on gold with these forces, can effectively tested.

7.2 Experimental

Samples of C8C8–C18C18 were prepared using the standard concentrations of Seimiya et al. (see chapter 5 for a justification) dissolved in a 1:1 volumetric mixture of alcohol and water. In comparison to Seimiya et al. who used aqueous solutions, we had switched to this solvent because the addition of alcohol had proven superior in terms of preparation and was shown to promote the extent of conformational order in the SAMs (see chapter 5).

XPS measurements were performed on all these samples, in order to measure the chemical composition of the surface region and to verify the chemical integrity. The presence of counterions like bromide (protons from the water are not detectable) would give rise

to characteristic peaks and the ratio between the nitrogen and the oxygen signal yields the degree of coverage relative to that of C18C18 (see previous chapter 6). NEXAFS measurements were carried out under standard conditions (see chapter 1) at the K-edges of carbon and nitrogen. An angle dependence of the alkane-related electronic transitions unambiguously proves order and the extent of the angular variations can be transformed into an average tilt angle of the alkanechains. Based on this value, the degrees of conformational order in films of different surfactants can be compared with each other. Complementary to XPS and NEXAFS, water contact angles were measured. In contrast to other systems, their interpretation in terms of surface chemistry, respectively the presence of conformational order is not readily possible for dialkylammonium ions on mica as discussed in the previous chapter (see chapter 6). Building up on the previous chapter, we instead assumed the surface to consist of two chemical species and used the contact angles to deduce the relative fraction of "ideal" SAM chemistry.

7.3 Results

XPS All the XPS results shown here, were obtained on films prepared from methanolic solutions under standard experimental conditions (see chapter 2.2). We have shown in the previous chapter (see chapter 6), that this does not affect the film structures strongly enough that any differences in the chemical composition would be measurable with XPS (under the chosen experimental conditions) and that these results are hence also valid for the methanol/ water mixtures. No sign of the bromide counterions was found in any of the spectra, so that adsorption most probably takes place via ion exchange (see the previous chapter 6 for a more detailed discussion) for all the surfactants. The features in the XPS spectra indicate, that the chemical integrity is warranted for all the samples.

Table 7.1 shows the amounts of nitrogen, carbon and potassium, normalised to the bulk oxygen signal (thus compensating the attenuation in the organic adlayer) and not corrected for the instrumental transmission factor or the elemental sensitivity factors. Within the experimental limit of the XPS machine, the degree of coverage as calculated from the nitrogen signal is indistinguishable for all the surfactants. The amount of carbon

	N/ O $\cdot 10^{-2}$	C/ O $\cdot 10^{-2}$	K2s/ O $\cdot 10^{-2}$
C8C8	1.3(3)	8(2)	3.4(1)
C12C12	1.1(1)	15(2)	4.0(3)
C14C14	1.3(1)	16(1)	3.7(1)
C16C16	1.1(1)	15(3)	3.7(5)
C18C18	1.2(2)	11(1)	—

Table 7.1: Amount of nitrogen, carbon and potassium on the surface normalised to the bulk oxygen signal (no calibration of the experimental transmission function) in films of dialkylammonium ions with variable chainlengths.

scales very roughly linearly with the chainlength as expected, with the exception of a disproportionately low amount for C18C18 films. Its lower amounts of both nitrogen and carbon, is attributed to experimental problems in that particular batch of samples and not necessarily to fundamental differences in these films (see water contact angles). Because Li-mica was used, the potassium signal does not reveal any information on the amount of ions exchanged in the second ion-exchange but only confirms that all the surface potassium ions had been replaced.

NEXAFS. NEXAFS experiments were carried out under standard conditions (see chapter 1) at the core edges of carbon and nitrogen. All the spectra qualitatively match the description presented in chapter 5. The left side of figure 7.1 shows the electron yield as a function of photon energy at grazing (20°) and normal (90°) angle of photon incidence.

For the shortest surfactant C8C8, no angle dependence can be observed, so that the distinguishing mark of internally ordered alkanechains is missing. In all the other spectra, the intensities of the two alkanechain-related resonances (i.e. R* and σ^*(CC) see chapter 5) vary with the angle of incidence, while the other spectral features are angle-independent. The extent of the angular variations between grazing and normal incidence systematically increases with the chainlength to be maximised in C18C18, as shown in the right panel of figure 7.1. An average tilt angle of the associated TDMs can be calculated from the quantitative extent of angle dependence, using the method of "difference spectra"(see

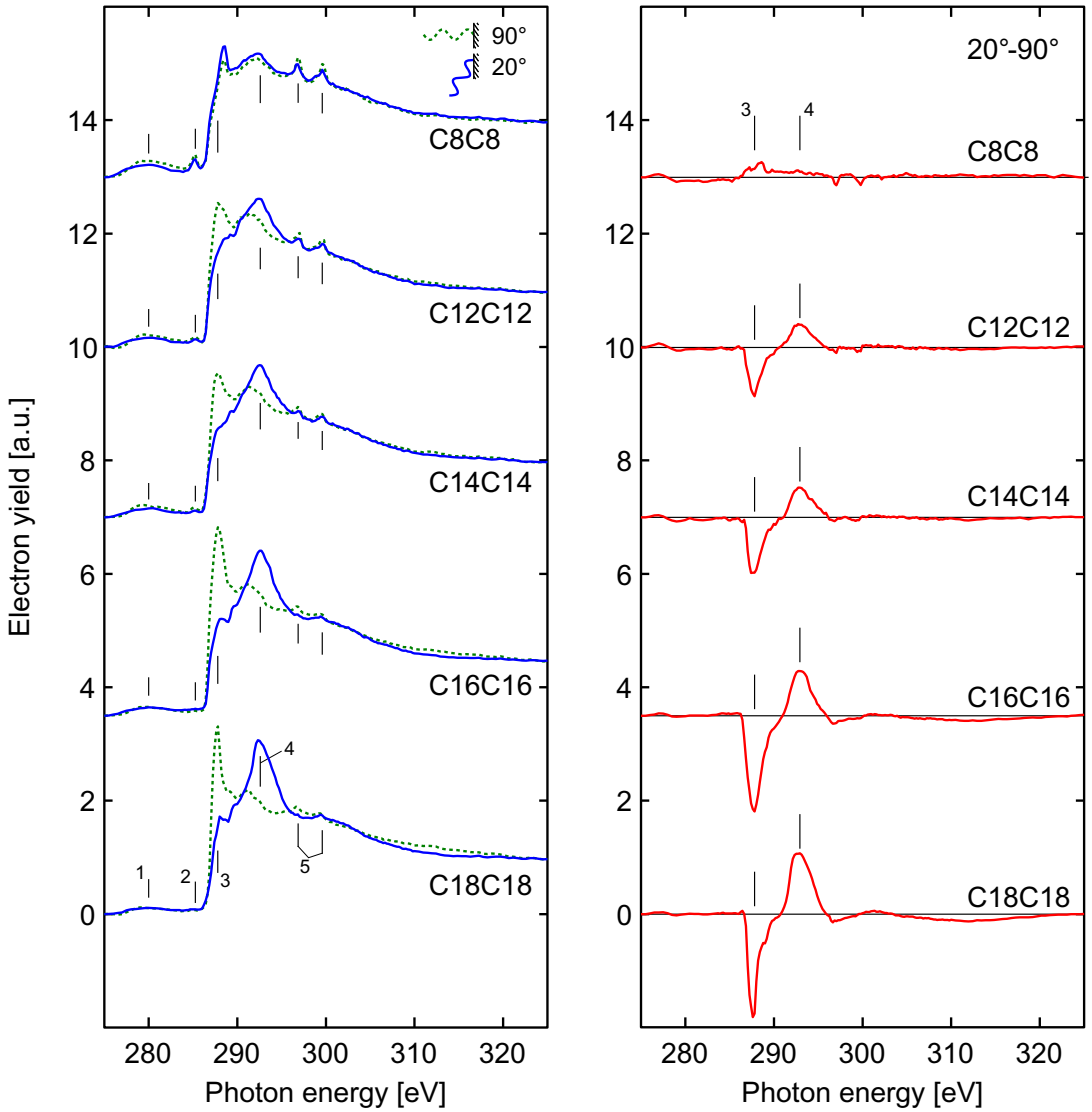

Figure 7.1: NEXAFS spectra of C8C8–C18C18 at grazing and normal angle of photon incidence (left) as well as the difference between the two angles (right) clearly show the correlation between order and chainlength in dialkylammonium films.

chapter 1.7) and the results of this calculation are shown in table 7.2:

As already mentioned, films of C8C8 did not show any significant angle dependence in the spectra and hence average tilt angles close to the "magic angle" of an amorphous layer, resulted. The "ideal" tilt angle of the alkanechains in a SAM is determined by the arrangement of the alkanespacers on the surface but not by their lengths, so that

	R*	σ(CC)
C8C8	57.6(24)°	49.3(13)°
C12C12	47.5(15)°	43.2(13)°
C14C14	44.4(35)°	42.3(12)°
C16C16	33.7(29)°	32.6(12)°
C18C18	31.8(42)°	25.2(27)°

Table 7.2: Average tilt angles of the chain-related resonances for dialkylammonium ions on mica.

	Contact angle	% Order CH_3	%Order CH_2
C8C8	61(3)°	0.38(4)	0.42(4)
C12C12	91(1)°	0.76(2)	0.83(2)
C14C14	92(2)°	0.77(3)	0.84(3)
C16C16	92(2)°	0.77(3)	0.84(3)
C18C18	89(2)°	0.73(3)	0.80(3)

Table 7.3: Advancing water contact angles for dialkylammonium ions with varying alkane chainlength, and the fraction of methyl- respectively methylene terminated surface, they amount to.

the differences in chain tilt angles between C12C12 and C18C18 were not interpreted as chains in all-trans conformation, which are tilted by different angles but rather as a measure of the number of gauche defects in the films. In the following section (section 7.4) two model interpretations of these average tilt angles will be presented.

Water contact angles. Table 7.3 shows the advancing water contact angles for films of C8C8–C18C18. As in the case of the XPS measurements, the films were prepared from methanolic solutions, which was shown in the previous chapter (see chapter 6) to leave the experimental contact angle unaffected. We measured the contact angles according to our standard protocol, the choice of which can itself influence the outcome of the experiments (see chapter 5).

C8C8 is again fundamentally different to the other films, showing advancing water contact angles, which are about 30° lower than all the other surfactants. In the standard

view of areas with the ideal SAM-contact angle and such with vanishing contact angle (i.e. 0°) this is equivalent to lower fraction of the surface being covered by the ideal SAM. This discrepancy can be the result of a substantially lower coverage (which was however not detected with XPS), or a higher fraction of molecules in the "flip-flop" conformation. For C12C12–C18C18, the water contact angles lie closely together and lie 10–20° below the reference values of methylene- or methylterminated surfaces (i.e. 103° respectively 110° [24]). Similarly to the previous chapter, the experimental contact angles were also interpreted as a mixture of regions with the ideal SAM chemistry and such with a vanishing contact angle (i.e. bare mica or molecules in "flip-flop" conformation) via the Cassie equation (equation 6.1). The match with the prediction for an ideal SAM, resulting from this two component model is also shown in table 7.3 for both the "SAM-reference" values of both methylene- and methylterminated layers. Apart from C8C8, which deviates from a completely SAM-covered mica much stronger than the rest of the surfactants, only relatively small differences in "SAM-coverage" were found. It amounts to about 20–25% as in in the previous chapter 6 for all the films between C12C12 and C18C18. While differences in coverage as resulting from the water contact angles of C12C12–C18C18 cannot be resolved with XPS and their values are nearly equal to completely ion-exchanged films within the experimental limits, it surprises that the nitrogen signal of C8C8 was not substantially lower than for the other samples.

7.4 Discussion

With all the dialkylammonium ions between C8C8 and C18C18 ultrathin films can be prepared under the standard conditions (see chapter 5 and 6). No differences in the ease of preparation exist between the different surfactants, the chemical composition is in qualitative agreement with the theoretical prediction and no sign of the counterion was ever found. Based on the XPS results, all the surfactants form films of a similar density, which is indistinguishable to the coverage in C18C18 films within the experimental limitation of the XPS machine. Advancing water contact angles were very similar for all molecules, except C8C8, where the contact angle only reached 61° – approximately 30° less than all

the other surfactants. As in the previous experiments (see chapter 6), the experimental values of the advancing water contact angles, lay substantially below the reference value for a methyl(ene)-terminated surface [24].

In the NEXAFS spectra of all the ions with chainlengths longer than 8 methylene units, signs of conformational order are found. The anisotropy in the alkane features systematically increases, as manifested in the difference spectra (see right panel of figure 7.1). Accordingly, the average tilt angles of the alkanechain-related TDMs lie further and further below the "magic angle" of a completely amorphous film. Films of C18C18, in which the angle dependence of the electron yield reaches its maximum, show experimental tilt angles even lower than those of the alkanethiol reference (see chapter 1.7). As a consequence, the alkanechains may be standing more upright on mica than alkanethiols on gold. This is, however, doubtful since the average area per alkane spacer is about 15% higher on mica than on gold [19] so that, if anything, a slightly higher tilt angle would be expected [19]. Alternatively, the degree of internal ordering reached with SAMs of C18C18, may also have been higher because fewer gauche defects were present in these films, than on the reference samples for the machine factor [10]. Possible explanations for this are imperfect reference samples (hexadecanethiol on gold, approx. 1 week old in comparison to the freshly prepared C18C18 films) or a lower number of terraces on the substrate and hence less, perturbed, domain boundaries.

Differences in TDM tilt angle can logically be explained by a fraction of disordered parts, which drive the experimental tilt angle towards the "magic angle" of an amorphous system. In this view, the experimental tilt angles yield an estimation of the relative fraction of ordered alkanechains relative to C18C18-SAMs, which served as a reference for an "ideally" ordered film, according to equation 7.1:

$$f \cdot \cos^2 \theta_{\text{ideal}} + (1 - f) \cdot \cos^2 \theta_{\text{magic}} = \cos^2 \overline{\theta} \tag{7.1}$$

Where f denotes the fraction of the "ideally" ordered film (and hence (1-f) disordered), θ_{ideal} and θ_{magic} are the reference angles for the two fractions and $\overline{\theta}$ is the experimentally determined tilt angle. As discussed in more details in chapter 4, this equation is based on the decomposition of the electron yield of a molecule multiple molecular blocks, the angle-dependent contributions of which are individually added up ("building block"-

principle [2]).

Equation 7.1 can also be used to test the hypothesis of ideally ordered films which contain 2–4 disordered methylene units because of a kink near the ammonium headgroup. In this case, the disordered fraction in equation 7.1 is fixed to 1–2 disordered units per chain (depending on whether the end of the non-kinked chains protrudes out of the surface) and the variable rest is completely ordered. Using a value of 2 methylene units (in both chains), equation 7.1 would change to:

$$\frac{(N-2)\cdot\cos^2\theta_{\text{ideal}} + N\cdot\cos^2\theta_{\text{magic}}}{N} = \cos^2\overline{\theta} \tag{7.2}$$

In addition to the variables introduced above, N indicates the total number of methylene units in the molecules. All the methylene units are weighted equally so that electron attenuation is neglected in first approximation. By using equation 7.2, the disordered parts hence have maximal impact on the resulting tilt angle so that the presented tilt angles represent an upper limit (i.e. closest to the "magic angle"). In the proposed model, the effect of the kink is expected to be substantially lower since the kink occurs directly at the headgroup and the electrons from it are attenuated more than any other part of the film. θ_{ideal} was calculated with C18C18 (R* 28.6(50)° , σ^*(CC) 20.3(36°) and then used as the reference for the other molecules.Table 7.4 shows the fractions of ideally ordered chains, the theoretical predictions for molecules with a kink, as well as the relative fractions of disorder, the kinks would amount to.

Disordered methylene units around the headgroup are not sufficient to explain the experimental tilt angles, so that the films of the shorter ions like C12C12 are, on average, not as well-ordered as those C18C18. VdW forces between neighbouring alkanespacers hence appear to play an important role for the establishment of conformational order. They have to reach a minimal strength before any ordering is induced into the films like in other SAM-forming molecules [90] and the relative number of gauche defects decreases as the VdW forces grow stronger for longer alkanechains. This explains, why ions with longer alkanespacers form films with a high degree of internal order, while the regular arrangement is strongly reduced for shorter molecules and a substantial fraction of the deposited functional endgroups is consequently not located at the surface any more. In comparison to alkanethiols on gold, the relative degree of order at a fixed spacer chainlength is lower

Values calculated from the R* resonance.			
	% Order	Predicted tilt angle	Associated % of order
C8C8	$\equiv 0\%$	35.6(34)	84(20)%
C12C12	32(7)%	33.3(38)	94(22)%
C14C14	45(7)%	32.7(40)	96(23)%
C16C16	92(11)%	32.2(41)	98(24)%
C18C18	100%	—	100(24)%
Values calculated from the $\sigma^* R$(CC) resonance.			
C8C8	19(5)%	30.4(20)	84(9)%
C12C12	40(6)%	27.4(24)	94(10)%
C14C14	44(5)%	26.5(25)	96(10)%
C16C16	78(7)%	25.8(26)	98(10)%
C18C18	100%	—	100(11)%
	% Order	Predicted tilt angle	Associated % of order

Table 7.4: Interpretation of the resulting tilt angles as a fraction of order in comparison to C18C18, respectively the predictions of the tilt angle for the model of perfectly ordered films with a kink and the associated fraction of order relatively to C18C18.

in SAMs of dialkylammonium ions on mica, possibly due to the higher area per alkane chain and an associated reduction in VdW binding energy per methylene unit.

As in the case of singlechained molecules, these discoveries are all in full agreement with predictions from standard SAM theory and match the experimental results of Suter et al. [123]. Seimiya et al., whose work has already been discussed in context of singlechained quaternary ammonium ions, also performed studies of conformational order in function of the symmetric chain length. In opposition to our results, they found highly ordered films for all the dialkylammoniumions between C10C10 and C18C18. An independence of conformational order on the chain length and the absence (respectively not reported presence) of islands or "flip-flop" molecules suggests, that fundamental differences exist between our films of doublechained alkylammonium ions and those of Seimiya et al. It is again not clear, whether any changes occur to the (incomplete) monolayers because of the imaging

AFM tip, in proximity of the surface. The authors are fully aware, that the images of bare mica, mica covered with singlechained alkylammonium ions and films with dialkylammonium ions all look identical and that further information, such as force-vs-distance curves are necessary for an interpretation of the images in terms of conformational order. The discussion of these discrepancies between our results and those of Seimiya et al., would be stimulated by the application of a technique, with which a direct proof (and maybe quantification) of conformational order can be furnished (e.g. NEXAFS), to the films of Seimiya et al.

With respect to the water contact angle, C8C8 strikes out in comparison to the other surfactants by being substantially lower, but apart from this, all the surfactants are nearly indistinguishable with no statistically significant differences between C12C12 and C18C18. In all these cases, the experimental contact angles again lie below the reference values for both methyl- and methylene terminated surfaces and were, just as in the previous chapter, used to measure the degree of match with ideal model surfaces.

Again, a homogenous mixture of two fractions with a contact angle of 0° and 103° respectively 110° was postulated, with which the coexistence of conformational order as well as the experimental contact angles can be consistently explained. From the average tilt angles of the TDMs, as resulting from the NEXAFS experiments, the assumption of 103° makes more sense, for C12C12 and C14C14, because only weak signs of ordering exists. Gauche defects preferentially occur in the topmost parts of partially ordered SAMs [34], so that the positional guarantee of the endgroups is lost long before the conformational order completely vanishes. Consequently an assumption of methylterminated surfaces is not justified for C12C12 and C14C14.

The discoveries of the previous chapter on the influence of the solvent and the formation mechanism of these films crystallised into a model, in which the resulting film structures were explained by a deviation from other SAMs due to shifted importance of individual force components (see chapter 6). These effects include the interactions of the alkane-spacers with solvent molecules as well as their neighbours in the dense films, the force between functional endgroups and the solvent and the energy gain due to the headgroup-substrate bond. Manifestations of the predicted shift include the formation of dense, highly ordered islands or the adsorption of molecules in “flip-flop” conformation, none of which

the experimental results were in favour of over the others on the basis of our experimental results. However, in combination with results from other groups, the concept of island formation gained in attention.

By using molecules of different chainlengths, the relative influence of chain-related interactions, was varied without affecting the other force components. If the significance of the alkanechains indeed gives rise to the differences in comparison to other SAM-forming surfactants, in which the headgroup is strongly attached to the substrate and the surface is completely covered with a monomolecular film [19], then the extent of this experimental deviation, will show variations with the chainlength. However, based on the experimental contact angles, the chainlength does not appear to strongly influence the fraction of the surface with a contact angle of 0° between C12C12 and C18C18, where an increase of 50% in the length of the alkanechains occurs. Despite the proven effect of the chainlength on the conformational order, the hypothesis of the alkane spacers as the explanation for the water contact angle is not verified and rather weakened instead.

Alternatively, the functional endgroups and their interactions with other molecular blocks or the very hydrophilic edges of terraces on muscovite mica, in the proximity of which the regular SAM structure is most likely to be disturbed, may be other reasons for the contact angles. While step edges occur, and will, if anything, lower the experimental contact angle, the flatness of mica is generally perceived to extend over large areas, so that the density of such edges on the mica surface would be insufficient to account for the observed discrepancies. Suter et al. have measured the ion exchange into partially delaminated particles [92] to amount to 80% of the maximum of ion sites. This may imply, that the surface coverage is effectively limited by the ion-exchange capacity and that this is very similar for all the investigated surfactants.

Two consequences arise for the aim to flexibly control the surface chemistry of muscovite mica with SAMs. Functional endgroups can only be deposited on the surface with longer-chained molecules such as C18C18 because the degree of conformational order in thinner films (e.g. C12C12) is not high enough to fix their position at the interface. Even with the longest molecules investigated by us (C18C18), the desired chemical functionality can only be established on about 80% of the mica surface and the independence of the water contact angle on the chainlength does not promise substantial improvements by switching

to even longer chains but suggests a fundamental limit for this group of surfactants. In respect to producing mica/ polymer composites, only experiments can show, whether the effect achieved in this way is sufficient.

7.5 Conclusions

Studies of the films formed by dialkylammonium ions, with differently long alkane chains provided valuable information in respect to the fundamental science of this family of films as well as for the concrete idea of functionalising mica particles with such films and using the coating to control their interaction with a surrounding polymer matrix. The chemical composition of all the investigated films was similar and matched the expectation from the molecular structures of the surfactants. Based on the water contact angle, about 80% of the surface cations are exchanged in solution after prolonged immersion, except for the shortest surfactant C8C8, where only about 40% of the surface are methyl(ene)-covered. Surprisingly, this was not reflected in the XPS nitrogen signals, where the differences are much smaller.

Upon shortening the alkanechains from C18C18 to C8C8, the relative fraction of conformational order in thin films of dialkylammonium ions on mica gradually decreases to vanish completely in C8C8. This discovery from NEXAFS experiments, with which the degree of conformational order can be quantified, is in excellent agreement with the predictions from the standard SAM-models and proves the pivotal role of interchain VdW forces on the resulting film structures. Their influence on the degree of conformational order is much stronger than on the coverage, where only small differences were found between C12C12 and C18C18 with both XPS and contact angle measurements. While a lower boundary of chainlength for the establishment of conformational order is found in many SAM-forming systems, the gradual increase of order with the chainlength is more pronounced in this system. It is only partially explained by complications due to the unification of two alkanespacers at one headgroup, so that the topmost parts of the monolayers are also affected. Important consequences for a targeted chemical functionalisation of mica arise from this discovery and necessitate the use of longerchained adsorbents, since the location of the functional endgroups can only be fixed at the topmost part of the films, if the alkane-

spacers adapt the tilted all-trans conformation.

The results of the previous two chapters round off the first stage of establishing SAMs on mica using quaternary ammonium ions. With the present best preparative procedures and surfactants it was possible to deposit films, which deliver the desired chemical functionality onto approximately 80% of the surfaces, while the rest remains undefined, possibly uncovered. It is not clear, whether the achieved effect is sufficient for the use in polymer composites and the observed deviations make the use of such films in fundamental surface scientific studies difficult. We consider the resulting films as limited by fundamental effects (e.g. ion exchange capacity [93]) and do hence not think, that changes in the spacer group or the preparation would provide a substantial improvement of the film quality.

Chapter 8

Change of binding head-group — Pyridinium ions

8.1 Introduction/ Motivation

As a change to the commonly used ammonium group we also investigated how ions containing the pyridinium ($C_5H_5N^+-$) group as ionic head group bind to mica. Such films possess the advantage that their adsorption onto mica particles can be monitored with UV-spectroscopy [109]. The applicability of this technique is helpful because it allows the determination of adsorption kinetics or of the specific area and hence the particle size. Another potential benefit of the pyridinium group ist the numerous docking sites to which other molecular blocks could be attached. Owing to this flexibility diverse compounds can potentially be synthesized so that the surface chemistry in pyridinium-containing SAMs could potentially be flexibly tailored.

We wanted to test, whether the pyridinium head-group could be used as an alternative to the ammonium group. The main question that awaited to be answered was whether these surfactants formed ordered films which are apt for a functional chemical modification of muscovite mica surfaces. D. Brovelli (LSST, ETHZ) measured and analysed the NEXAFS spectra for hexadecylpyridinium chloride [112] so that my experiments with methylpyridinium iodide supplemented already established knowledge about such films allowing a more comprehensive interpretation of it — most notably the influence that an additional (bulky)

alkane chain exerts on the pyridinium ring. Her experiments are described elsewhere [112] but are presented again here for the sake of consistency. The results of these experiments as well as their impact on the intended chemical functionalisation of muscovite mica have bee published and this chapter follows the argumentation of the corresponding article [128].

8.2 Experimental

Surfactants Hexadecylpyridinium chloride (HDP) is commercially available and was used as bought from Fluka (≥98% Fluka, Switzerland) while W. Caseri (IfP, ETHZ) synthesized methylpyridinium iodide(MP) according to the standard procedure [129]. For practical reasons I will use the abbreviations MP and HDP for both the salts and the cations, wherever their use is clear in the context. All surfactants were used without further cleaning. Glassware was carefully cleaned in a solution of RBS50 (Fluka, Switzerland) and a subsequent bath in nitric acid (approx. 30% acid, 70% ultrapure water). All aqueous solutions were prepared using ultrapure water (Easypure, Barnstead, ≥18.2MΩ cm^{-1}).

Sheets of muscovite mica (Provac, P-OTS-06027 T, BALZERS Liechtenstein) were cleaved on both sides using adhesive tape and then immersed into a 1M aqueous solution of LiCl(≥98% Fluka, Switzerland, no further purification) where we left them for 3–7 days. During this pre-treatment all the surfacial cation sites are occupied by lithium ions which can subsequently be replaced by other ions easier. HDP ions for instance only replace about half of all the ion sites if the surface layer consists of potassium ions but rapidly establish films of full coverage on lithium-bearing mica [109]. After this initial ion exchange, the samples were taken out of the LiCl solutions and thoroughly rinsed with pure water to remove any abundance of the salt, which remained loosely bound on the surface. Attempts to detect the adsorbed lithium with XPS and correlate it with the decrease of the potassium signal failed, due to the relatively low sensitivity factor (only about 5% compared to that of oxygen) and the atomic fraction of lithium

The cleaned samples were then immersed into aqueous solutions of the pyridinium ions. As discussed in more detail in a designated section 6, the critical micelle concentration may be a crucial parameter for the kinetics of film formation from aqueous solutions. To

ensure a monomolecular film with maximal coverage and an efficient adsorption process, a concentration close to, but below, the CMC was chosen for HDP with a reference CMC of 0.2mM [107]. The CMC of MP cannot be found in reference tables. For comparison, micellisation in aqueous solutions of octylpyridinium bromide ($C_5H_5N^+C_8H_{17}Br^-$) occurs at 0.2M [107] and MP is most probably even less amphiphilic so that its CMS is certainly much higher than the used concentration. Both solutions hence contained an abundance of free cations which could adsorb onto the substrates and form monomolecular films [39]. A 0.1mM solution of HDP and a 10mM solution of MP were prepared and samples stayed in them for ≈40h (HDP) respectively ≥ 72h (MP). One sample of MP was additionally prepared in a 10mM ethanolic (p.a. quality) solution to determine the influence of the solvent (6). Again, residual surfactant molecules were removed from the samples by rinsing them with the clean solvent. Finally, the samples were dried in a stream of nitrogen and then immediately inserted into the experimental chamber.

NEXAFS experiments were carried out under standard conditions (see chapter 1 for detailed information). Muscovite mica is a highly insulating material so that an electron floodgun had to be used in order to counterbalance the severe charging of the samples. As always, the necessary precautions were taken to prevent the neutralising electrons from saturating the channeltron and no electron-induced film damage was detected in the course of our experiments (approx. 1h per sample, see section 1.6). In accordance with the molecular structure, we measured carbon (C1s 275-325eV) and nitrogen (N1s 380-430eV) spectra. Carbon spectra were energy calibrated according to the R* resonance of an alkanethiol (287.6eV [48]) on gold as an "absolute" energy reference. For nitrogen, the pre-edge π^*-resonance (400.8eV [111, 130]) served as energy reference.

8.3 Results

Chemical composition. Carbon. Figure 8.1 shows carbon spectra of MP and HDP. The first feature in the carbon spectra is a broad, relatively weak resonance at approximately 279(1)eV (1). Its associated transition does not have the C1s orbital as an initial state but the peak rather arises from transitions from inner shells of oxygen atoms (O1s), which manifest themselves in the carbon spectra because the beam monochromator

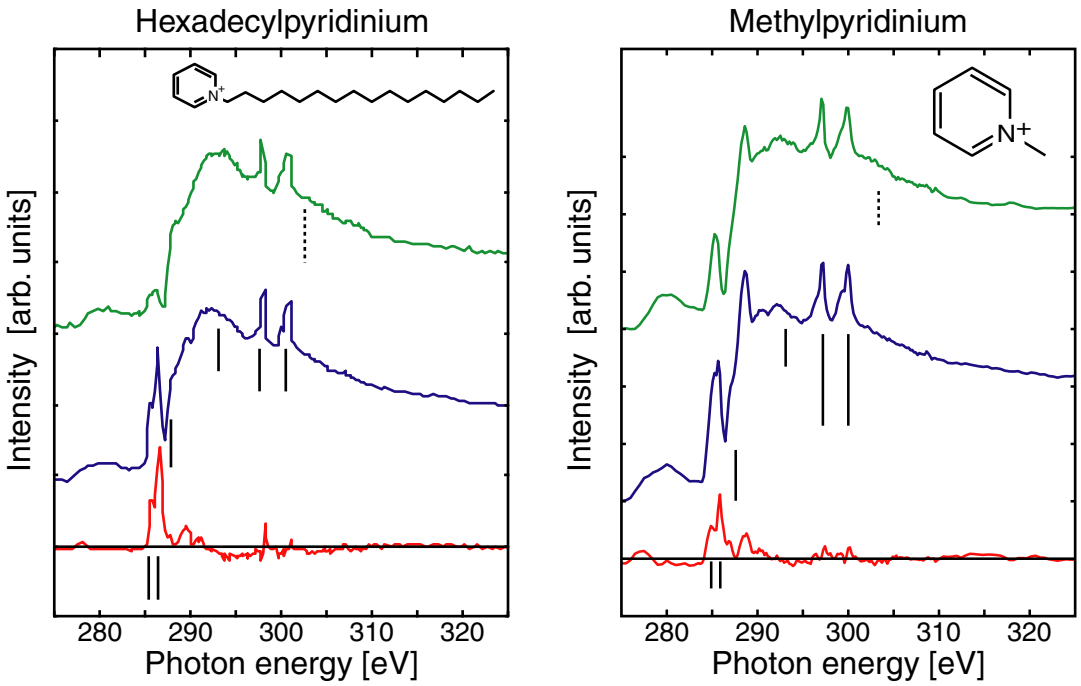

Figure 8.1: Carbon 1s spectra of MP and HDP.

allows a fraction of photons with double energy to pass (see section 1.6). The lack of oxygen atoms in the adsorbents implies that this resonance stems from the mica substrate and not from the surfactants. Accordingly, it is more pronounced in the spectra of MP because the organic overlayer is thinner and hence the electrons from the substrate are less attenuated. At 285.4(5)eV a second peak (2) arises which consists of two similar transitions C1s$\rightarrow$ π^* at 285.0eV and 285.5(MP) (respectively 285.9eV in HDP) . Both final states belong to the aromatic system of the pyridinium ring. In contrast to adsorbed benzene, where only one such pre-edge resonance (at 285.2(1)eV [111]) into a π^* orbital the "double-bond" orbitals are separated into two resonances as a consequence of the relatively reduced symmetry of the pyridinium unit and hence lower energy degeneracy of the different orbitals [111]. The lower extent of degeneracy is also observed for pyridine molecules that were condensed onto Ni(111) [111] and furthermore the energies of the two transitions also match the transition energies for adsorbed pyridine.

The transition dipole moment of these resonances points into the same direction for both transitions, namely perpendicular to the aromatic ring. Thanks to this parallelism, their

intensities can be added and treated as the total intensity of one single resonance. It is maximised at grazing angles of incidence which indicates a flat-lying orientation of the pyridinium rings. At higher energy, the R* resonance (3), which is associated with a final state of CH-orbitals [48], appears at 287.6eV. It lacks any visible angle dependence and is partially superimposed by the absorption step (approx. 289.1–289.4eV [131] depending on the chemical shift). A next angle-independent resonance which is associated with transitions into another unfilled CH orbital(CH_{Ring}) or alternatively into a σ(CN) orbital can be detected at approx. 289(5)eV [132].

We distinctively find the σ^*(C-C and C=C) resonance centered at 292.5eV (4) [132]. In the case of HDP it is dominated by the carbon atoms of the alkane chain and its angle dependence hence yields information about a potential ordering of this molecular building block. For both surfactants such an indicator of order was however missing as this spectral region revealed the same intensity for all angles of photon incidence. Another two substrate peaks lie at 297.2eV (5) and 300.0eV (6) and originate from transitions K2p→K3d [112]. Finally, a further resonance of the type C1s→ σ^*(C-C) (7) lies at 301–302eV [132, 50]. Because it is partially overlapped by the higher potassium peak (i.e. 6) and due to a relatively low oscillator strength it is however barely recognisable in the signal and lacks any angular variations.

Nitrogen spectra of MP and HDP are shown in figure 8.2 only manifest three distinct features. The energetically lowest — a pronouncedly pre-edge resonance — served as energy reference and lies at (fixed) 400.8(10)eV [130]. This is attributed to transitions of the kind N1s→ π^* of the aromatic (π-like) system of the aromatic (π-like) system of the molecules just as its analogue in the case of carbon spectra [111, 130]. However, in contrast to the carbon resonance, the nitrogen peak only contains one component.

For nitrogen the symmetry of the initial state is fixed to a_1 while it can be a_1 or a_1+b_2 at the carbon edge. The final states are the same for both the nitrogen and the carbon region and have a_2 or b_1 symmetry. Group theory predicts that the TDM for the nitrogen transition in to the a_2 final state vanishes (i.e. is symmetry-forbidden) so that there is only one π^* resonance in the nitrogen 1s region [111]. The angle dependence of this resonance is however the same as in the carbon spectra and maximises the intensity for grazing photon incidence. At approximately 405(1)eV, ionisation starts and evokes

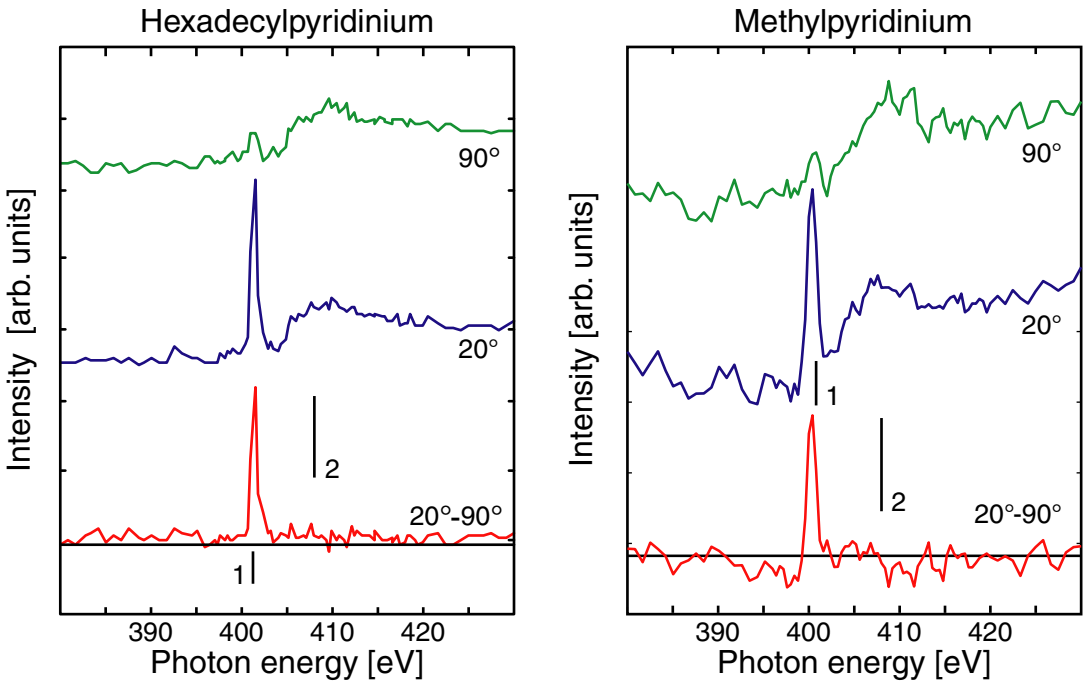

Figure 8.2: Nitrogen 1s spectra of MP and HDP at grazing and normal photon incidence.

the typical absorption step. A second transition into σ^* (N-C, N=C) final states, with comparatively low oscillator strength occurs at 408(1)eV and and does not depend on the angle of photon incidence.

Average tilt angles. The angle-dependent π^*-resonances in both the nitrogen and the carbon spectra prove, that at least some molecular blocks adapt a well-defined orientation upon adsorption. For this reason, we calculated the tilt angles of the TDMs belonging to the different resonances. No angle reference was available for quantifying the angle-dependence of the π^* resonance so that we were not able to use the analysis with the method of "difference spectra". Its analysis was fortunately relatively simple because it is situated below the absorption edge and well separated from other spectral features so that the intensity of the resonance equals the experimental signal and a quantification is commensurately straightforward (i.e. numerical integration). This advantage holds for both the nitrogen and the carbon spectra. The tilt angle was determined from the quantified intensities according to equation 1.12 under the assumption of 85% linearly polarised radiation [9]. In the case of the R*- and the σ^*(CC)-resonances in the carbon

	Pyridine ring		Hydrocarbon	
	π^* (**N**=C)	π^* (**C**=C)	R* / CH	σ^*(CC/CN)
HDP	34(6)°	32(5)°	55(1)°	55(1)°
MP_{water}	35(3)°	48(2)°	55(4)°	55(3)°
$MP_{ethanol}$	37(5)°	47(3)°	55(4)°	55(3)°

Table 8.1: Average orbital tilt angles for the different pyridinium ions on mica.

spectra, the method of difference spectra can in principle be applied, but an examination of difference spectra rapidly reveals that the π^*-resonances are the only ones that exhibit an angle-dependence. The same is also true for the nitrogen spectra.

The statistical error calculations are based on the experimental noise in difference spectra which is converted into an uncertainty in the tilt angle as would result from the ratio of intensities at different angles of incidence. Table 8.3 displays the average tilt angles that were determined in this fashion.

It becomes clear why the σ^* resonances (C-C, N-C) do not show any preferential order even though the rings are regularly arranged. The TDMs of the π^*-resonances, which stand perpendicular to the ring plane, are tilted by approximately 35° , which is equivalent to an average tilt angle of about 55° for the TDMs which lie in the pyridinium ring plane (e.g. R* respectively σ^*[1]). This value coincides with the "magic angle" for a disordered system so that the self-assembled structures do not leave a distinctive mark in the σ^*-region.

For HDP, the tilt angles of the aromatic rings in the carbon spectra and those of the nitrogen spectra match within the experimental limits in contrast to MP, where a systematic and significant deviation occurs. Indeed its apparent carbon tilt angle approaches that of a disordered system, which would indicate that the order in the films is lost to a significant extent without the information from the nitrogen edge. Several possible explanations for such a disagreement exist, the most prominent being other carbon species in or on the mica which would influence the carbon tilt angle while the nitrogen signal would remain

[1]Strictly speaking this is an approximation since we do not know the exact 3-dimensional orientation of the ring.

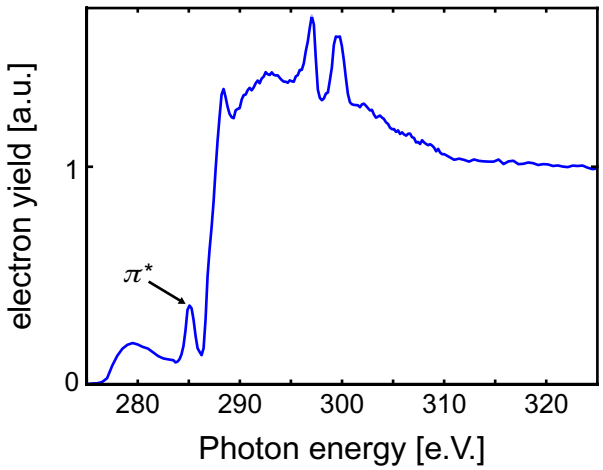

Figure 8.3: Carbon 1s spectra of MP and HDP at grazing and normal photon incidence.

unaffected. We tested this hypothesis by performing another NEXAFS experiment on non-functionalised, freshly cleaved mica. This spectrum is shown in figure 8.3 and indeed reveals a pronounced, π^*-resonance. Carbon is not contained in the ideal mica crystal lattice but muscovite mica —being a natural material — can incorporate graphite into the bulk during its formation [101, 102] so that this resonance does not need to be taken as the proof for adventitious surface contamination. Indeed the cleaning and preparation procedures were not relaxed for the MP samples compared to the HDP samples, where carbon and nitrogen render the same tilt angles. However, a different batch of mica sheets was used in the experiments of the MP films. We hence attribute the deviations in these samples to carbon that was within the mica and, at most, only minutely influenced the structure of adsorbed films. As a consequence of this interpretation, the tilt angle of the aromatic ring in MP is likely to be appropriately described by the nitrogen signal, while the carbon spectra can be ignored in this context

Interpretation in the terms of the molecular building blocks. For both ions, the only peaks which vary with the angle of photon-incidence are the π^*-resonances. These arise from transitions into orbitals of the aromatic system. Their angle dependence stems from a regular alignment of the pyridinium ring and is not affected by the conformation of the alkane moieties. Additionally, for HDP the σ^*-(C-C) and R*-resonances are dominated

by the fraction of carbon atoms in the alkane chain, so that we are able to study the orientation of the two connected molecular blocks (nearly) separately. However, no angle dependence and hence no order were detected in any of alkane-chain connected resonances. This completes the image of ordered rings with disordered, randomly arranged alkane blocks.

Influence of the solvent. The single sample of MP which was prepared from an ethanolic solution showed exactly the same tilt angles as its analogues from aqueous solutions. As described in a designated chapter 6, the solvent may influence the adsorption kinetics and with it the film formation in the case of amphiphilic ions. MP is only slightly amphiphilic so that it should in principle form the same films independently of the solvent as long as this is polar and the equilibrium constant allows the ion exchange.

8.4 Discussion

Cations of hexadecylpyridinium and methylpyridinium both strongly adsorb onto muscovite mica surfaces via ion exchange. Nitrogen and carbon 1s NEXAFS spectra reveal the tilt angles of the different molecular blocks "independently" of each other. The π^*-resonances are characteristic for the arrangement of the pyridinium rings and prove that these align regularly and adapt a flat orientation (i.e. tilt angle of 35° from the surface).

By the matches between the tilt angles of the aromatic groups in both MP and HDP we conclude that the change from a short to a longer alkane block does not influence the arrangement of the rings. Unfortunately the attempt to measure the orientation of pyridinium ions which would have an even shorter "extension" attached to the nitrogen atom (hindering an upright positioning of the aromatic rings) failed because the pyridinium ions did not adsorb onto mica — probably because of concurrent adsorption of protons from the aqueous solutions [112].

Apart from the π^*-related resonances, none of the spectral features showed any angle-dependence. This observation is interpreted differently for MP and HDP. Both the R∗'and the σ^*-resonances are dominated by transitions in the pyrindinium ring in the case of

MP. Its tilt angle of ∼55° with respect to the surface normal however implies that all the corresponding transitions of R* or σ^*-type will exhibit no or nearly no angle-dependence (i.e. "magic angle"). In the case that the R^*-resonance (287.6(2)eV [49]) arises solely from the methyl group, we would not expect an angle dependence either, since the three CH-bonds nearly completely span an (angle independent) tetrahedron. However, even for HDP films where these resonances arise mainly from atoms in the alkane chains, no preferential order was found. In our opinion these results are not caused by a regular chain conformation which, "per coincidence", renders the "magic angle" but we rather interpret the angle-independence in these spectral regions as a proof, that the alkane chains are disordered instead.

Connected with this discovery is the issue of the principal driving forces behind the molecular arrangement in these films. In order for alkane chains to adopt a highly ordered conformation, the inter-chain VdW forces have to reach a substantial strength [24]. In comparison to highly ordered films, such as alkanethiols on gold or the related dialkylammonium ions on mica [104], the net chain density in HDP is much lower (1 chain per 48Å^2 for HDP compared to 1 chain per 24Å^2 for dialkylammonium ions on mica). The pyridinium units cannot replace the "missing" chains because they could at best stabilise the lowest pars of the much longer chains (i.e. $<$ 5Åring diameter, hexadecane chain ≈18Å). As a consequence of the low chain density on the surface, these are hence not ordered and their conformational disorder means that the chemical end-groups are not in a defined position at the top of these films so that they do not predominantly determine the surface chemistry and that a versatile control over this via the "SAM-method" is not yet possible.

The tilt angle of the aromatic pyridinium units is a compromise between the electrostatic forces of the different parts of the rings with the negatively charged mica substrate. One of these force components is the ionic interaction between the substrate and the pyridinium ring which is one-fold positively charged at the nitrogen. Owing to this interaction, the ring seeks a conformation in which the nitrogen atom is in closest proximity to the substrate. Because the methyl group (MP) respectively the alkane chain (HDP) induce rigidity into the molecule, this force favours a flat adsorption pattern of the pyridinium rings. On the other hand, the electrons in the π^*-orbitals of the pyridinium ring are

repelled from the substrate — which would prefer upright standing pyridinium rings. Intermolecular VdW forces between neighbouring adsorbate molecules are again (compare the discussion of the chain ordering) expected to play an inferior role for the tilt angle of the pyridinium rings because of their small size.

8.5 Conclusions and Outlook

Ionic surfactants containing the pyridinium unit adsorb onto muscovite mica from aqueous solutions at concentrations slightly below the CMC. In the course of adsorption, their pyridinium blocks adapt a regular arrangement with rings that lie tilted at a flat angle of 34° with respect to the surface. This orientation is a compromise between the ionic interaction attraction and other electrostatic interactions between substrate and the surfactant molecules. We did not detect any sign of ordering of the alkane chain of HDP, most likely because the strength of the inter-chain VdW forces is insufficient to stabilise the alkane chains. Alkane chains such as that in HDP generally order themselves in monolayers because of intermolecular VdW interactions between neighbouring surfactant molecules. A comparatively low packing density of surfactant atoms and the small size of the pyridinium units explain why these forces do not possess the required magnitude to induce order in this case.

With respect to the applicability, for the variable and controlled chemical modification of mica surfaces using the full potential of SAMs, the films fall short of meeting the requirements, if the full potential of SAMs is crucial. The knowledge acquired in these experiments, however, opens a route to ordered, pyridinium-based SAMs on mica. Since the chain density appears to be a pivotal factor for the inter-chain VdW forces and these in term determine whether alkane chains will be driven towards an ordered arrangement, better results are likely to be achieved with pyridinium ions that have more than one alkane chain attached to them. The pyridinium ring offers five sites to which further alkane chains could be attached via a chemical synthesis. After the attachment of a second chain, the overall chain density would resemble that of alkanethiols on gold and closer at hand, equal that of dialkylammonium ions on mica which have already been shown to

posses ordered alkane chains in all-trans conformation and for which the mechanism of self-assembly is well understood (see chapter 5). An educated guess would hence be, to attach two octadecyl chains to the pyridinium ring, thus reaching the "critical number" of methylene groups to ensure highly ordered films.

As a consequence of the increased amphiphilicity, the adsorption kinetics of such adsorbates could become a problem for a successful film formation because the CMC would probably be commensurately low and necessitate unsuitably low working concentrations. This problem can however been overcome by the addition of alcohol to the solvents (6, a change in the preparational procedure which was in principle successfully shown to work for MP.

Acknowledgement

I did not spend my last three years entirely with preparing and analysing samples or studying research articles. Science brought me into contact with people who were fascinated by their jobs and it gave me the chance to travel to London and St. Andrews. Wherever, the journey took me, I always met friends and received help from my colleagues. For the tremendous support, received during this time, I would like to express my sincere gratitude, in particular to:

Prof. N. D. Spencer, for offering me the opportunity to work in his research group and for his ever-open door.

PD. G. Hähner, for thorough scientific guidance, lots of intensive and fruitful discussions, the good times at the NSLS in Brookhaven and for showing me Great Britain.

Prof. S. Virtanen, for willingly accepting the duty of co-examiner.

PD. W. Caseri, for providing invaluable help in chemical questions and for the synthesis of surfactants.

Prof. M. Textor, S. Tossatti, for sample preparation and help in the investigation of phosphate- /phosphonate-based SAMs on titanium oxide

C. Dicke, for being a soulmate during our "odyssey" through Europe and for the preparation of EG-films on gold.

Irene Klingenfuss-Hähner, for valuable assistance with computer problems and for help in XPS- and NEXAFS measurements

Dr. Venkataraman Nagaiyanallur, for his open ear and the inspiring discussions about SAMs on mica

The research groups at CMMP (University college London), LSST (ETH Zürich) and the surface science group of the University of St. Andrews, especially Louise

Dash, Tanja Drobek, Che Gannarelli, Andrew Gormanly, Sara Harris, Seeungwhan Lee, Marcus Müller, Martin Widmer and Stefan Zürcher

Sascha Khakshouri, for the interest he took in my work, inspiration and for his friendship

Jamie Kleiber, David Traynor, Harry Wright for the excellent time in London and for welcoming me in your flat and your group

Mischa Mahler, Reinhard Brunner and Christian Paratore for staying in Zürich and remaining great friends

Anja Hahn, for immeasurable love, encouragement, and the tremendous patience during my long absence. I (still) love you!

My family, for continuous love and support and for believing in me during all the times

Curriculum Vitae

Mathias Zwahlen

Nov. 1st 1975	born in Zürich (ZH), Switzerland citizen of Wahlern (Be), Switzerland
1982–1983	Primary school Farnham Common, Bucks., UK
1984	Middle school Farnham Common, Bucks., UK
1984–1987	Primarschule Dänikon, Switzerland
1987–1994	Gymnasium Oerlikon ZH, Switzerland (Matura Typus B)
1994–2000	Studies in experimental physics at the university of Zürich Academic degree: Diplom in Experimentalphysik
2000–2003	Work towards the PhD-Degree in the Laboratory of surface science and technology, D-Werk, Swiss Federal Institute of Technology (ETH) Zürich
2001–2002	External part of the PhD thesis at the Condensed Matter and Materials Physics (CMMP) Group, Dep. of Phys. and Astr., University College London, UK
2002–2003	External part of the PhD thesis at the Surface Science group, School of Chemistry, University of St. Andrews, UK

Zürich, 2003

List of publications

[1] Mathias Zwahlen Samuele Tosatti Marcus Textor and Georg Hähner. Orientation in methyl- and hydroxyl-terminated self-assembled alkanephosphate monolayers on titanium oxide surfaces investigated with soft x-ray absorption. *Langmuir*, 18(10):3957–3962, 2002.

[2] Mathias Zwahlen Dorothee Brovelli Walter Caseri Georg Hähner. Orientation and electronic structure of ion-exchanged pyridinium compounds on mica. *Journal of Colloid and Interface Science*, 256:262–267, 2002.

[3] Mathias Zwahlen Sascha Herrwerth Wolfgang Eck Michael Grunze and Georg Hähner. Conformational order in oligo(ethylene glycol) self-assembled monolayers on gold determined by soft x-ray absorption. *Langmuir*, in press, 2003.

Bibliography

[1] M.O. Krause. *J. Phys. Chem. Ref. Data*, 8:307, 1979.

[2] Stöhr J. *NEXAFS spectroscopy.* Number 25 in Springer Series in Surface Science. Springer Verlag, Berlin, Germany, June 1992.

[3] K.-J. Kim, editor. *Characteristics of Synchrotron Radiation*, volume 184. AIP, 1989. page 565.

[4] Sham T.K., editor. *Chemical applications of Synchrotron Radiation*, volume 12 of *Advanced Series in Physical Chemistry.* World Scientific, New Jersey USA, 2002.

[5] V. Schmidt. *Electron Spectroscopy of Atoms using Synchrotron Radiation*, volume 6 of *Cambridge monographs on atomic, molecular and chemical physics.* Cambridge University Press, Cambridge, UK, 1997.

[6] R.P. Feynman. *The Feynman Lectures on Physics.* Number 1. Addison-Wesley Pub. cop., Redwood City, USA, 1970.

[7] F.A. Cotton. *Chemical Applications of Group Theory.* Wiley-Interscience, NY, USA, 2. edition, 1971.

[8] J.N. Murrell S.F. Kettle J.M. Tedder. *The Chemical Bond.* Wiley, Chichester UK, 2. edition, 1985.

[9] J.D. Jackson. *Classical electrodynamics.* Wiley, New York, USA, 3. edition, 1999.

[10] Kinzler M. Schertel A. Hähner G. Wöll Ch. Grunze M. Albrecht G. Holzhüter G Gerber T. *J. Chem. Phys*, 100(10):7722–7735, 1994.

[11] http://www.nslsweb.nsls.bnl.gov/nsls/operations/ring-parameters. Electronic, 2002.

[12] Kittel C. *Introduction to Solid State Physics*. Wiley, NY USA, 7. edition, 1996.

[13] Henry R C Beer P, editor. *Henry Rowland and astronomical spectroscopy: celebration of the 100th anniversary of Henry (A.) Rowland's introduction of the concave diffraction grating: proceedings of a symposium*, volume 29 of *Vistas in astronomy*. Baltimore, USA, 1984.

[14] divers. U1a beamline manuals. stored at beamline U1A, NSLS, USA, 1996.

[15] BURLE TECHNOLOGIES INC. http://www.burle.com/cgi-bin/byteserver.pl /pdf/channelbook.pdf. Electronic.

[16] Heister K. Frey S. Gölzhauser A. Ulman A. Zharnikov M. *J. PHYS. CHEM. B*, 103(50):11098–11104, 1999.

[17] COMPAQ INC. http://h18002.www.hp.com/alphaserver/vax/. Electronically.

[18] Briggs D. Seah M.P., editor. *Practicle Surface Analysis: Auger and X-Ray Photoelectron Spectroscopy*, volume 1. John Wiley & Sons, Chichester, UK, 1983.

[19] Ulman A. *CHEM. REV.*, 96(4):1533–1554, 1996.

[20] Pruys H. Datenanalyse. Lecture notes.

[21] Levine I.N. *Physical Chemistry*. McGraw Hill, NY USA, 1978.

[22] Somorjai G.A. *Introduction to Surface Chemistry and Catalysis*. John Wiley & Sons, NY, USA, 1994.

[23] Adamson A. *Physical Chemistry of Surfaces*. Interscience, NY USA, 1967.

[24] Ulman A. *An introduction to ultrathin organic films : from Langmuir-Blodgett to self-assembly*. AP Academic Press, Boston, USA, 1 edition, 1991.

[25] Tosatti S. Michel R. Textor M. Spencer N.D. *Langmuir*, 18(9):3537–3548, 2002.

[26] Nachtigall W. *Vorbild Natur: Bionik-Design für funktionelles Gestalten*. Springer, Berlin, Germany, 1 edition, 1997.

[27] Nachtigall W. Blüchel. *Das grosse Buch der Bionik: neue Technologien nach dem Vorbild der Natur*. Deutsche Verlags-Anstalt, Stuttgart, Germany, 2. edition, 2001.

[28] Lindau I. Spicer W.E. *J. Elec. Spectroscopy*, 3:409, 1974.

[29] Powell C.J. *Surf. Science*, 44:29, 1974.

[30] Shirley D.A. *Phys. Rev. B*, 5(12):4709–4714, 1972.

[31] Camillone N Chidsey C. E. D. Liu G. Y. Putvinski T. M. Scoles G. *J. Chem. Phys.*, 94(12):8493–8502, 1991.

[32] Hähner G Wöll C Buck M Grunze M. *LANGMUIR*, 9(8):1955–1958, 1993.

[33] Himmelhaus M Eisert F Buck M Grunze M. *J. PHYS. CHEM. B*, 104(3):576–584, 2000.

[34] Schertel A H"ahner G Grunze M Wöll C. *J. VAC. SCI. & TECH. A*, 14(3):1801–1806, 1996.

[35] Brown G.E. Henrich V. E. Casey W. H. Clark D. L. Seaborg G.T. Eggleston C. Felmy A. Goodman D. W. Grätzel M. Maciel G. McCarthy M. I. Nealson K. H. Sverjensky D. A. Toney M. F. Zachara J. M. *Chem. Rev.*, 99(1):77–174, 1999.

[36] Brunette D.M. Tengvall P. Textor M. Thomsen P., editor. *Titanium in Medicine: Material Science, Surface Science, Engineering, Biological Responses and Medical Applications*. Springer Verlag, Berlin, Germany, 2001.

[37] Hähner G Hofer R Klingenfuss I. *Langmuir*, 17(22):7047–7052, 2001.

[38] Rosen M. J. *Surfactants and interfacial phenomena*. Wiley cop., New York, USA, 2. edition, 1989.

[39] Chen Y.L. Chen S. Frank C. Israelachvili J. *J. coll. int. sci.*, 153(1):244–264, 1992.

[40] Zwahlen M. Tosatti S. Textor M. Hähner G. *Langmuir*, 18(10):3957–3962, 2002.

[41] Tosatti S. *unknown.* PhD thesis, ETH Zürich, Zürich, Switzerland, 2003.

[42] Kryshtab T.G. Gomez J.P Lytvyn P.M. Lytvyn O.S. *Thin Solid Films*, 373(1–2):79–83, 2000.

[43] Hofer Rolf. *Surface Modification for Optical Biosensor Applications.* PhD thesis, ETH Zurich, Zurich, CH, 2000. Nr. 13873.

[44] Bunton C A Diaz S v.Fleteren G M Paik C. *J. org. chem.*, 43(2):258–261, 1978.

[45] Cassie A B D. *Discuss. Faraday Soc.*, 4:5041, 1952.

[46] Israelachvili J.N. Gee M.L. *Langmuir*, 5(1):288–289, 1989.

[47] Textor M. Ruiz L. Hofer R. Rossi A. Feldmann K. Hähner G. Spencer N.D. *Langmuir*, 16(7):3257–3271, 2000.

[48] Bagus P.S. Weiss K. Schertel A. Wöll C. Braun W. Hellwig C. Jung C. *Chem. Phys. Lett.*, 248(3–4):129–135, 1996.

[49] Himmel H.J. Weiss K. Jäger B. Dannenberger O. Grunze M. Wöll C. *Langmuir*, 13(19):4943–4947, 1997.

[50] Hähner G. Marti A. Spencer N.D. Brunner S. Caseri W.R. Suter U.W. Rehahn M. *Langmuir*, 12(3):719–725, 1996.

[51] Urquhart S.G. Hitchcock A.P. Priester R.D. Rightor E.G. *J. Polym. sci. polym. phys.*, 33(11):1603–1620, 1995.

[52] Hofer R. Textor M. Spencer N.D. *Langmuir*, 17(13):4014–4020, 2001.

[53] Brovelli D. Hähner G. Ruiz L. Hofer R. Kraus G. Waldner A. Schlösser J. Oroszlan P. Ehrat M. Spencer N.D. *Langmuir*, 15(13):4324–4327, 1999.

[54] More SD Graaf H Baune M Wang C S Urisu T. *JPN J APPL PHYS PT 1*, 41(6B):4390–4394, 2002.

[55] Losic D Shapter JG Gooding JJ. *LANGMUIR*, 17(11):3307–3316, 2001.

[56] Rowe G K Creager S E, Hockett L A. *Langmuir*, 8(3):854–861, 1992.

[57] Folkers J P Gorman C B Laibinis P E Buchholz S Whitesides G M Nuzzo R G. *LANGMUIR*, 11(3):813–824, 1995.

[58] Allara D L Atre S V Elliger C A Snyder R G. *J. Am. Chem. Soc.*, 113(5):1852–1854, 1991.

[59] Sprik M Delamarche E Michel B Röthlisberger U Klein M L Wolf H Ringsdorf H. *Langmuir*, 10(11):4116–4130, 1994.

[60] Bielka H u.a. *Molekularbiologie1.* Gustav Fischer Verlag, Stuttgart, Germany, 1 edition, 1985.

[61] Dreyer und Rusconi Fachschaft Medizin according to Prof. Conzelmann. *Biochemie Skript.* University of Fribourt CH, 2000.

[62] Alberts B Johnson A Lewis J Raff M Roberts K Walter P. *Molecular biology of the cell.* Garland Science, Taylor & Francis Group, New York, USA, 4. edition, 2002.

[63] G.M Pale-Grosdemage C. Simon E.S. Prime K.L. Whitesides. *J.Am.Chem.Soc.*, 113(1):12–20, 1991.

[64] Jeon S.I. Andrade J.D. *J. coll. int. sci.*, 142(1):159–166, 1991.

[65] Harder P. Grunze M. Dahint R. Whitesides GM. Laibinis PE. *J. PHYS. CHEM. B*, 102(2):426–436, 1998.

[66] Matsuura H. Miyazawa T. Machida K. *Spectrochim. Acta*, 29(A):771–779, 1973.

[67] Tadokoro H. Chatani Y. Yoshihara T. Tahara S. Murahashi S. *Makromol. Chem.*, 73:109–127, 1964.

[68] Matsuura H. Miyazawa T. *J. polymer sci.*, 7:1735–1744, 1969.

[69] Pertsin A.J. Grunze M. Garbuzova I.A. *J. Phys. Chem. B*, 102:4918–4926, 1998.

[70] M. Wang R.L.C. Kreuzer H.J. Grunze. *Phys.Chem.Chem.Phys.*, (2):3613–3622, 2000.

[71] Pertsin A.J. Grunze M. *Langmuir*, 16(23):8829–8841, 2000.

[72] Prime K.L. Whitesides G.M. *J.Am.Chem.Soc.*, 115:10714–10721, 1993.

[73] Ostuni E. Chapman R.G. Homlin R.E. Takayama S. Whitesides G.M. *Langmuir*, 17(18):5605–5620, 2001.

[74] Dicke C. Hähner G. *J. Am. Chem. Soc.*, 124(42):12619–12625, 2002.

[75] Hähner G. Dicke C. Feldman K. Eck W. Herrwerth S. *Abstr. Pap. Am. Chem. Soc.*, 220, 2000.

[76] Feldman K. Hähner G. Spencer N.D. Harder P. Grunze M. *J. Am. Chem. Soc.*, 121:10134–13141, 1999.

[77] Nelson K.E. Gamble L. Jung L. S. Böckl M. S. Naeemi E. Golledge S. L. Sasaki T. Castner D. G. Campbell C. T. Stayton P. S. *Langmuir*, 17(9):2807–2816, 2001.

[78] Hähner G. Kinzler M. Wöll Ch. Grunze M. Scheller M.K. Cederbaum L.S. *Phys. Rev. Lett*, 67(7):851–854, 1991.

[79] Takahashi Y. Tadokoro H. *Macromolecules*, 6(5):672–675, Sept-Oct 1973.

[80] Zharnikov M Frey S Heister K Grunze M. *J. Electron Spectrosc. Relat. Phenom.*, 124(1):15–24, 2002.

[81] Mathworks inc. www.mathworks.com. electronically.

[82] Jager B. Schurmann H. Muller HU. Himmel HJ. Neumann M. Grunze M. Wöll C. *Z PHYS CHEM*, 202:263–272, 1997.

[83] Tokumitsu S Liebich A Herrwerth S Eck W Himmelhaus M Grunze M. *Langmuir*, 18(23):8862–8870, 2002.

[84] Stöhr J. Samant M.G. Luning J. Callegari A.C. Chaudhari P. Doyle J.P. Lacey J.A. Lien S.A. Purushothaman S. Speidell J.L. *SCIENCE*, 292(5525):2299–2302, 2001.

[85] Stöhr J. Samant M.G. Cossy-Favre A. Diaz J. Momoi Y. Odahara S. Nagata T. *MACROMOLECULES*, 31(6):1942–1946, 1998.

[86] Herrwert S. PhD thesis, Chemie Institut, University of Heidelberg, Germany, 2002.

[87] Theng B K G. *Formation and Properties of Clay-Polymer Complexes.* Elsevier, Amsterdam, 1979.

[88] diverse. Encyclopedia britannica. electronically, 2002.

[89] Collings R K Andrews P R A. *Mica and vermiculite*, volume 1. Canadian Communication Goup - Publishing, Ottawa, Ca, 1 edition, 1989.

[90] Schreiber F. *Progress in Surface Science*, 65:151–256, 2000.

[91] Moore J. H. Spencer N. D., editor. *Encyclopedia of chemical physics and physical chemistry.* Institute of Physics publishing, Bristol, 1 edition, 2001.

[92] Meier B.H. Suter U.W. Osman M.A. Ernst M. *J. Phys. Chem. B*, 106(3):653–662, 2002.

[93] Shelden R.A. Caseri W.A. Suter U.W. *J. coll. int. sci.*, 157:318–327, 1993.

[94] Fujii M. Li B. Fukada K. Kato T. Seimiya T. *Langmuir*, 17(4):1138–1142, 2001.

[95] Chen Y.L. Chen S. Frank C. Israelachvili J. *J. coll. int. sci.*, 153(1):244–264, 1992.

[96] Liu Y. Evans D.F. Song Q. Grainger D.W. *Langmuir*, 12(5):1235–1244, 1996.

[97] Benitez J.J Lopta S. Ogletree D.F. Salmeron M. *Langmuir*, 18(16):6096–6100, 2002.

[98] Herder P. C. Claesson C. E. Herder J. *J. coll. int. sci.*, 119:155, 1987.

[99] Grunwaldt JD Atamny F Gobel U Baiker A. *Appl. Surf. Sci.*, 99(4):353–359, 1996.

[100] Derose J A Thundat T Nagahara L A Lindsay S M. *Surf. Sci.*, 256(1–2):102–108, 1991.

[101] Biino G.G. Groning P. *EUROPEAN J MINERAL*, 10(3):423–437, 1998.

[102] G. G. Biino. *Schweiz. Miner. Petrog.*, 78(1):21, 1998.

[103] Claesson Herder Berg Christenson. *J. coll. int. sci.*, 136:541, 1990.

[104] Brovelli D. Caseri W. R. Hähner G. *J. coll. int sci*, 216:418–423, 1999.

[105] Ralston A. W. Reck R. A. Harwood H. J. DuBrow P. L. *J.org. chem*, 13(2):186–190, 1947.

[106] Davey T.W. Ducker W.A. Hayman A.R. Simpson J. *Langmuir*, 14(12):3210–3213, 1998.

[107] Mukerjee P. and Mysels K. J., editors. *Critical Micelle Concentrations of Aqueous Surfactant Systems*. Number 36 in NSRDS-NBS. U.S. Dept. of Commerce, Washington, 1971.

[108] Christenson H.K. *J. Phys. Chem.*, 97(46):12034–12041, 1993.

[109] E. Herzog. *Nr. 11362*. PhD thesis, ETH Zürich, Zürich, Switzerland, 1996.

[110] Beamson G Briggs D. *High resolution XPS of organic polymers: The scienta ESCA 300 database*. Wiley cop., Chichester, 1 edition, 1992.

[111] Aminpirooz S. Becker L. Hillbert B. Haase J. *SURF. SCI. Lett.*, 244(3):L152–L156, 1991.

[112] Brovelli D. *Nr. 13001*. PhD thesis, ETH Zürich, Zürich, Switzerland, 1999.

[113] Solomon J. L. Madix R. J. Stöhr J. *Surface science*, 255:12–30, 1991.

[114] Salmeron M. Bluhm H. Inoue T. *Surf. Sci.*, 462:L599–L602, 2000.

[115] Pfüller U. *Mizellen - Vesike - Mikroemulsionen : Tensidassoziate und ihre Anwendung in Analytik und Biochemie*. Number 22 in Anleitung für die chemische Laboratoriumspraxis. Springer Verlag, Berlin, Germany, 1986.

[116] Doudevski I. Schwartz D.K. *J. Am. Chem. Soc.*, 123(28):6867–6872, 2001.

[117] D.W. Fuerstenau. *J. Phys. Chem.*, 60:981, 1956.

[118] Manne S. Gaub H.E. *Science*, 270:1480–1482, 1995.

[119] Li B. Fujii M. Fukada K. Kato T. Seimiya T. *J. coll. int sci*, 209:25–30, 1999.

[120] Doudevski I. Schwartz D.K. *Appl. surf. sci.*, 175-176:17–26, 2001.

[121] Osman M. A. Seyfang G-Suter U. W. *J. Phys. Chem. B*, 104(18):4433–4439, 2000.

[122] Lide D. R., editor. *CRC Handbook of Chemistry and Physics. A ready-reference of Chemical and Physical Data*. CRC Press, Boston, USA, 72 edition, 1991–1992.

[123] Heinz H. Castelijns H. J. Suter U. W. *J. Am. Chem. Soc.*, 125(31):9500–9510, 2003.

[124] Mugele F. Salmeron M. *J. Chem. Phys.*, 114(4):1831–1836, January 2001.

[125] Brady J. E. Evans D. F. Warr G. G. Griesser F. Ninham B. W. *J. of phys. Chem.*, 90(9):1852–1859, 1986.

[126] Wall J.F. Zukoski C.F. *Langmuir*, 15(22):7432–7437, 1999.

[127] Okuyama K Soboi Y Iijima N Hirabayashi K. *Bull. Chem. Soc. Jpn.*, 61:1485–, 1988.

[128] Zwahlen M Brovelli D Caseri W H"ahner G. *J. coll. int. sci*, 262:262–267, 2002.

[129] Barlet R. Moi A. Poignet J.C. Vidal M. *J. Chim. Phys. Chim. Phys. Biol.*, 81(5):349–354, 1984.

[130] Hähner G. Marti A. Spencer N.D. Caseri W.R. *J. CHEM. PHYS.*, 104(19):7749–7757, 1996.

[131] DAVIES PR; SHUKLA N. *SURFACE SCI*, 322(1–3):8–20, 1995.

[132] Huang S.X. Fischer D.A. Gland J.L. *J PHYS CHEM*, 100(24):10223–10234, 1996.